

**Editor-in-Chief B.E.Paton**

**Editorial board:**

Yu.S.Borisov	I.A.Ryabtsev
A.Ya.Ishchenko	V.F.Khorunov
B.V.Khitrovskaya	I.V.Krivtsun
S.I.Kuchuk-Yatsenko	
Yu.N.Lankin	L.M.Lobanov
V.N.Lipodaev	A.A.Mazur
V.I.Makhnenko	I.K.Pokhodnya
O.K.Nazarenko	K.A.Yushchenko
A.T.Zelnichenko	

**International editorial council:**

N.P.Alyoshin	(Russia)
U.Diltey	(Germany)
Guan Qiao	(China)
D. von Hofe	(Germany)
V.I.Lysak	(Russia)
N.I.Nikiforov	(Russia)
B.E.Paton	(Ukraine)
Ya.Pilarczyk	(Poland)
P.Seyffarth	(Germany)
G.A.Turichin	(Russia)
Zhang Yanmin	(China)
A.S.Zubchenko	(Russia)

**Promotion group:**

V.N.Lipodaev, V.I.Lokteva  
A.T.Zelnichenko (exec. director)

**Translators:**

I.N.Kutianova, T.K.Vasilenko,  
V.F. Orets

PE «Melnik A.M.»

**Editor**

N.A.Dmitrieva

**Electron galley:**

I.S.Batasheva, T.Yu.Snegiryova

**Address:**

E.O. Paton Electric Welding Institute,  
International Association «Welding»,  
11, Bozhenko str., 03680, Kyiv, Ukraine

Tel.: (38044) 287 67 57

Fax: (38044) 528 04 86

E-mail: journal@paton.kiev.ua

http://www.nas.gov.ua/pwj

State Registration Certificate  
KV 4790 of 09.01.2001

**Subscriptions:**

**\$324**, 12 issues per year,  
postage and packaging included.  
Back issues available.

All rights reserved.

This publication and each of the articles  
contained herein are protected by copyright.  
Permission to reproduce material contained in  
this journal must be obtained in writing from  
the Publisher.

Copies of individual articles may be obtained  
from the Publisher.

**CONTENTS**

**SCIENTIFIC AND TECHNICAL**

*Yushchenko K.A., Yarovitsyn A.V. and Zvyagintseva A.V.*  
Properties of microplasma powder welded joints on  
heat-resistant nickel alloys ..... 2

*Makhnenko O.V.* Increase of efficiency of thermal  
straightening of welded thin-sheet structures on basis of  
mathematical modeling ..... 6

*Poklyatsky A.G.* Influence of oxide film macroinclusions on  
the strength of welds in plate joints of AMg6 alloy ..... 10

*Borisova A.L., Borisov Yu.S., Adeeva L.I., Tunik A.Yu.,  
Karpets M.V. and Burlachenko A.N.* Effect of parameters  
of mechanical-chemical synthesis on structure, phase  
composition and properties of thermal spraying Al-Cu-Fe  
system powders containing quasi-crystalline phase ..... 14

*Tsaryuk A.K., Skulsky V.Yu., Moravetsky S.I. and  
Sokirko V.A.* Influence of electromagnetic treatment on  
residual welding stresses in welded joints of carbon and  
low-alloyed steels ..... 22

**INDUSTRIAL**

*Kovtunenkov V.A., Gerasimenko A.M., Zadorozhny V.A. and  
Ryndich V.V.* Application of 10KhSNDA, 15KhSNDA rolled  
stock in metal structures of the railway-road bridge across  
the Dnieper river in Kiev ..... 26

*Kuchuk-Yatsenko S.I., Shvets Yu.V., Kavunichenko A.V.,  
Shvets V.I., Taranenkov S.D. and Proshchenko V.A.*  
Performance of flash butt welded joints on railway frogs ..... 30

*Lentyugov I.P., Ryabtsev I.A., Kuzmenko O.G. and  
Kuskov Yu.M.* Metal-abrasive grinding wastes, methods of  
their processing and experience of application in surfacing  
materials ..... 34

**BRIEF INFORMATION**

Theses for a scientific degree ..... 39

News ..... 41

**NEWS**

International Conference «Titanium-2008 in CIS» ..... 43

Fourth International Conference «Mathematical Modelling  
and Information Technologies in Welding and Allied  
Processes» ..... 44

Developed at PWI ..... 13, 33, 40, 42, 45



# PROPERTIES OF MICROPLASMA POWDER WELDED JOINTS ON HEAT-RESISTANT NICKEL ALLOYS

K.A. YUSHCHENKO, A.V. YAROVITSYN and A.V. ZVYAGINTSEVA  
E.O. Paton Electric Welding Institute, NASU, Kiev, Ukraine

It has been established that increase in the content of oxygen and nitrogen in the weld metal has a negative effect on ductility of welded joints in heat-resistant nickel alloys at a working temperature. The range of the content of oxygen and nitrogen in the weld metal, within which the quality formation of the weld and satisfactory mechanical properties of the welded joints are provided, has been determined for repair microplasma powder welding.

**Keywords:** *microplasma powder welding, cladding, heat-resistant nickel alloy, welded joint, content of oxygen and nitrogen, short-time mechanical properties*

Oxygen and nitrogen, along with some other elements, are known to act as harmful impurities in heat-resistant nickel alloys, as they decrease heat [1] and crack resistance [2] during welding. Their content in modern heat-resistant nickel alloys after vacuum induction remelting is limited to 0.0015 wt.% for each element [1]. The metallurgical method of control of hot cracking of nickel and its alloys during welding is limitation of the oxygen content of the weld metal to 0.005 wt.%, in addition to refining of structure of the weld metal and heat-affected zone (HAZ) and formation of the optimal thermal-deformation cycle [3]. Peculiarity of the technology of welding heat-resistant nickel alloys consists in the presence of refractory oxide films on the surface of metal welded [4, 5]. In this connection, it is recommended to apply the technological approaches that limit oxidation of the deposited metal [6].

The plasma arc welding methods using an additive powder hold promise for repair of blades of heat-resistant nickel alloys [7, 8]. However, microplasma powder welding used to repair blades [9] may induce microstructural defects (Figure 1) because of decrease in the efficiency of shielding of the welding zone, while increase in the content of oxygen and nitrogen

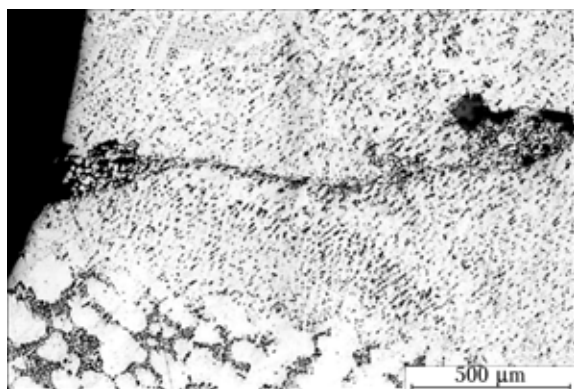


**Figure 1.** Microstructure of region of the deposited metal with oxide inclusion resulting from repair microplasma powder welding of blades made from heat-resistant nickel alloys

in the deposited metal may cause changes in mechanical properties of the welded joints.

In contrast to widely applied TIG welding in argon atmosphere using a filler [5, 6], repair microplasma powder welding of heat-resistant nickel alloys is characterised by a number of factors that decrease the efficiency of shielding of the welding zone. They include an increased arc length, disturbance of gas flows caused by an addition of powder, and introduction of extra impurities with the powder into the weld pool.

One of the ways of evaluating the efficiency of shielding of the weld pool with inert gases is determination of the content of oxygen and nitrogen in the weld metal [10], which depends not only upon the chemical composition of base metal and welding consumables, but also upon the welding method [11].

The purpose of this study was to investigate the effect of process parameters on the content of oxygen and nitrogen in the weld metal, as well as to evaluate changes in mechanical properties of welded joints in microplasma powder welding of heat-resistant nickel alloys.

Bead on plate welding by using an additive powder of the nickel alloy containing 50 vol.% of the  $\gamma$ -phase was performed for quantitative estimation of gas content of the deposited metal, the plates being 2.5–4.0 mm thick and having similar chemical composition (Table 1).

Argon of grade 1 (GOST 10157–79) with the following content of impurities, wt.%: 0.002 O<sub>2</sub>, 0.001 H<sub>2</sub>O, was used as a plasma, carrier and shielding gas for welding. Residual pressure in a gas bottle was not less than 3 MPa. The flow rates of gases were as follows: 1 l/min for plasma gas, and 6–7 l/min for carrier and shielding gases. Plasmatron travel speed  $v_w$  was 3 m/h. The baked powder with a particle size of 40–160  $\mu$ m, produced by dry atomisation in argon atmosphere, was used as an additive material. The process variables were the plasmatron to work-piece distance and weight of the powder fed to the arc. The flow diagram of welding is shown in Figure 2. To estimate the effect of the state of the additive powder on the content of oxygen and nitrogen in the deposited metal, the beads were also deposited by using the unbaked powder and powder oxidised in the arc. In the latter case, welding was performed to evaluate the possibility of reusing the additive material to reduce its losses.

**Table 1.** Chemical composition (wt.%) of heat-resistant nickel alloys under investigation

Alloy	C	Si	Mn	W	Cr	Mo	Ti	Al
With 50 vol.% of $\gamma$ -phase	$\leq 0.17$	$\leq 0.3$	$\leq 0.5$	2.6	16.0	1.8	3.4	3.4
EI-698	$\leq 0.08$	$\leq 0.4$	$\leq 0.4$	–	13.0–16.0	2.8–3.2	2.35–2.75	1.3–1.7

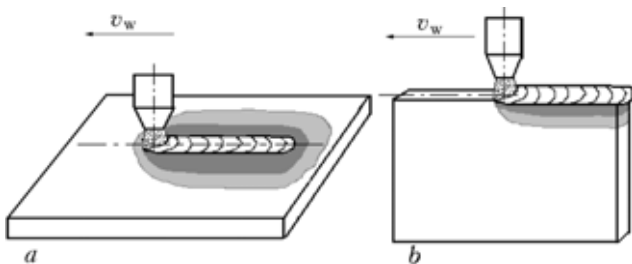
**Table 1 (cont.)**

Alloy	Nb	Co	Fe	B	Ta	Zr	[O]	[N]
With 50 vol.% of $\gamma$ -phase	0.9	8.5	$\leq 0.3$	$\leq 0.01$	1.8	0.1	0.0007	0.0018
EI-698	1.8–2.0	–	$\leq 2.0$	–	–	–	0.0009	0.0014

Note. Contents of oxygen and nitrogen in the alloys are not specified, the data on oxygen and nitrogen were derived by the authors.

To conduct investigations, specimens in the form of a cube with a side of 3–4 mm were cut out from the deposited metal at a height of not less than 1 mm from the base metal by the electroerosion method, and their surfaces were machined to remove oxide films. Quantitative estimation of the gas content of the deposited metal was performed by measuring the total content of oxygen and nitrogen in reduction melting in a carrier gas flow using the LECO instruments RO316 and TN114. The quality of formation of the deposited metal was assessed visually from the appearance of a bead and oxide film on its surface (Figure 3).

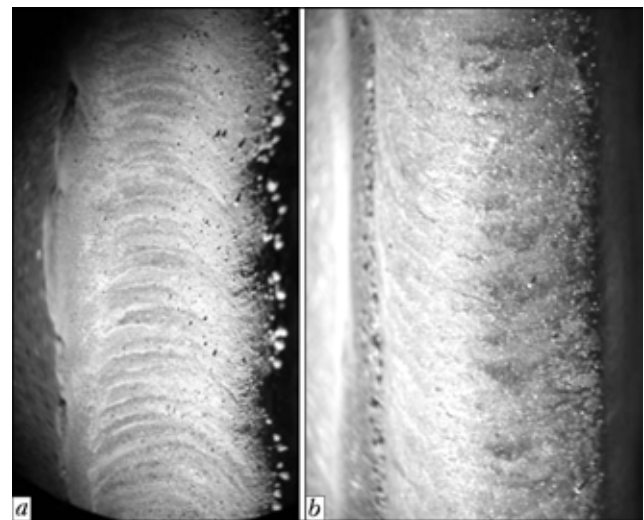
Results of the investigations on the gas content of the deposited metal are shown in Figures 4–7. As established, the content of oxygen in the deposited metal ranges from 0.007 to 0.022 wt.%, and that of nitrogen is 0.0026–0.008 wt.%, depending upon the welding process parameters. The quality and satisfactory formation of the deposited metal is provided at its oxygen content of 0.007–0.017 wt.%, and nitrogen content of 0.0026–0.0055 wt.%. In this case, the content of gases introduced into the deposited metal directly from the powder is not less than 0.007 wt.% for oxygen, and not less than 0.0022 wt.% for nitrogen. It was established that the process parameters affecting to a substantial degree the content of oxygen and nitrogen in the deposited metal are the plasmatron to workpiece distance, flow diagram of the welding process, and amount of an additive powder fed to the arc. Decrease of the weight content of gases in the deposited metal in welding on a narrow substrate (end surface of a plate) can be explained by the fact that the corresponding welding parameters are characterised by an insignificant consumption of powder and a short plasmatron to workpiece distance (about 3 mm).

**Figure 2.** Flow diagrams of microplasma powder welding on a plate (a) and its end surface (b)

Heat-resistant nickel alloy EI-698 (Tables 1 and 2) with 14–17 vol.% of the  $\gamma$ -phase [12] in the as-received condition [13] was chosen to investigate mechanical properties of the welded joints on heat-resistant nickel alloys with a range of the oxygen and nitrogen content of the weld metal as given above. This alloy belongs to a category of hard-to-weld alloys and is applied for making disks and blades of gas turbines operating at a temperature of up to 750 °C [13].

Microplasma welding of two restrained butt joints on plates measuring 100 × 50 × 2.5 mm was performed for the investigations. The additive powder of alloy EI-698 with a particle size of 40–160  $\mu\text{m}$  was fed in an amount of 7 g/min. The welding speed was 3 m/h. Parameters of the microplasma welding process were selected for the experiments so that they could provide a minimal and maximal content of oxygen and nitrogen in the weld metal. To ensure the satisfactory weld formation at the maximal gas content of the weld metal, the welding current was increased by 30 %, the welding speed being left unchanged.

Mechanical properties of the welded joints in the as-welded condition were evaluated with the ALA-TOO unit [8] by testing sectional specimens cut out across the weld. Cross section of the gauge length was 1.5 × 2 mm (Figure 8). Surfaces of the specimens

**Figure 3.** Appearance of the deposited beads of heat-resistant nickel alloy containing 50 vol.% of the  $\gamma$ -phase with poor (a) and satisfactory (b) formation ( $\times 10$ )



**Table 2.** Properties of welded joints on alloy EI-698

Test object	$\sigma_t$ , MPa		$\sigma_y$ , MPa		$\delta$ , %		[O], wt. %	[N], wt. %
	20 °C	750 °C	20 °C	750 °C	20 °C	750 °C		
Base metal	$\frac{1206}{1}$	$\frac{800}{1}$	$\frac{920}{1}$	$\frac{770}{1}$	$\frac{34}{1}$	$\frac{18}{1}$	0.0009	0.0014
Welded joint: No. 1	$\frac{973}{0.806}$	$\frac{726}{0.908}$	$\frac{600}{0.652}$	$\frac{490}{0.636}$	$\frac{30}{0.882}$	$\frac{17.2}{0.956}$	0.0060	0.0032
No. 2	$\frac{885}{0.774}$	$\frac{579}{0.723}$	$\frac{550}{0.598}$	$\frac{510}{0.662}$	$\frac{33}{0.971}$	$\frac{10}{0.556}$	0.0150	0.0079

*Note.* Denominator gives values of strength factor for  $\sigma_t$ ,  $\sigma_y$  and  $\delta$  compared to the base metal at the given temperature.

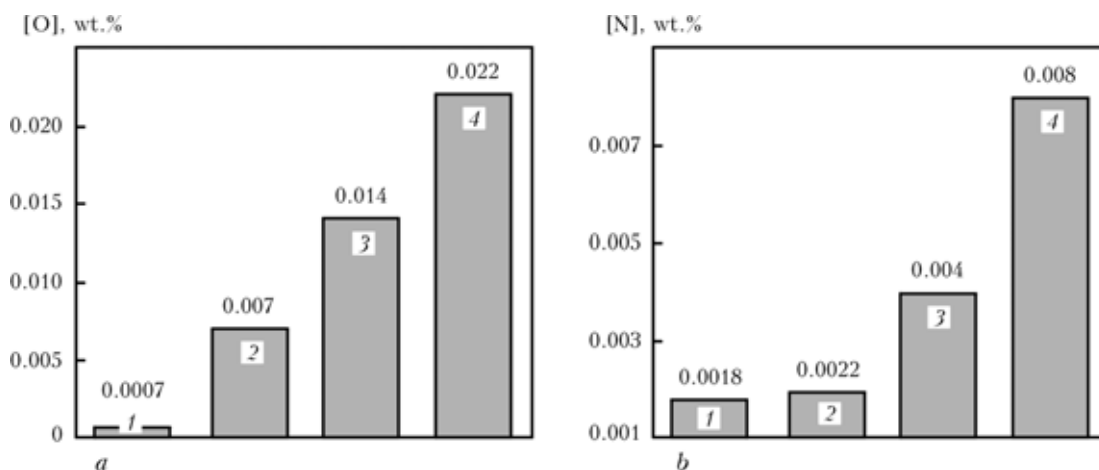


**Figure 4.** Content of oxygen (a) and nitrogen (b) in the deposited metal of heat-resistant nickel alloy containing 50 vol.% of  $\gamma$ -phase in multilayer welding using an additive powder at its consumption of 5 g/min: 1 — cast alloy; 2 — additive powder; 3, 4 — deposited metal produced at plasmatron to workpiece distance  $L = 4$  and 10 mm, respectively

before the tests were inspected by the dye penetrant method to detect defects. To avoid the effect of air oxygen, the specimens were heated by the radiation method in vacuum. Short-time mechanical properties of the base metal were evaluated to eliminate any influence of the scale factor. The tests were carried out at a temperature of 20 and 750 °C. The choice of this temperature was based on the temperature conditions of operation of the alloy [13], as well as on the presence of the ductility-dip temperature range for materials of this class [8], within which the sensitivity to cracking of the welded joints is especially

pronounced. The specimens fractured in the weld metal. Results of the tests are given in Table 2.

It was established that tensile strength of the specimen of welded joint No. 1 with the minimal content of oxygen and nitrogen in the weld metal at a temperature of 750 °C is 20 % higher compared with that of the specimen of welded joint No. 2. Ductility of specimen No. 1 at 750 °C remains at a level of the base metal, whereas ductility of specimen No. 2 at the same temperature is only 55.6 % of that of the base metal.

The data obtained are in good agreement with the results of the earlier metallographic examinations [1, 2]. Decrease in ductility of heat-resistant nickel alloys is caused by enrichment of grain boundaries with oxygen, and by formation of low-melting point compounds with other impurity elements. In particular, this is confirmed by the data of Auger spectroscopy of the fracture surface of a specimen of polycrystalline heat-resistant nickel alloy with 65 vol.% of the  $\gamma$ -phase, which was tested within the ductility-dip temperature range [2].

Increase of the content of oxygen and nitrogen in the weld metal decreases ductility and tensile strength of the welded joints in the ductility-dip temperature range, which may have a negative effect on crack resistance of the welded joints in welding and heat treatment.

Therefore, it is necessary to improve shielding of the microplasma powder welding zone in welding

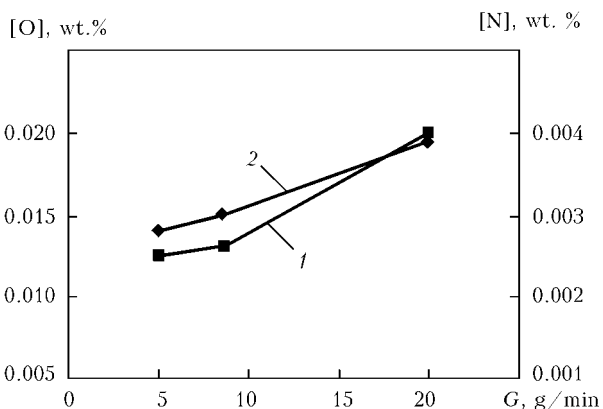


**Figure 5.** Content of oxygen (1) and nitrogen (2) in the deposited metal of heat-resistant alloy with 50 vol.% of the  $\gamma$ -phase against the amount of the additive powder fed to the arc

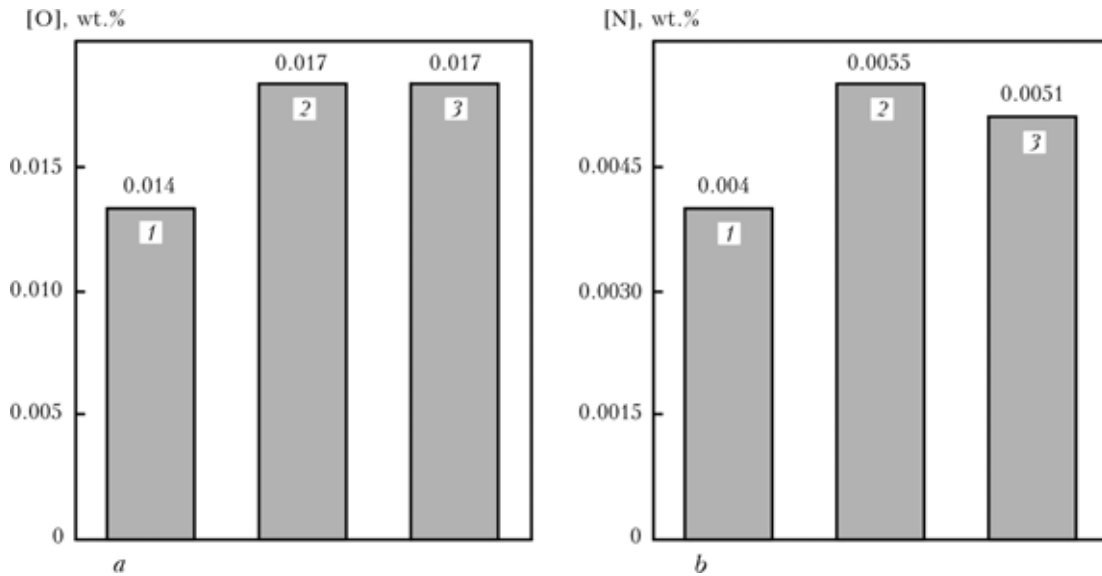


**Figure 6.** Content of oxygen (a) and nitrogen (b) in the deposited metal of heat-resistant nickel alloy with 50 vol.% of the  $\gamma$ -phase against the condition of the additive powder fed to the arc in an amount of 5 g/min in multilayer welding: 1 — baked; 2 — unbaked; 3 — oxidised in the arc

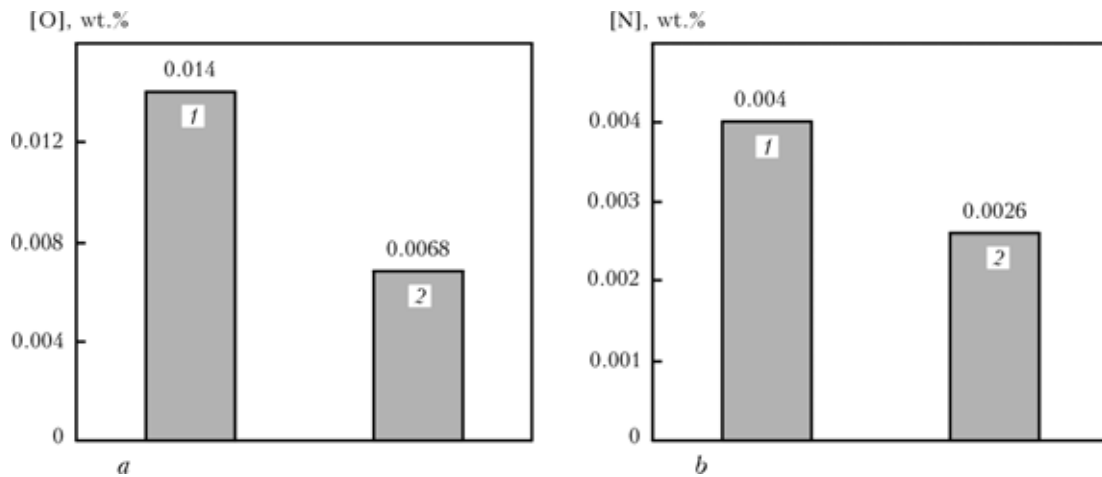


**Figure 7.** Content of oxygen (a) and nitrogen (b) in the deposited metal of heat-resistant nickel alloy with 50 vol.% of the  $\gamma$ -phase against the flow diagram of multilayer welding on a plate (1) and its end surface (2) by using the additive powder in an amount of 5 g/min

(cladding) of heat-resistant nickel alloys with a total aluminium and titanium content of over 3 wt.%.

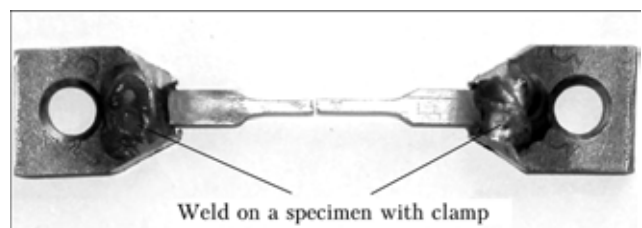


**Figure 8.** Appearance of the sectional specimen after testing to short-time mechanical properties

1. Stroganov, G.B., Chepkin, V.M. (2000) *Cast high-temperature alloys for gas turbines*. Moscow: ONTI, MATI.
2. Savchenko, V.S., Yushchenko, K.A., Zvyagintseva, A.V. et al. (2007) Investigation of structure and crack formation in welded joints of single crystal Ni-base alloys. *Welding in the World*, 51(11/12), 76–81.
3. Lebedev, V.K., Kuchuk-Yatsenko, S.I., Chvertko, A.I. et al. (2006) *Mechanical engineering: Encyclopedia. Technology of welding, soldering and cutting*. Ed. by B.E. Paton. Moscow: Mashinostroenie.
4. Zinke, M., Neubert, G., Herold, H. (1999) Properties of welded joints of nickel-base heat-resistant alloys. *Automatich. Svarka*, 4, 35–38.
5. Sorokin, L.I. (2004) Welding repair of cracks with oxidised surfaces on heat-resistant nickel alloys. *Svarochn. Proizvodstvo*, 12, 30–31.
6. Sorokin, L.I. (2004) Argon-arc surfacing of tread-band webs of heat-resistant nickel alloys. *Ibid.*, 7, 36–39.
7. Savchenko, V.S., Yushchenko, K.A., Savolej, N.I. et al. (1993) Peculiarities of welding of high-nickel strain-hardened alloys and repair of products made from them. *Automatich. Svarka*, 10, 31–33.
8. Yushchenko, K.A., Savchenko, V.S., Chervyakova, L.V. et al. (2005) Investigation of weldability of nickel superalloys and development of repair technology for gas turbine blades. *The Paton Welding J.*, 6, 2–5.
9. Kalina, P.P., Yarovitsyn, A.V., Yushchenko, K.A. (2005) Peculiarities of the microplasma powder cladding process. *Ibid.*, 4, 7–13.
10. Fedorenko, G.A., Shvedikov, V.M., Grishchenko, L.V. (1986) About validity of methods for examination of spray shielding. *Svarochn. Proizvodstvo*, 6, 35–37.
11. Pokhodnya, I.K., Yavdoshchin, I.R., Paltsevich, A.P. et al. (2004) *Metallurgy of arc welding. Interaction of metal with gases*. Kiev: Naukova Dumka.
12. Sorokin, L.I. (1999) Stresses and cracks in welding and heat treatment of heat-resistant alloys. *Svarochn. Proizvodstvo*, 12, 11–15.
13. Zubchenko, A.S., Koloskov, M.M., Kashirsky, Yu.V. et al. (2003) *Reference book on grades of steels and alloys*. Ed. by A.S. Zubchenko. Moscow: Mashinostroenie.



# INCREASE OF EFFICIENCY OF THERMAL STRAIGHTENING OF WELDED THIN-SHEET STRUCTURES ON BASIS OF MATHEMATICAL MODELING

O.V. MAKHNENKO

E.O. Paton Electric Welding Institute, NASU, Kiev, Ukraine

Analysis of efficiency of different shapes of heating spots in thermal straightening of thin-sheet steel structures with buckling deformations was carried out on basis of mathematical modeling. Ratio of the volume of residual plastic shrinkage strains in plane of the sheet to the heating energy input was used as a criterion of thermal efficiency of straightening. It was shown that due to optimization of the shape of heating and its parameters efficiency of thermal straightening may be increased several times.

**Keywords:** welded thin-sheet structures, welding deformations, thermal straightening, mathematical modeling

Expenditures for thermal straightening in manufacturing of welded thin-sheet structures may be rather significant [1, 2], which is stipulated by both big volume of manual skilled labor input and significant consumption of energy. Recently attempts were made to reduce expenditures for thermal straightening using automation of this process [3] for the purpose of sharp reduction of the volume of manual labor. During performance of works for automation of thermal straightening of welded thin-sheet structures with buckling deformations on basis of mathematical modeling of this process it was found out that significant saving of energy consumption may be achieved due to optimization of the heating parameters.

In this work results of the calculations, directed at increase of the thermal straightening efficiency (TSE) by optimization of the heating parameters, are presented.

Experience of manufacturing of thin-sheet structures shows that frequently occurring kind of local deformations --- buckling of the sheet metal --- is formed as a result of loss of stability because of compression stresses, caused by longitudinal shrinkage of welded joints during welding of stiffening ribs. If these deformations exceed permissible level, usually thermal straightening is used, due to which in plane of the sheet metal occur plastic shortening strains, which remove «extra» metal.

Values of residual plastic strains in thermal straightening depend upon a whole number of parameters, such as shape of the heating spot, power of the source and time of heating, material and thickness of the structure sheet, conditions of cooling, maximum temperature of heating and its distribution. Ratio of the volume of residual plastic shrinkage strains in plane of the sheet  $V_{p,s}$  to the heating energy input  $Q_h$  was taken as a criterion of TSE:

$$\text{TSE} = \frac{V_{p,s}}{Q_h} \text{ [mm}^3\text{/kJ]}. \quad (1)$$

As far as in thermal straightening of buckling deformations of a thin sheet of casing the determining factor is shrinkage in plane of the sheet, volume of residual plastic strains may be presented as product of area of the latter  $F_{p,s}$  in the sheet plane and its thickness  $\delta$ . Such assumption may be assumed for thin sheets at relatively uniform distribution over their thickness of plastic shrinkage strains. Respectively heating energy input may be determined as product of the source power  $P_h$  and time of heating  $t_h$ :

$$\text{TSE} = \frac{F_{p,s}\delta}{P_h t_h} \text{ [mm}^3\text{/kJ]}. \quad (2)$$

Traditionally in thermal straightening round heating spots (in thin-wall ( $\delta \leq 5$  mm) structures) or heating strips (in big-thickness structures) are used. It is considered that long heating strips ( $L \geq 50\delta$ ) are more efficient (approximately 4 times) in straightening, but they have higher risk of local loss of the sheet stability during heating [1, 4]. Such shapes of heating in thermal straightening as heating over spiral and over ring are also known, but they are rarely used in practice.

For investigation of TSE of thin-wall structures using heating spots of different shapes, the 2D calculation model of the heating spot in a plate of a limited size with fixed or free over the boundary edges was used, assuming presence of the plane stressed state. In order to exclude influence of the plate edges, heating spots were arranged at different distance from them.

Problem of thermoplasticity was solved using the Prandtl–Rice theory of plastic flow, associated by the Mises condition of fluidity. Temperature and mechanical problems were viewed sequentially in time --- from beginning of heating up to full cooling of the metal. At each stage of monitoring a linearized problem was solved using method of finite elements. Physical non-linearity was implemented by means of

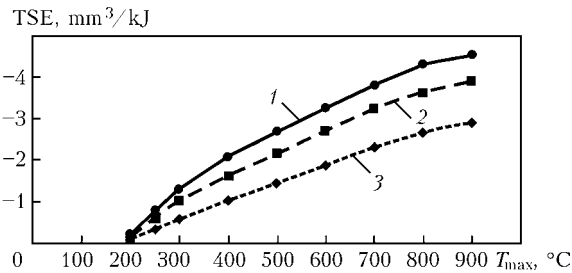


**Figure 1.** Dependence of TSE of St3 steel using heating spots of diameter  $d = 10$  mm upon maximum temperature of heating  $T_{max}$  at different time of heating prior to it: 1 —  $t_h = 5$ ; 2 — 10; 3 — 30 s

iterations [5]. As a material of a thin-sheet structure the St3 low-carbon steel was selected, whereby the calculation model took into account dependence of physical-mechanical properties of the material upon temperature.

For assessment of TSE (1), (2) area of residual plastic strains in plane of the sheet was determined by integration of respective components of plastic strains over area of the sheet:

$$F_{p,s} = \iint \epsilon_{xx}\epsilon_{yy} dx dy \text{ [mm}^2\text{]}. \quad (3)$$

The calculation model also could take into account process of local loss of the metal sheet stability during heating of the spot. For this purpose the developed approach was used, in particular, loss of stability (buckling) takes place within a rather big area, where temperature compression stresses occur. For assessment of critical state, in which loss of stability occurs, the approximate energy method was used [6, 7]. According to this method, risk of loss of stability in a certain arbitrary area is determined by sign of the sum

$$E = U + W, \quad (4)$$

where  $U$  is the potential bend energy;  $W$  is the work of welding stresses. If  $E < 0$ , risk of stability loss is rather high. Influence of initial bending flexure of the sheet surface was not taken into account in assessment of the critical state. All presented below calculation results are obtained for such parameters of heating, which should not cause local loss of stability of a metal sheet of respective thickness and are accessible for thermal straightening.

The calculation results, presented in Figure 1, confirmed well known from the practice fact that TSE sharply increases by means of growth of the maximum heating temperature. However, heating of steels above  $650^\circ\text{C}$  may cause undesirable change of the metal structure and degradation of its mechanical properties. That's why heating of steels at TSE is limited by temperature  $600\text{--}650^\circ\text{C}$ .

The calculation results, presented in Figures 1 and 2, show that TSE depends upon time of the spot heating up to maximum temperature: the shorter is the time, the higher is TSE. This means that for TSE increase a powerful heating source is needed which,

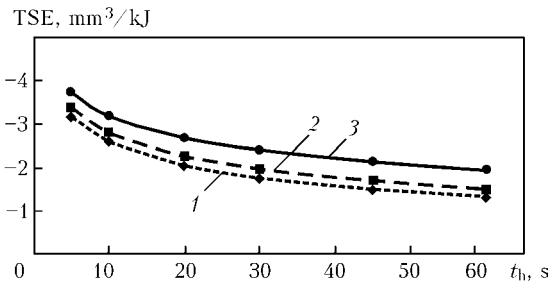


**Figure 2.** Dependence of TSE of St3 steel using round heating spots of different diameter upon time of heating up to  $T_{max} = 625^\circ\text{C}$ : 1 —  $d = 6$ ; 2 — 10; 3 — 20 mm

however, should not cause melting of the sheet surface.

As one may see from Figure 2, TSE may be increased by increase of the heating spot diameter, whereby it is necessary to take into account that by means of its increase probability of local loss of stability (buckling) of the metal sheet at its heating gets higher. That's why maximum diameter of the heating spot for a certain thickness of a sheet should be selected in such way that local loss of stability not to occur. In Figure 3 data, taken from [4], about recommended diameters of the heating spot up to  $600^\circ\text{C}$  are presented, as well as data, obtained in [3], concerning maximum diameters of heating spots at which local loss of stability still does not occur. The calculated data match well experimental data if assumption is made that in case of increase of the metal sheet thickness, time of the spot heating up to the maximum temperature gets longer as well. One may see from Figure 3 that maximum diameter of the heating spot gets bigger by means of increase of the metal sheet thickness and reduction of the time of heating up to the maximum temperature.

So, due to reduction of time of heating up to the maximum temperature and increase of diameter of the round heating spot up to the maximum possible one it is possible to increase without local loss of stability TSE using round heating spots approximately 2 times in comparison with parameters of heating that are usually used in gas-flame heating.

Heating strips in thermal straightening may be produced by a stationary distributed or a moving concentrated source of heating. In first case heating is performed simultaneously over the whole length of

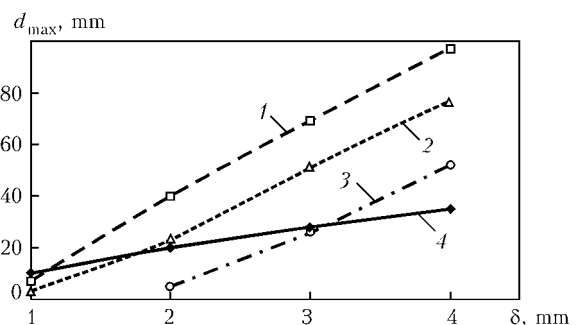


**Figure 3.** Dependence of maximum diameter  $d_{max}$  of heating spots, at which local loss of stability does not occur, upon thickness  $\delta$  of St3 steel sheet at different time of heating up to  $T_{max} = 600^\circ\text{C}$ : 1 —  $t_h = 10$ ; 2 — 30; 3 — 60 s; 4 — data of [4]

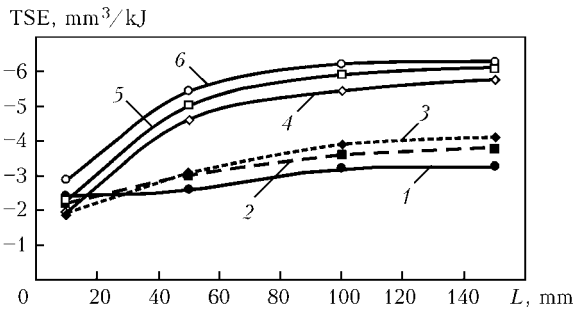


**Figure 4.** Dependence of TSE of St3 steel upon length  $L$  of heating strip of 10 mm width in case of use of distributed heating source at different time of heating up to  $T_{max} = 625\text{ }^{\circ}\text{C}$  and speed of movable source of heating: 1–3 — the same as in Figure 3; 4 —  $v = 1.12$ ; 5 — 2.5; 6 — 5.0 mm/s

the strip. Example of such heating source is equipment for thermal straightening of ship-building structures of Norwegian company «Thermex» which works on basis of induction heating. Traditionally used heating of the strip by a gas-flame torch is performed using a moving concentrated source of heating.

In Figure 4 calculation data of the TSE dependence upon length of the heating strip are presented. TSE in case of a moving source of heating is significantly (1.5–2 times) higher than in case of a distributed one. As far as the data were obtained for the heating strip of 10 mm width, calculation points at length of the strip 10 mm approximately correspond to the round heating spot. It is easy to draw conclusion that at transition from the round spot to the heating strip and by means of increase of length of the latter, TSE gets significantly higher and at a certain length of the strip gets constant. In case of heating of a long strip, TSE is approximately 2 times higher than in case of a round spot, time of heating up to the maximum temperature with application of a distributed source of heating being the same, and 3 times higher at equal power of heating in case of using a movable source.

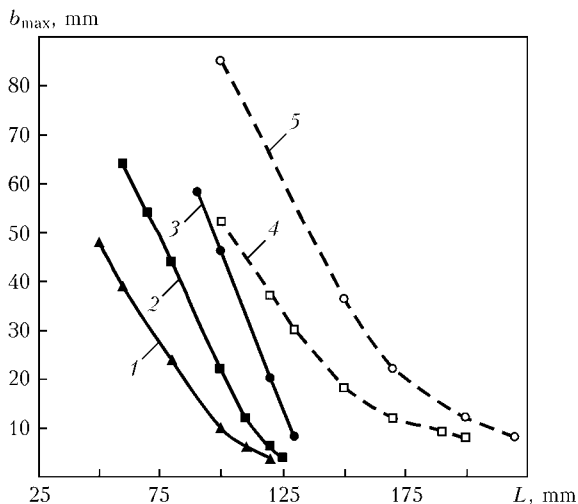


**Figure 5.** Dependence of maximum width  $b_{max}$  of heating strip (at immovable heating source), at which local loss of stability does not occur, upon its length  $L$  at different thickness of metal sheet and time of heating up to  $T_{max} = 600\text{ }^{\circ}\text{C}$ : 1 —  $\delta = 3$  ( $t_h = 10$  s); 2, 4 — 4 (respectively 30 and 10 s); 3, 5 — 5 mm (respectively 60 and 30 s)

One more difference of the heating strip from a round heating spot is observed. At reduction of the time of heating up to the maximum temperature using round spots TSE increases, while in case of using strips heated by a distributed source it reduces (see crossing of lines in Figure 4) at transition from a round spot to the heating strip in case of a distributed source of heating.

So, widely used at present in thermal straightening gas-flame heating with application of long strips and a moving torch is rather efficient, i.e. parameters of heating of long strips are sufficiently optimal for producing maximum residual plastic shrinkage strains. This is confirmed by existing opinion that TSE in case of using long heating strips is significantly higher than in case of using round spots. Results of this computational investigation showed that TSE with application of long strips, heated by a moving source, may be increased due to increase of speed of movement of the heating source, maximum heating being the same, i.e. due to increased power of the concentrated source.

It is known that long heating strips have higher propensity to local loss of the metal sheet stability during heating than round spots. The calculation data were obtained concerning change of maximum width of the heating strips (an immovable source), when local loss of stability still did not occur, depending upon their length, thickness of the St3 steel sheet and time of heating up to  $T_{max} = 600\text{ }^{\circ}\text{C}$  (Figure 5). The data, obtained for steel sheets of small thickness (3, 4 and 5 mm), explain the fact that for such thickness heating with application of strips with an immovable heating source, i.e. simultaneous heating over the whole length of the strip, for example, with application of induction heating, is not used. One may see that at minimal (10–20 mm) width of the heating strip its maximal length at real time of heating 30 s ( $\delta = 4$  mm) and 60 s ( $\delta = 5$  mm) is not more than 100 mm.

Usually at small thickness of a steel sheet heating using strips is performed by a movable source, for example, a gas-flame torch. For heating of strips using a movable source the calculation data were obtained (Figure 6) that demonstrate dependence of maximum length of the heating strip at its assigned width upon speed of the source movement. One may see from the Figure that the higher is maximal speed of the movement, the bigger is maximal possible length of the

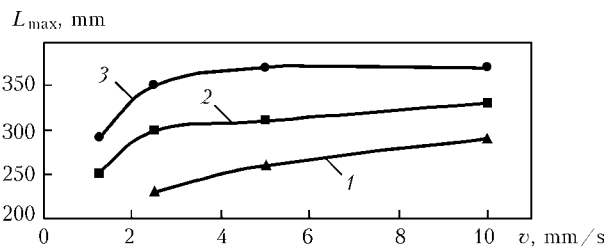


**Figure 6.** Dependence of maximum length  $L_{max}$  of heating strip, at which local loss of stability does not occur, upon speed of movement  $v$  of heating source at  $\delta = 3$  mm and  $b = 20$  mm (1),  $\delta = 4$  and  $b = 30$  (2),  $\delta = 5$  and  $b = 40$  mm (3)

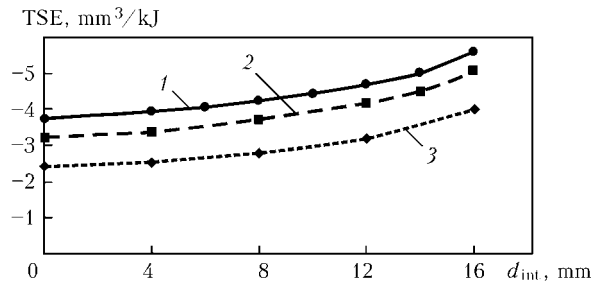


**Figure 7.** Dependence of TSE of St3 steel at heating using rings with external diameter 20 mm upon internal diameter of rings at time of heating up to  $T_{max} = 625\text{ }^{\circ}\text{C}$ ,  $t_h = 5$  (1), 10 (2) and 30 (3) s

heating strip. This is explained by reduction of running energy of heating by means of the source speed increase for achievement of the assigned maximum temperature. In comparison with an immovable distributed heating source, it is possible to heat significantly longer strips without hazard of their stability loss using a moving source. So, at the metal thickness 3 mm it is possible to heat using a distributed source strips of 20 mm width and maximum length 80 mm within time of heating up to maximum temperature 10 s, while using a movable source it is possible to increase length of the strips up to 280 mm at speed of the heating source movement 10 mm/s. The calculation showed that at the metal thickness 3 mm and width of the heating strip 10 mm its length in case of using a movable source of heating is not limited at any speed of its movement. Similar results were obtained for the metal of 4 and 5 mm thickness at width of the heating strips 20 and 25 mm respectively. These calculation data match well recommended values of width of the heated strips (at which a casing usually does not lose stability), obtained on basis of big volume of experimental works in shock-free straightening of structures at ship-building plants [4].

It is rather difficult to implement annular heating in practice, whereby it is characterized by high efficiency. In Figure 7 the calculated TSE data are presented for heating spots in the form of rings with external diameter 20 mm at different internal diameters of the ring and time of heating up to the maximum temperature. Calculated points at internal diameter of the ring  $d_{int} = 0$  correspond to the cases of heating using a round spot. It is easy to see that at transition from a round spot to the ring of heating and then at reduction of the ring width, TSE noticeably increases, whereby similar to the case with a round spot, reduction of the time of heating up to the maximum temperature enables significant increase of TSE.

Like in case of heating with application of a long strip, TSE is higher when a moving over the ring source of heating is used (Figure 8) than in case of application of a distributed source of heating. Increase of TSE is especially noticeable at big width of the ring. By means of reduction of its external diameter and rate of heating TSE diminishes.

The calculations, carried out proceeding from the risk of local loss of the metal sheet stability at heating, showed that values of maximum external radii of the

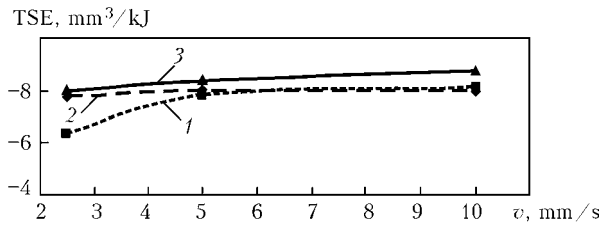


**Figure 8.** Dependence of TSE upon speed of movement of heating source over ring at thickness of metal sheet 3 mm and different external  $d_{ext}$  and internal  $d_{int}$  diameters of rings ( $T_{max} = 625\text{ }^{\circ}\text{C}$ ): 1 —  $d_{ext} = 20$  mm,  $d_{int} = 15$  mm; 2 —  $d_{ext} = 30$ ,  $d_{int} = 20$ ; 3 —  $d_{ext} = 30$ ,  $d_{int} = 25$

heating rings, at which does not occurs local loss of stability, depend insignificantly upon width of the ring and correspond to calculated values of maximum radii of the round heating spots (see Figure 3). So, heating over the ring is a promising method in case of its implementation using state-of-the-art heating sources (for example, laser ones).

In practice in case of a spherical shape of the buckling deformation of a casing specialists recommend to perform straightening using local heating over a spiral [8]. In order to assess TSE at such heating, calculations of heating of a sheet from a low-carbon steel of 3 mm thickness were carried out. A movable source with different width of heating ( $b = 5$  and 10 mm) moved at a speed 2.5, 5 and 10 mm/s over trajectory in the form of a spiral with the pitch, value of which also varied ( $h = 10$  and 30 mm). Maximum temperature of heating was 625 °C. Results of the calculation (Figure 9) demonstrate high TSE values, which get higher by means of increase of the heating source speed, reduction of the heating width, and increase of the spiral pitch. However, the calculations showed that risk of local loss of stability of the sheet metal at heating over spiral is rather high, especially if number of the spiral turns is more than two-three. It was determined that risk of stability loss reduces in case of increase of the heating source speed and reduction of the spiral pitch. So, performing straightening of buckling using local heating over a spiral, it is advisable to increase speed of the heating source which simultaneously increases TSE and reduces risk of local loss of the metal sheet stability.

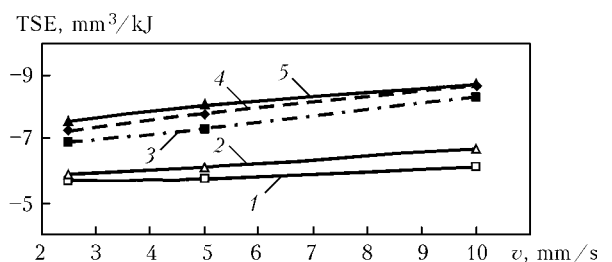


**Figure 9.** Dependence of TSE upon speed of movement  $v$  of heating source over spiral at thickness of metal sheet 3 mm and different values of width  $b$  of heating and pitch  $h$  of spiral ( $T_{max} = 625\text{ }^{\circ}\text{C}$ ): 1 —  $b = 10$  mm,  $h = 10$  mm; 2 —  $b = 10$ ,  $h = 10$ ; 3 —  $b = 5$ ,  $h = 10$ ; 4 —  $b = 5$ ,  $h = 20$ ; 5 —  $b = 5$ ,  $h = 30$



## CONCLUSIONS

1. TSE may be increased approximately 2 times, in comparison with heating parameters used at present in gas-flame heating, and approach TSE values using long strips and a distributed heat source due to reduction of time of heating up to the maximum temperature and increase of diameter of the round heating spot up to the maximum possible one without occurrence of local loss of stability of the metal sheet.

2. As far as at heating with application of long strips and a movable source of heating TSE values are significantly (1.5–2 times) higher than in case of using a distributed source, widely used at present gas-flame heating is sufficiently efficient. TSE in case of using a movable source of heating may be increased both due to increase of its speed, i.e. increase of its power, and reduction of the heating strip width. In case of using a distributed heating source on the opposite — increase of the heating rate (reduction of time of the strip heating up to the maximum temperature) and reduction of the strip width causes reduction of TSE, whereby in case of a movable source it is possible to heat much longer strips without hazard of local loss of the metal sheet stability.

3. At heating of a spot in the form of a ring it is possible to reach due to increase of external diameter and reduction of the ring width high TSE values both using a distributed and a movable source of heating, whereby in case of heating using the rings the TSE values are comparable with efficiency of straightening using long strips with a movable source of heating.

1. Mikhajlov, V.S. (1972) *Straightening of ship welded hull structures*. Leningrad: Sudostroenie.
2. Matsui, S. (1982) Prevention of welding deformations in thin-skin welded structures. *J. Light Metal Welding & Construction*, 20(1), 3–11.
3. Paton, B.E., Lobanov, L.M., Tsybulkin, G.A. et al. (2003) Automated thermal straightening of welded thin-sheet structures. *The Paton Welding J.*, 7, 2–6.
4. Kuzminov, S.A. (1974) *Welded strains of ship hull structures*. Leningrad: Sudostroenie.
5. Makhnenko, V.I. (1976) *Calculation methods of study of welding stress and strain kinetics*. Kiev: Naukova Dumka.
6. Volmir, A.S. (1967) *Stability of deformable systems*. Moscow: Nauka.
7. Makhnenko, V.I., Barvinko, A.Yu., Barvinko, Yu.P. et al. (2002) Estimation of stressed state of the wall of coiled vertical cylindrical tanks in welding-in of insert plates. *The Paton Welding J.*, 5, 2–6.
8. Zaikin, V.M. (1984) Calculation of smooth thermal straightening of welded structures of aluminium-magnesium alloys. *Automatich. Svarka*, 6, 62–66.

# INFLUENCE OF OXIDE FILM MACROINCLUSIONS ON THE STRENGTH OF WELDS IN PLATE JOINTS OF AMg6 ALLOY

A.G. POKLYATSKY

E.O. Paton Electric Welding Institute, NASU, Kiev, Ukraine

Effect of oxide film macroinclusions on mechanical properties of welds made on aluminium alloy AMg6 6–12 mm thick by TIG welding in argon atmosphere has been investigated. Dependencies of strength of the welds on surface area of such defects escaping to the surface on the side of penetration and located inside the weld have been derived. The relationships can be used to estimate the admissibility of oxide film macroinclusions in the welds in fabrication of welded structures.

**Keywords:** argon-arc welding, nonconsumable electrode, AMg6 aluminium alloy, oxide film macroinclusions, ultimate tensile strength, defect length

In fabrication of critical welded structures from aluminium alloys a considerable part of welds are made by nonconsumable electrode argon-arc (TIG) welding. This welding process allows producing sound welds with a smooth face surface, smooth transition to the base metal, without undercuts, overlaps or spatter. Strength of butt joints of AMg6 alloy 6–12 mm thick produced by single-pass TIG welding in argon is equal to 95 or 75 % of that of the base metal in the annealed or work-hardened condition, respectively [1, 2]. However, in fabrication of large-sized welded structures

oxide film macroinclusions quite often form in welds, because of violation of the requirements to preparation of the edges being welded, accuracy of their assembly and fixing, as well as change of the technological parameters of welding [3]. Presence of such defects may lead to lowering of the mechanical properties of welded joints [4, 5].

The purpose of this work is determination of the extent of the influence of oxide film macroinclusions on the strength of welds made by TIG welding in argon on aluminium alloy AMg6 of 6–12 mm thickness.

Butt joints made on sheets of aluminium alloy AMg6 of 400 × 200 mm size by automatic single-pass TIG welding at the speed of 12 m/h using filler wire SvAMg6 of 2.5 mm diameter were studied. The arc



was powered from test power source I-160 developed at PWI. This source allows independent adjustment of duration  $\tau_{SP}$ ,  $\tau_{RP}$  and amplitude  $I_{SP}$ ,  $I_{RP}$  of current of straight and reverse polarity, respectively. Material of 6 mm thickness was welded by symmetrical current ( $I_{SP} = I_{RP} = 360$  A;  $\tau_{SP} = \tau_{RP} = 10.4$  ms). Current of asymmetric amplitude ( $I_{SP} = 780$  A,  $I_{RP} = 440$  A) was used in welding 12 mm thick metal to ensure the required resistance of the nonconsumable electrode (yttriated tungsten rod of 10 mm diameter). For a guaranteed formation of oxide film macroinclusions in the welds the butts were assembled with a fixed gap (1.2 mm at sheet thickness of 6 mm and 1.6 mm at sheet thickness of 12 mm) between the edges [6]. Before welding the sheets and welding wire were subjected to chemical etching by the generally accepted technology. To obtain defects in welds of a large area, part of butt joints were welded without preliminary mechanical scraping of the surfaces and end faces of the edges being welded.

The obtained joints were used to make standard samples to determine the ultimate strength of weld metal. To have the samples fail through the weld in the point of defect location, the reinforcement and penetration were removed flush with the base metal. At sample testing under static tension, actual load  $P$ , at which fracture occurred, was recorded. Weld cross-sectional area,  $F_w$ , was measured on the sample before its testing to determine ultimate strength of weld metal. After sample fracture the area of oxide film macroinclusions  $F_{o,f}$  was determined in weld fractures using MBS-2 microscope. All the defects by the nature of their location in the welds were divided into open (located on the surface from the penetration side) and closed (located inside the weld) (Figure 1). Relative area  $F_{o,f}/F_w$  of macroinclusions was determined separately for each defect group. Average values of the indices obtained from testing 10–15 samples were used for calculations.

In order to clarify to what extent such macroinclusions behave as stress raisers at tension of samples 6 mm thick, we calculated the area of the weld working section  $F_{w,s} = F_w - F_{o,f}$  without allowing for the defect area. Then, proceeding from the ultimate strength of sound welds, load value  $P_c$  was calculated, at which sound samples with different area of weld cross-section would fail. In addition, impact toughness and bend angle of welds, the metal of which contains oxide film macroinclusions, were assessed on individual samples.

Analysis of sample fracture showed that in most of the cases oxide film macroinclusions are located in the lower (root) part of the weld, which is equal to approximately 25 % of welded metal thickness. All of them have different shape and extent, but by their appearance they may be conditionally divided into two groups — thin (0.30–0.45 mm) extended (Figure 1, *a*) and concentrated, close to a triangular shape (Figure 1, *b*). As a rule, after removal of weld reinforcement, the main quantity of such defects turns out to be open and can be readily detected visually.

A small part of the defects remain inside the weld and X-ray or ultrasonic testing should be used for a comprehensive evaluation of the quality of welded joints of plate AMg6 alloy produced by TIG welding in argon.

All the oxide film macroinclusions studied using a scanning microscope were very thin (from  $6 \cdot 10^{-4}$  to  $2 \cdot 10^{-2}$  mm) and had different colour shades. The thinnest films are shiny, fragments of metal structure are clearly seen under their surface (Figure 2, *a*). Black-coloured films had greater thickness, and were characterized by brittleness, which is indicated by presence of microcracks in their structure (Figure 2, *b*).

Curves were plotted (Figure 3) to evaluate the influence of oxide film macroinclusions on the strength of welds made by TIG welding on a sheet of AMg6 alloy 6–12 mm thick. Obtained results are indicative of a substantial influence on weld strength of defects of even a small area. Presence of a closed defect which amounts to just 1 % of weld area, lowers its ultimate strength  $\sigma_t$  from 315 to 300 MPa, and that of an open defect of the same area — to 285 MPa. At increase of the relative area of oxide film macroinclusions to 2 % the ultimate strength of welds decreases to 285 MPa at their location inside the weld and to 248 MPa at their coming to the surface. If the relative defect area is equal to 6 % of weld area, then depending on their location the ultimate strength of weld metal may drop by 20–30 %.

Apparently, open defects not only reduce the weld working section, because of absence of a strong adhe-



**Figure 1.** Oxide film macroinclusions in fractures of samples of the metal of welds made by TIG welding in argon on aluminium alloy AMg6 12 mm thick: *a*, *b* — open, thin extended and concentrated; *c* — closed

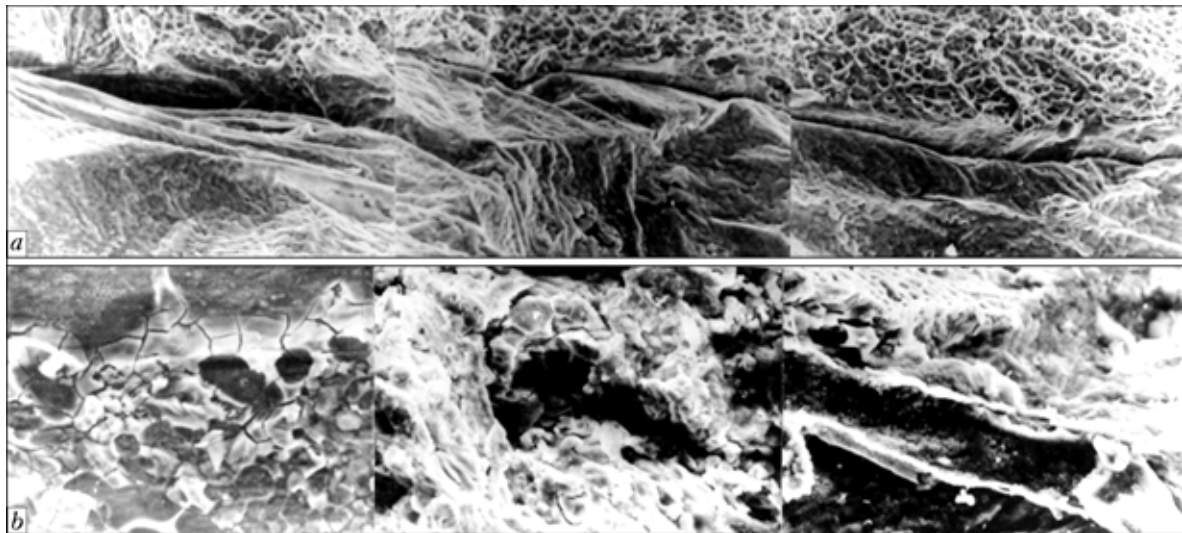


**Figure 2.** Fractograms of fractured weld surfaces, made on AMg6 alloy, in the region of oxide film macroinclusions: *a, b* — see the text (×500)

sion interaction between the surfaces of oxide film macroinclusions and weld metal, but also act as stress raisers at load. This is fully confirmed at comparison of calculated load values, at which sound samples with different cross-sectional area failed, and actual loads, at which defective samples fail (Figure 4). Calculated load values are greater than the actual ones at any defect area, but with its increase the difference between them becomes greater.

Therefore, longitudinal macroinclusions of the oxide film can be the most dangerous for longitudinal welds of cylindrical vessels, circumferential and circular welds of spherical vessels, as in these joints the greatest principal stresses act normal to the weld at loading. In critical welded structures high requirements are made of weld strength. Therefore, proceeding from the purpose and operating conditions, the branch standards and production instructions specify the dimensions of the admissible oxide film macroinclusions in the weld metal.

The length of admissible defects in the welds can be determined proceeding from the derived dependencies (Figure 3). For instance, for a critical structure

ultimate strength of welds on the level of 280 MPa should be ensured. As is seen from the graph, the area of open defects in welds can be equal to approximately 1 % of the sample cross-sectional area, i.e. about 1 mm<sup>2</sup> for 6 mm thick metal. As the maximum depth of location of concentrated defects is not greater than 1/4 of weld height (1.5 mm), and their shape is close to the triangular one, their length on a tested sample should not be more than 1.3 mm. For 12 mm thick metal the cross-sectional area of a tensile testing sample is 300 mm<sup>2</sup>, and, therefore, the admissible area of oxide film macroinclusions is equal to 3 mm<sup>2</sup>, and the maximum defect length is 2 mm. However, thin (0.30–0.45 mm) extended defects amount to approximately half of the total quantity of defects. Assuming such defects to be rectangular, their admissible length for metal samples 6 mm thick should not exceed 3.5 mm, and of those of 12 mm thick metal — 6.7 mm.

Averaging the calculated values of defect length, we establish that in fabrication of structures of AMg6 alloy 6 mm thick the length of the admissible macroinclusions of the oxide film coming to the surface from

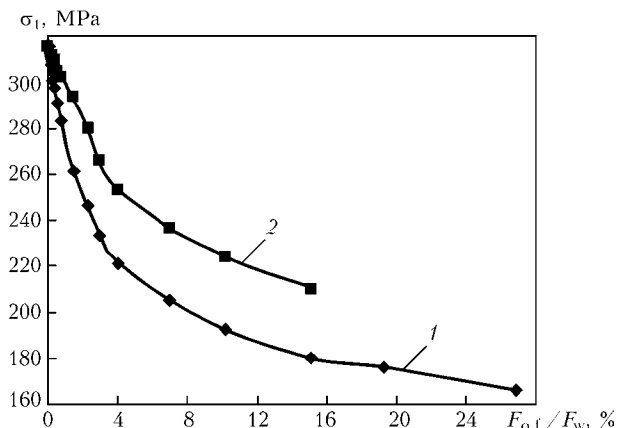


**Figure 3.** Dependence of ultimate strength  $\sigma_1$  of the metal of welds made by TIG welding in argon on aluminium alloy AMg6 6–12 mm thick on relative area of oxide film macroinclusions at open (1) and closed (2) defects

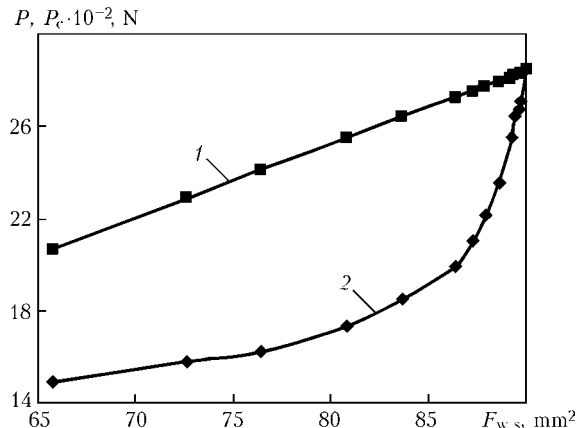


**Figure 4.** Dependence of actual  $P$  (1) and calculated  $P_c$  (2) load leading to fracture of the samples of welds, made by TIG welding in argon on aluminium alloy AMg6 6 mm thick, on the weld working section area  $F_{w,s}$



the penetration side, is equal to 2.4 mm. With increase of the welded metal thickness up to 12 mm, the admissible length of such defects in welds rises up to 4.3 mm.

Obtained results are in agreement with the requirements made by the existing industrial standards to welded joint quality. So, for instance, in fabrication of aerospace casing items of AMg6 alloy presence of not more than 2.5 mm long oxide film macroinclusions at 6 mm thickness of welded metal and not more than 4 mm long ones at welded metal thickness of 12 mm is admissible in the weld. Two times increase of defect length can be allowed for closed defects, as they lower weld strength to a smaller degree.

Impact toughness and bend angle of welds at increase of the area of oxide film macroinclusions decrease more abruptly than their strength. If the strength of welds containing open defects of the area of 1 % of that of the weld, decreases by approximately 10 %, the impact toughness and bend angle of welds containing oxide film macroinclusions of the same area, decrease by approximately 20 %. This is indicative of a higher sensitivity of the above indices to stress concentration under the impact of loads at testing. Therefore, at TIG welding of AMg6 aluminium alloy products it is necessary to provide the required accuracy of preparation, fit-up and fastening of the edges, and also strictly observe the technological parameters of the welding process to avoid formation of oxide film macroinclusions in the weld metal. In the case of subsequent deformation or impact loading of welds during structure fabrication, it is more rational to make them by plasma-arc welding, which allows avoiding formation of defects in the weld root part

characteristic for TIG welding, due to a high concentration of the plasma jet, and ensuring high mechanical properties of welded joints.

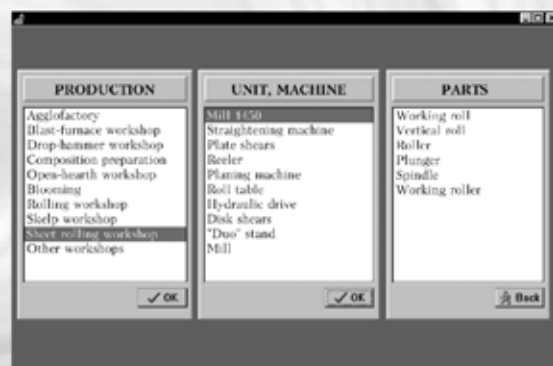
This leads to the conclusion that the oxide film macroinclusions in the weld metal, which are the most characteristic defect in TIG welding of aluminium alloy AMg6, essentially lower the mechanical properties of welds. The most hazardous are the defects coming to the surface on the penetration side, as they not only reduce the weld working section, but also are stress raisers at loading. In the presence of an open defect in the sample which takes up 1 % of the section of a weld made by TIG welding on aluminium alloy AMg6 6–12 mm thick, the ultimate strength of welds decreases by 10 %, and their impact toughness and bend angle --- by 20 %. The derived dependence of ultimate strength on the relative area of oxide film macroinclusions in the weld metal allows determination of the dimensions of admissible defects proceeding from the requirements made of welded structures.

1. Mashin, V.S., Poklyatsky, A.G., Fedorchuk, V.E. (2005) Mechanical properties of aluminium alloys in consumable and nonconsumable electrode arc welding. *The Paton Welding J.*, **9**, 39–45.
2. Rabkin, D.M. (1986) *Metallurgy of fusion welding of aluminium and its alloys*. Kiev: Naukova Dumka.
3. Poklyatsky, A.G. (2001) Peculiarities of formation of macroinclusions of oxide film in weld metal of aluminium alloys (Review). *The Paton Welding J.*, **3**, 36–38.
4. Voropaj, N.M., Manzhelej, G.P. (1969) Detection of oxide inclusions in welds of aluminium alloys. *Avtomatich. Svarka*, **3**, 71–72.
5. Makarov, I.I., Volynsky, V.N., Prokhorov, N.N. (1976) Influence of pores and oxide inclusions on strength of AMg6 alloy welded joints. *Ibid.*, **4**, 27–30.
6. Ishchenko, A.Ya., Poklyatsky, A.G., Yavorskaya, M.R. (1989) Prevention of oxide film inclusions in argon arc welds of aluminium alloys. *Ibid.*, **6**, 38–41.

## COMPUTER SYSTEM TO DESIGN TECHNOLOGIES FOR REPAIR AND HARDENING OF METALLURGICAL EQUIPMENT PARTS

**Purpose.** The system is intended to design technologies for repair and hardening of metallurgical equipment parts by the electric arc surfacing methods. The computer system is based on the experience accumulated by 16 metallurgical plants in the field of surfacing. It allows design of a surfacing technology for 350 different parts (selection of surfacing consumables, methods, conditions, equipment, etc.) at a level of a highly skilled specialist. The system operation result has the form of a process sheet.

**Application.** The system can be used at metallurgical enterprises. It is intended for welding technologists working at a plant engineering department.



Selection of a part to be surfaced

Contacts: Prof. Makhnenko V.I.  
E-mail: d34@paton.kiev.ua



# EFFECT OF PARAMETERS OF MECHANICAL-CHEMICAL SYNTHESIS ON STRUCTURE, PHASE COMPOSITION AND PROPERTIES OF THERMAL SPRAYING Al–Cu–Fe SYSTEM POWDERS CONTAINING QUASI-CRYSTALLINE PHASE

A.L. BORISOVA, Yu.S. BORISOV, L.I. ADEEVA, A.Yu. TUNIK, M.V. KARPETS and A.N. BURLACHENKO  
E.O. Paton Electric Welding Institute, NASU, Kiev, Ukraine

Composite powders containing quasi-crystalline  $\psi$ -phase, along with amorphous and crystalline phases, were produced from a mixture of aluminium, copper and iron powders by the method of mechanical-chemical synthesis. Subsequent annealing at 680 °C for 2 h allows increasing the  $\psi$ -phase content up to 96 %.

**Keywords:** mechanical-chemical synthesis, thermal spraying, Al–Cu–Fe system powders, production methods, quasi-crystalline phase, structure, phase composition

The concept of mechanical alloying (further on called «mechanical-chemical synthesis» — MCS) was suggested in the 1970s by J.S. Benjamin [1, 2]. Mechanical alloying is a solid-phase method of processing powder materials, which includes repeated operations of crushing, bonding and destruction of powder particles with a high-energy ball mill [3–5]. MCS can be used to synthesise various equilibrium and non-equilibrium phases in a mixture of elementary or preliminarily alloyed powders. Non-equilibrium particles synthesised in this way include oversaturated solid solutions, meta-stable crystalline and quasi-crystalline phases, nanostructures and amorphous alloys [3]. In general, the principle of the MCS process is that metal particles

are deformed, cold-worked and crushed between the balls in an attritor. A new juvenile surface formed as a result of destruction of the particles allows their bonding. This leads to increase in size of the particles and formation of conglomerates, which thus acquire a characteristic layered structure consisting of different combinations of initial components (Figure 1, *a*). Crushing is followed by a certain period of equilibrium between the bonding process promoting increase in sizes of the particles and crushing leading to decrease in sizes of the forming powder particles (Figure 1, *b*). The energy transferred to the particles at the moment of collision is partially transformed into the internal energy of molecules. Relaxation of the stored energy may take place in a different manner, including as a result of excitation of chemical reaction.

Occurrence of a chemical reaction during the MCS process is possible because the mechanical energy in collision is transferred for a short period of time ( $1 \cdot 10^{-12} - 1 \cdot 10^{-13}$  s) to the zone of a sub-microscopic contact. Local stresses formed in this case may exceed the energy of a chemical bond, while relaxation of the elastic energy is accompanied by regrouping of atomic bonds, i.e. the chemical event of formation of a new material.

MCS is a promising area in production of thermal spraying powders, and has a number of advantages over traditional methods used to produce such powders, including of the Al–Cu–Fe system, containing the quasi-crystalline phase [3, 6, 7]. Properties and structure of the powders are determined in many respects by their production methods. In our earlier publications [8–10] we analysed different methods for production of quasi-crystalline powders for thermal spraying.

In this study we give results of investigations of the processes employed to produce powders containing the quasi-crystalline phase by solid-phase diffusion in MCS. We studied the effect of parameters of MCS and subsequent heat treatment on phase com-

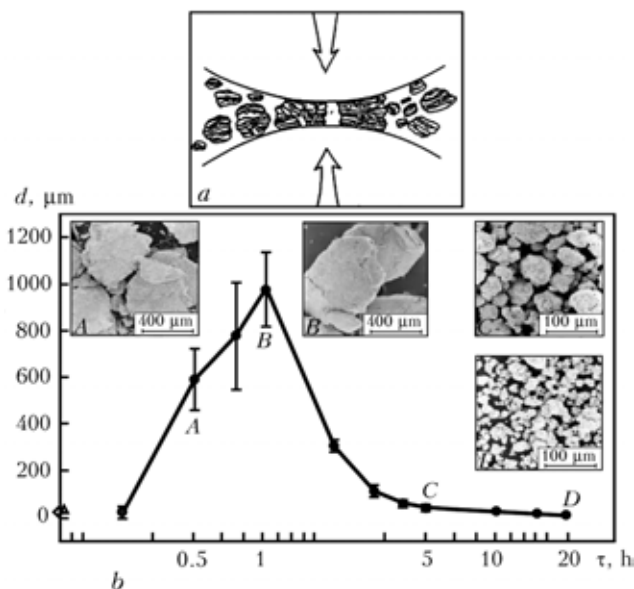


**Figure 1.** Formation of composite particles (*a*) and dynamics of distribution of their size  $d$  during the MCS process (*b*) [3];  $\tau$  — time of crushing

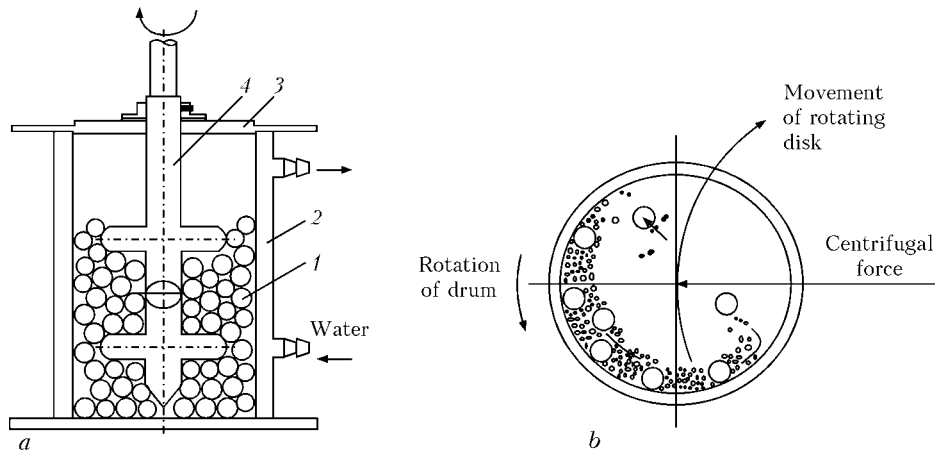


**Figure 2.** Schematic of work chamber of the attritor (*a*) (1 — steel balls; 2 — water-cooled stationary casing; 3 — cover; 4 — mixer) and drum of the planetary-type mill (*b*)

position and structure of the particles produced from the powder mixture close in composition to a region of existence of the quasi-crystalline  $\psi$ -phase [6].

**Experimental procedure.** The MCS process was performed in a laboratory attritor developed and manufactured by the E.O. Paton Electric Welding Institute (Figure 2, *a*), and in a triboreactor (planetary-type mill) manufactured by Closed Joint Stock Company «Aktivator», Novosibirsk, RF (Figure 2, *b*). Rotating mixer of the attritor mixes the balls, thus increasing their kinetic energy to a high level. The speed of rotation of the mixer can be varied in discrete steps from 63 to 960 rpm.

In the triboreactor, the drums with a reaction mixture and grinding balls rotating about their axis at speed  $v_2 = 1500$  rpm are secured to the central axis rotating at speed  $v_1 = 1000$  rpm.

The integrated procedure, including metallography, durometric analysis, scanning electron microscopy and X-ray diffraction phase analysis (XDPA), was used to study initial and synthesised powders. X-ray studies were performed both at room temperature and in heating within the 20–900 °C temperature range by using high-temperature attachment UVD-2000 in a helium atmosphere. The content of the  $\psi$ -phase was determined by the Sordelet's procedure [11]. For this, X-ray patterns were recorded in an angular range of location of the most intensive diffraction maxima of the main phases —  $40 < 2\theta < 50^\circ$ .

To investigate the effect of isothermal annealing on phase composition of the powders produced by MCS, they were placed in a compacted and non-compacted state into a tube furnace purged with argon, and annealed at a temperature of 680 °C for 2 h. Compaction was carried out by using the hydraulic press under a force of 40 kN.

As in the process of milling of powders a certain amount of iron is milled out into the charge as a result of wear of balls and chamber walls, composition of the charge should be constantly checked, so that it does not exceed the limits of existence of the quasi-crystalline  $\psi$ -phase having the icosahedral lattice. According to recommendations [12, 13], the composition of the charge should correspond to the  $\text{Al}_{70}\text{Cu}_{20}\text{Fe}_{10}$

formula, and with addition of an extra amount of iron powder in milling it should be close to the set one ( $\text{Al}_{63}\text{Cu}_{25}\text{Fe}_{12}$ ).

To eliminate adhering of powder to walls of the attritor chamber or planetary-type mill drum, and to facilitate the process of spheroidising of the composite particles formed during MCS, 30 drops of kerosene or 1 wt.% of zinc stearate were added to the charge.

Aluminium, iron and copper powders were used as the initial materials. Specifications of the initial powders are given in Table 1, and morphology of their particles is shown in Figure 3.

**Experimental results.** The MCS process performed at speed  $v_{pr} = 400$  rpm and processing time  $\tau_{pr}$  of up to 10 h results in refining of coarser particles of the powder mixture (aluminium and copper), whereas the fine spherical iron particles are introduced into the formed copper-aluminium composites (Figure 4, *a*). At the same time, at this stage the composite particles are small in number, the fine particles of individual components being dominant.

With increasing the MCS time to 20 h, there comes the equilibrium between the process of crushing of the particles and their bonding, thus leading to formation of composite particles and increase in their size. The major part of the powder mixture consists of the dense composite particles of a primarily rounded shape, 20–40  $\mu\text{m}$  in size (Figure 4, *b*). Spot-like oxide inclusions embedded into the aluminium matrix, along with fine spherical or slightly deformed iron particles, can be detected in structure of the particles.

Increasing the MCS time to 30 h leads to crushing of the particles in adhesion planes and formation of a large number of dispersed composite particles ( $d = 1\text{--}5 \mu\text{m}$ ) with components that are uniformly dis-

**Table 1.** Specifications of initial powders

Powder	Predominant particle size, $\mu\text{m}$	Microhardness $HV_{0.1}$ , MPa
Aluminium	60–80	$830 \pm 50$
Copper	50–80	$960 \pm 200$
Iron	1–3	Attempts to measure failed

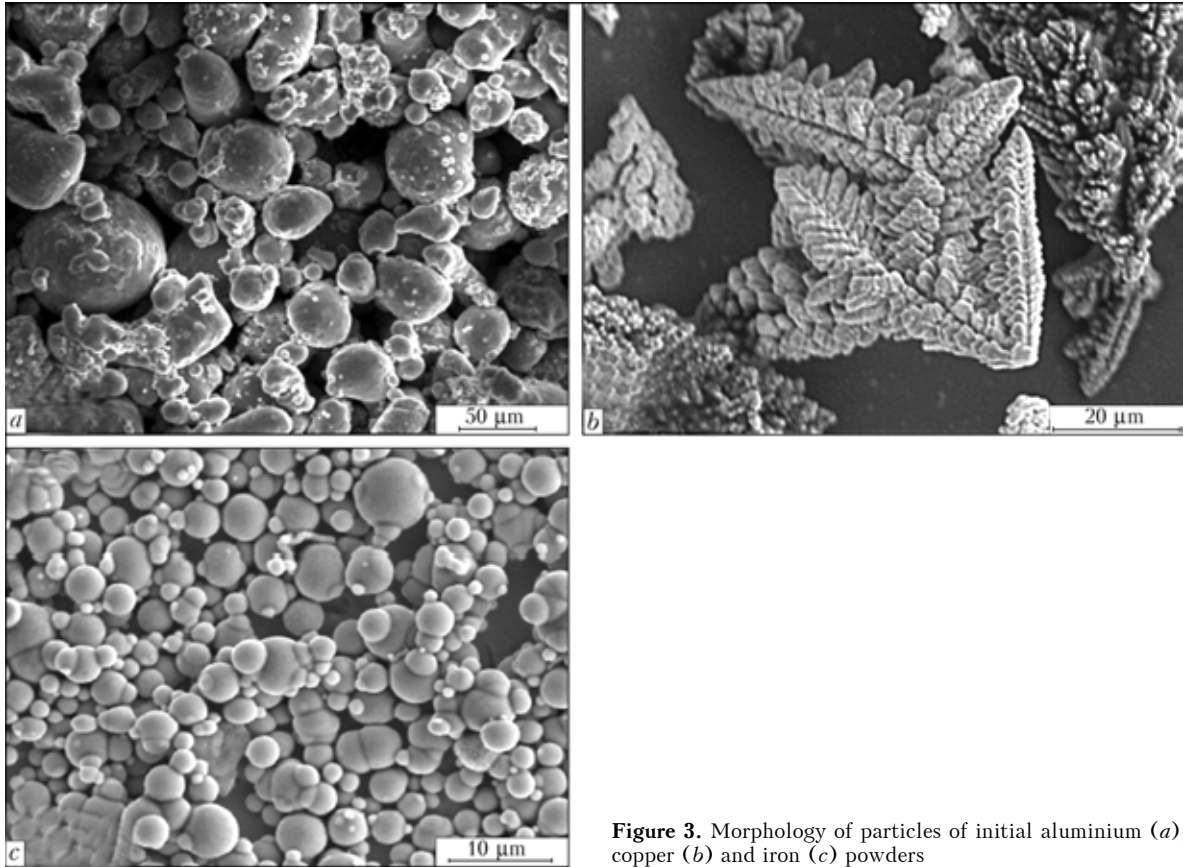


Figure 3. Morphology of particles of initial aluminium (a), copper (b) and iron (c) powders

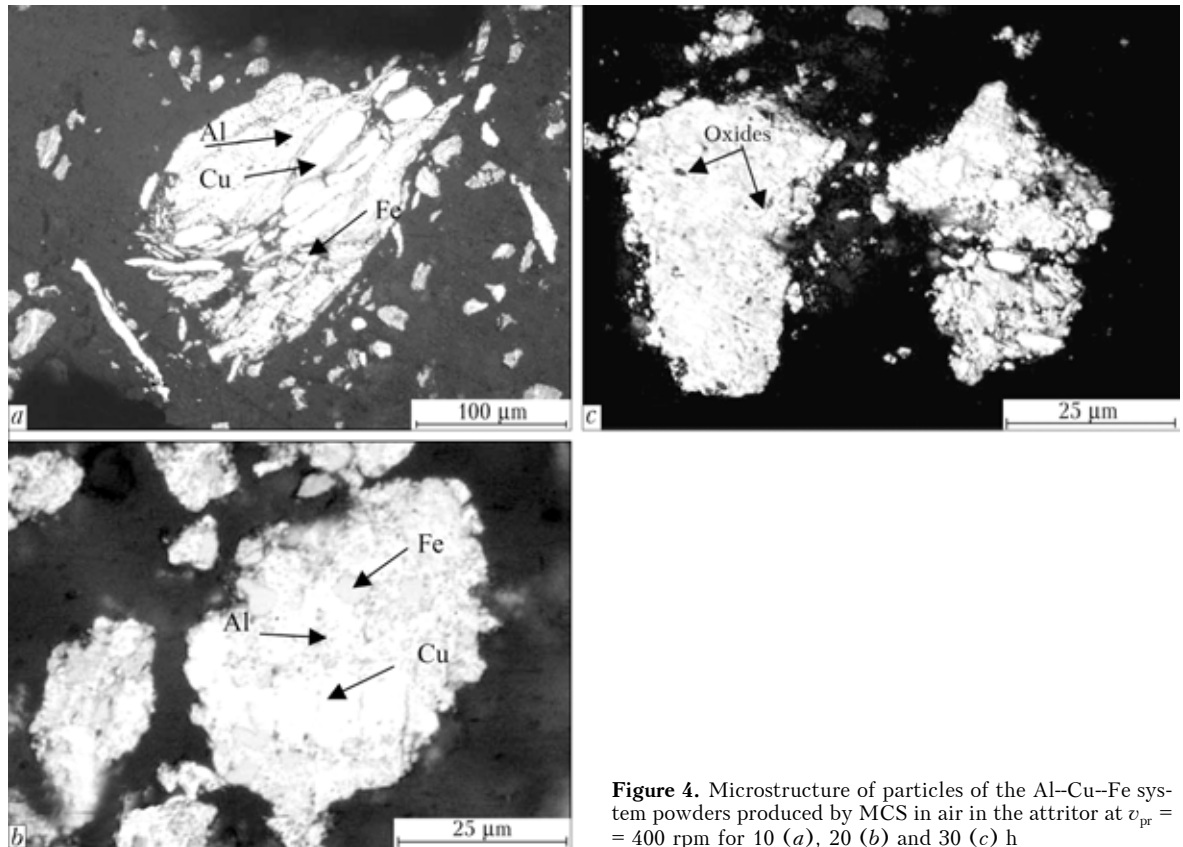


Figure 4. Microstructure of particles of the Al-Cu-Fe system powders produced by MCS in air in the attritor at  $v_{pr} = 400$  rpm for 10 (a), 20 (b) and 30 (c) h



**Table 2.** Specifications of Al-Cu-Fe system powders produced by MCS

No.	MCS conditions			Extra processing	Phase composition	HV 0.25 of particles, MPa
	$v_{pr}$ , rpm	$\tau_{pr}$ , h	Atmosphere			
<b>Attritor</b>						
1	400	10	Air	No	Al, Cu, $\alpha$ -Fe	1430 $\pm$ 110
2		10	Same	Compaction, annealing, crushing	$\beta$ , $\omega$ , $\psi$ , Al, Cu, $\alpha$ -Fe	4700 $\pm$ 1250
3		20	»	No	Al, Cu, $\alpha$ -Fe	3570 $\pm$ 980
4		20	»	Compaction, annealing, crushing	$\beta$ , $\omega$ , $\alpha$ -Fe, $\psi$	5390 $\pm$ 1150
5		30	»	No	Al, $\alpha$ -Fe, Cu	4440 $\pm$ 800
6		30	»	Compaction, annealing, crushing	$\beta$ , $\alpha$ -Fe, $\psi$	6220 $\pm$ 1250
7	960	4	Air	No	Al, Cu, $\alpha$ -Fe	Impossible to measure
8		4	Same	Compaction, annealing, crushing	$\psi$ (95 wt.%), $\beta$ , $\omega$ , $\theta$	6480 $\pm$ 520
9		5	»	No	Al, Cu, $\alpha$ -Fe	2000 $\pm$ 250
10		7	»	Same	Al, Cu, $\alpha$ -Fe	3450 $\pm$ 650
11		10	»	»	Al, Cu, $\alpha$ -Fe	3720 $\pm$ 510
12		15	»	»	Al, Cu, $\alpha$ -Fe, $\beta$ , $\theta$ , traces of oxides	5630 $\pm$ 500
13		20	»	»	Al, Cu, $\alpha$ -Fe, $\beta$ , $\theta$ , traces of oxides	Impossible to measure
14		5	Argon	»	Al, Cu, $\alpha$ -Fe	1920 $\pm$ 270
15		5	Same	Compaction, annealing, crushing	$\psi$ (88 wt.%), $\beta$ , $\omega$ , $\theta$	6040 $\pm$ 700
16		8	»	No	Al, Cu, $\alpha$ -Fe	3520 $\pm$ 540
<b>Planetary-type mill</b>						
17	$v_1 = 1000$ $v_2 = 1500$	0.5	Air	No	Al, Cu, $\alpha$ -Fe	2560 $\pm$ 350
18		1	Same	Same	$\alpha$ -Fe, Al, $\theta$ , Cu	3330 $\pm$ 250
19		1.5	»	»	$\alpha$ -Fe, Al, $\theta$ , $\omega$	3740 $\pm$ 400
20		2.5	»	»	$\beta'$ -, Al, $\theta$ , AP, $\omega$	7400 $\pm$ 600
21		5	»	»	$\beta'$ -, AP, $\psi$ , $\theta$ , $\omega$	4840 $\pm$ 600
22		5	»	Annealing, crushing	$\psi$ (80 wt.%), $\beta$	6620 $\pm$ 1200
23		5	»	Compaction, annealing, crushing	$\psi$ (96 wt.%), $\beta$	6800 $\pm$ 1100

Note. AP --- amorphous phase.

tributed in volume (Figure 4, c). The level of oxidation of the powder mixture particles increases with formation of dispersed oxides both in the form of individual particles and in the form of spot-like inclusions in the aluminium matrix.

As established by using the XDPA method (Table 2, Nos. 1, 2 and 5), the phase composition of the particles after MCS at a processing speed of 400 rpm and time of up to 30 h remains constant, and no new phases form in the Al-Cu-Fe system. It is likely that the oxidation processes taking place in MCS in air atmosphere hamper occurrence of chemical reaction to form the  $\psi$ -phase even at such low temperatures (about 150 °C) in the work chamber. At the same time, X-ray maxima of the initial phases broaden with increase in the crushing time, which is related to increase in internal stresses and decrease in size of the particles and regions of coherent scattering (Figure 5). In addition, growth of the intensity of reflection of iron and simultaneous decrease in the intensity of reflection of aluminium can be seen in the X-ray patterns.

The content of iron in the powder mixture increases because of milling out of balls and chamber walls. Losses of aluminium are attributable to the fact that it partially transforms into aluminium oxide, being most active to oxidation among other components

of the powder mixture. As noted above, the traces of oxides are detected in structure of the particles at a MCS time of 20 h or longer (see Figure 4). Longer processing leads to considerable cold-working and strain-hardening of the powder particles, which is proved by a gradual growth of their microhardness (Figure 6, curve 1).

Increasing the processing speed to 960 rpm allows reducing the MCS time and substantially decreasing the content of oxide inclusions in structure of the composite powder particles. In this case, formation of a layered structure of the particles can be seen as soon as after processing the powder mixture for 5 h, while after 7 h we can see formation of rounded composites consisting of dispersed particles of the initial components with a predominant size of 25–40  $\mu$ m. The powder does not lose its metallic lustre, which is indicative of the absence of oxidation on its surface. The spot-like oxide inclusions in the metal matrix are very rare (Figure 7, a–d; Table 2, Nos. 9 and 10). Intensive oxidation of the powder mixture occurs only in processing for over 10 h (Figure 7, e, f; Table 2, Nos. 12 and 13).

MCS was performed in argon at  $v_{pr} = 960$  rpm to prevent oxidation of the powders. The use of the shielding atmosphere provided absolute elimination of oxidation of the powder particles. After processing



$I$ , rel. un.

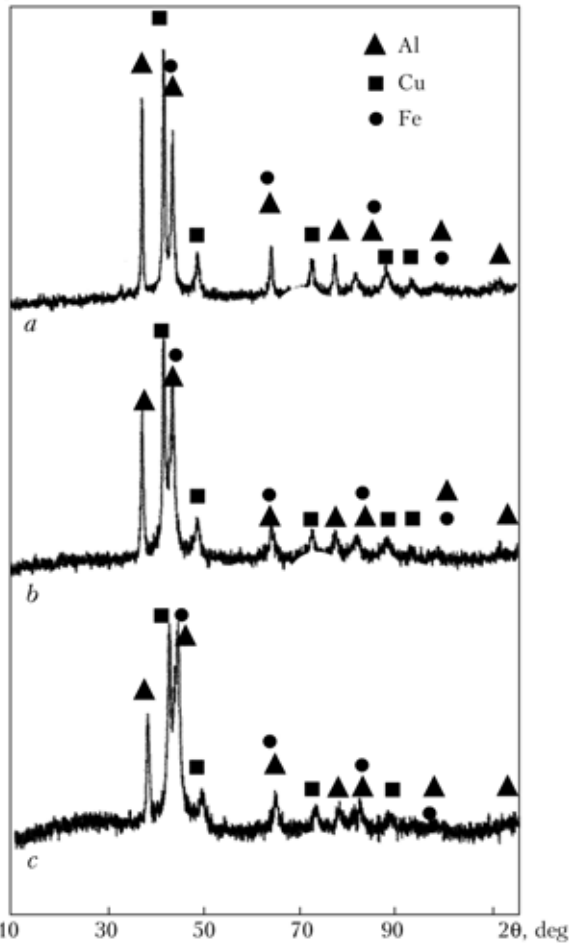


**Figure 5.** X-ray patterns of the Al–Cu–Fe system powders produced by MCS in air in the attritor at  $v_{pr} = 400$  rpm for 10 (a), 20 (b) and 30 (c) h:  $I$  — intensity of reflection of X-rays;  $\theta$  — diffraction angle

for 8 h, the particles acquired mostly the spherical shape, and retained their lustrous surface and structure consisting of dispersed particles of the initial components.

Formation of new crystalline phases of the Al–Cu–Fe system (ternary  $\beta$ -phase with body-centred cubic (bcc) lattice, and  $\theta$ -phase — intermetallic  $Al_2Cu$  with tetragonal lattice) takes place in MCS in the attritor at  $v_{pr} = 960$  rpm and processing time of more than 10 h (Figure 8; Table 2, Nos. 12 and 13). In this case, microhardness of the forming particles dramatically grows (see Figure 6, curve 2).

HV 0.25, MPa

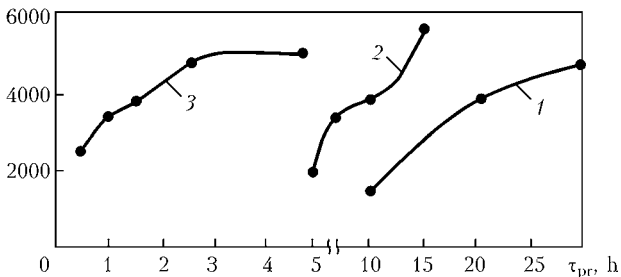


**Figure 6.** Effect of processing time  $\tau_{pr}$  on microhardness of particles of the Al–Cu–Fe system powders produced by MCS in air in the attritor at  $v_{pr} = 400$  (1) and 960 (2) rpm, and in the planetary-type mill at  $v_1 = 1500$  and  $v_2 = 1000$  rpm (3)

Therefore, with a sufficient intensification, the MCS process in the attritor results not only in refining of the initial components, but also in formation of the  $\beta$ -phase particles from them, this phase having bcc parameter  $a = 0.2923\text{--}0.2928$  nm and composition close to that of the quasi-crystalline  $\psi$ -phase [13].

In MCS in the planetary-type mill, the time of solid-phase reactions becomes much shorter, and the effect of oxidation on the formation processes decreases because of high rotation speeds of the drums (Figure 9, Table 2). Synthesis of new phases takes place in processing for 1 h. The XDPA results are indicative of formation of the  $\theta$ -phase (see Table 2, No. 18). In addition to the latter, also the  $\omega$ -phase is formed after 1.5 h, which is the phase of ternary intermetallic  $Al_7Cu_2Fe$  (see Table 2, Nos. 19 and 20). The powder particles are composites consisting of dispersed particles of both initial and new phases.

Starting from the processing time of 2.5 h, MCS results in formation of AP, and after 5 h the amorphous-crystalline structure becomes dominant in the powder mixture. Unlike the previous cases, the cubic  $\beta$ -phase in this structure has a smaller lattice parameter ( $a = 0.2898\text{--}0.2899$  nm) and is designated as a  $\beta'$ -phase (Figure 9, c; Table 2, Nos. 20 and 21). With further mechanical processing of the powders, some of the X-ray reflexes relating to this phase gradually broaden and disappear, while the rest of them shift to a position corresponding to the icosahedral quasi-crystalline  $\psi$ -phase. It is likely that AP also transforms into the quasi-crystalline phase because of formation of clusters, which are characterised by a short-range ordering of the  $\psi$ -phase.

Microhardness of the particles grows from 2560 to 4840 MPa with increase in the processing time from 0.5 to 5 h, the inflections of curve 3 in Figure 6 corresponding to formation of the quasi-crystalline ( $\tau_{pr} = 1$  h) and amorphous ( $\tau_{pr} = 2.5$  h) phases.

Powders of the two types, i.e. produced in the attritor in air at  $v_{pr} = 400$  rpm and  $\tau_{pr} = 30$  h, and produced in the attritor in argon atmosphere at  $v_{pr} = 960$  rpm and  $\tau_{pr} = 8$  h, were investigated by the high-temperature X-ray method to determine temperature limits of phase transformations in the synthesised powders.

The first type of the powder contained no new phases before heating. After heating to 400 °C in the X-ray apparatus chamber in argon, new crystalline phases, i.e.  $\beta$  and  $\theta$ , were revealed in the X-ray pattern, in addition to the  $\alpha$ -Fe phase (Figure 10, a). The  $\omega$ -phase formed instead of the  $\theta$ -phase at a temperature of 650 °C (Figure 10, b), and the quasi-crystalline  $\psi$ -phase formed at 750 °C (Figure 10, c). The phase composition of the powder heated to 750 °C ( $\beta$ -,  $\psi$ - and  $\alpha$ -Fe phases) persists even after cooling to room temperature. The presence of iron in the powder after annealing is related to its excessive content as a result of milling during a long-time (30 h) MCS process.

The second type of the powder, like the first one, contained no new phases in the initial state. At 400 °C

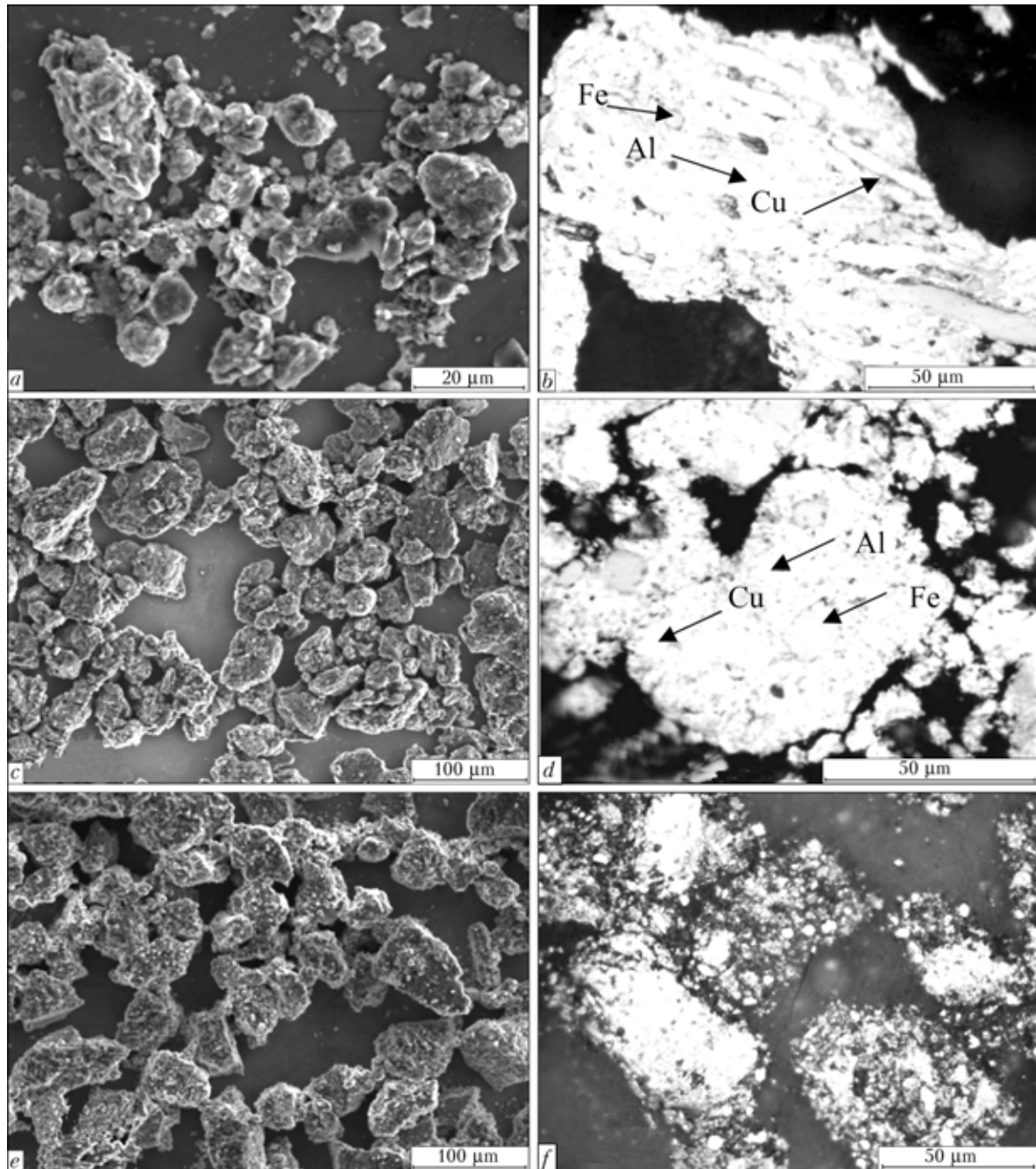


**Figure 7.** Morphology (*a, c, e*) and microstructure (*b, d, f*) of particles of the Al–Cu–Fe system powders produced by MCS in air in the attritor at  $v_{pr} = 960$  rpm for 5 (*a, b*), 7 (*c, d*) and 15 (*e, f*) h

it contained the crystalline  $\theta$ -phase, in addition to the initial components ( $\alpha$ -Fe, Al and Cu). Formation of the  $\psi$ -phase, along with the  $\omega$ - and  $\beta$ -phases, occurred already at a temperature of 650 °C. No X-ray maxima of iron were seen in X-ray patterns both at 650 and 750 °C, this being indicative of a decreasing amount of milled out iron with shortening of the processing time. The powders acquired a two-phase ( $\psi + \beta$ ) composition with predominance of the quasi-crystalline phase after cooling to room temperature.

It is shown in studies [8, 9] how the phase composition of the powders produced by argon or high-pressure water atomisation can be changed almost to a single-phase quasi-crystalline state by heat treatment. In our study we checked the possibility of this

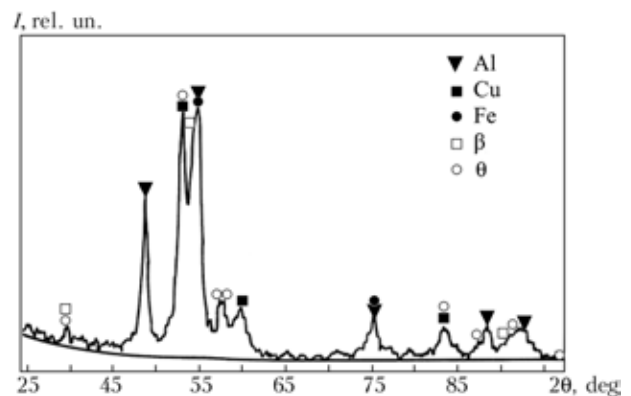


**Figure 8.** X-ray pattern of the Al–Cu–Fe system powder produced by MCS in air in the attritor at  $v_{pr} = 960$  rpm for 15 h

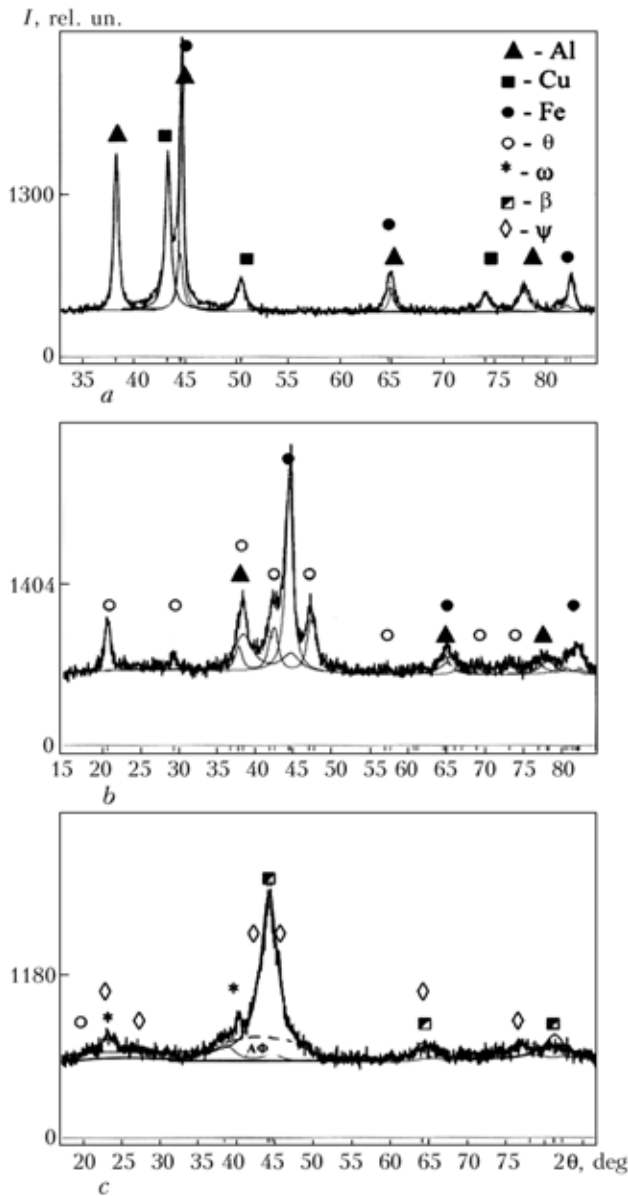


**Figure 9.** X-ray patterns of the Al-Cu-Fe system powders produced by MCS in the planetary-type mill in air for 0.5 (a), 1.5 (b) and 5 (c) h

transformation on powders produced by the MCS method. We established that structure of the particles and phase composition of the powders after heat treatment depend upon the MCS conditions (see Table 2, Nos. 2, 4, 6, 8, 15, 22 and 23).

The powder subjected to MCS at  $v_{pr} = 400$  rpm in air had the densest structure of the particles (Figure 11, a) and highest content of the  $\psi$ -phase after processing for 10 h. The  $\psi$ -phase content decreased with increase in the milling time. Most probably, this was caused by formation of oxides and milling out of iron.

Annealing of powders subjected to MCS at a higher rotation speed and shorter milling time can provide a higher content of the  $\psi$ -phase in the annealed material.

As a result of annealing of the powder produced by MCS in air in the attritor at a rotation speed of 960 rpm and  $\tau_{pr} = 4$  h, because of interaction its par-

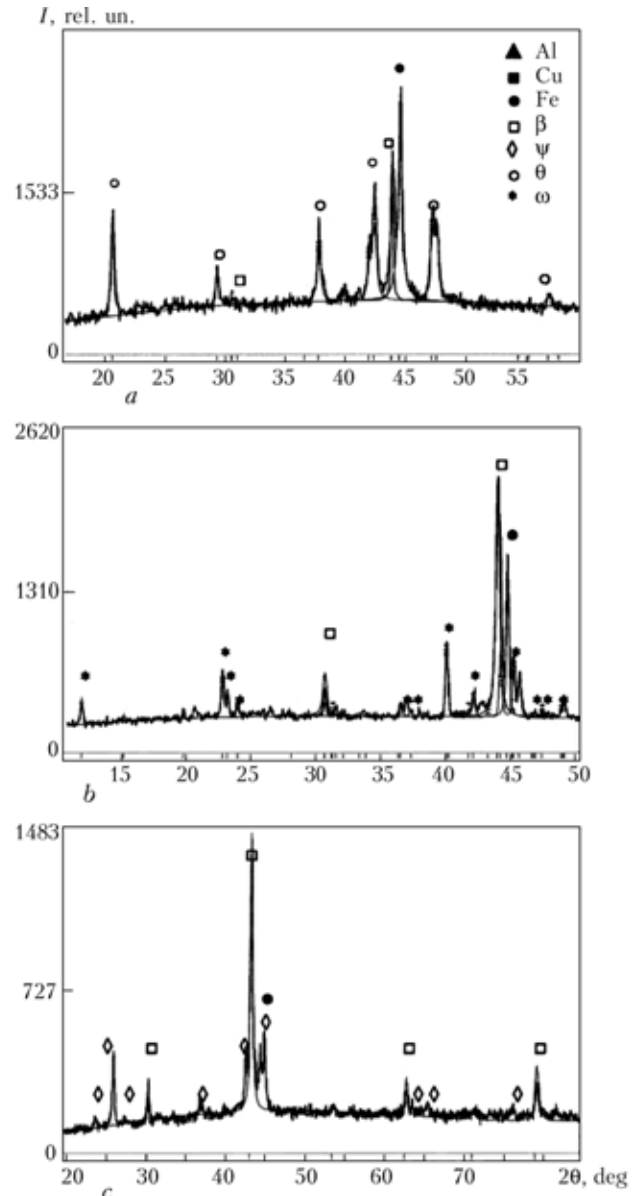


**Figure 10.** X-ray patterns of the Al-Cu-Fe system powders produced by MCS in air in the attritor at a speed of 400 rpm for 30 h, after heating to 400 (a), 650 (b) and 750 (c) °C

ticles consisting of the initial components acquired an almost single-phase quasi-crystalline structure with small admixtures of crystalline  $\beta$ -,  $\omega$ - and  $\theta$ -phases (Figure 11, b; Table 2, No. 8). Microhardness  $HV 0.25$  of the particles after heat treatment was  $(6480 \pm 520)$  MPa.

The  $\psi$ -phase content was 88 wt.% after annealing of the powders produced by MCS in argon in the attritor at the same processing speed and  $\tau_{pr} = 5$  h (Table 2, No. 15). In this case, the powder particles had a denser structure, as the MCS process in the shielding atmosphere caused no oxidation of the particle surfaces, this leading to a more complete solid-phase reactions occurring between them.

Annealing of the powders produced by MCS in the planetary-type mill in air for 5 h results in formation of a two-phase structure ( $\psi$ -phase with an admixture of the  $\beta$ -phase) (see Table 2, Nos. 22 and 23). The powders compacted before annealing contained

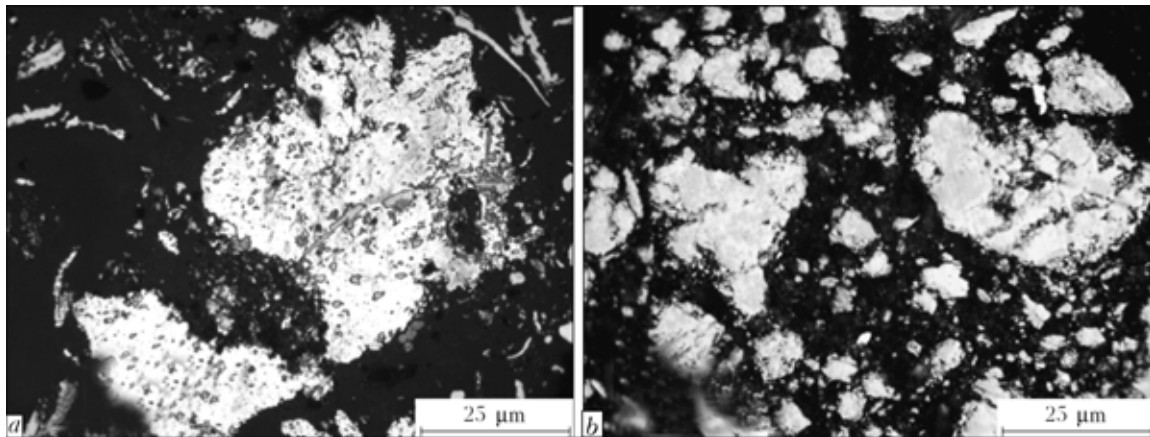


**Figure 11.** Microstructure of heat-treated particles of the Al-Cu-Fe system powders produced by MCS in air in the attritor at  $v_{pr} = 400$  rpm for 10 h (a), and at  $v_{pr} = 960$  rpm for 4 h (b)

96 wt.% of the quasi-crystalline phase, and those which were not compacted contained 80 wt.% of this phase, microhardness of the powders being  $HV 0.25 (6800 \pm 1100)$  and  $HV 0.25 (6620 \pm 1200)$  MPa, respectively. The  $\psi$ -phase content and microhardness of the particles were higher in the case of the compacting operation performed before annealing.

Investigation of behaviour of the synthesised powders under the plasma spraying conditions showed that phase transformations occurring in particles under the effect of the plasma jet were identical to those taking place in heat treatment. Short-time but intensive heating results in the processes of phase interactions taking place between the mixture components (aluminium, copper and iron) activated by MCS to form the  $\beta$ - and  $\psi$ -phases, as well as the formation of coatings containing the quasi-crystalline phase.

Therefore, the high-energy MCS process provides the possibility of producing powders with the non-equilibrium, including quasi-crystalline, structure. As shown by the investigation results, it is necessary to perform annealing of the powder mixture in argon at a temperature of 600–700 °C to provide a more complete phase formation of quasi-crystals and ordering of the nanocrystalline  $\psi$ -phase. The maximal content (96 wt.%) of the  $\psi$ -phase takes place in MCS performed in the planetary-type mill at  $v_1 = 1000$  and

$v_2 = 1500$  rpm, and subsequent annealing of the compacted powders at 680 °C for 2 h.

1. Arunachalam, V.S. (1990) Mechanical alloying. In: *Current problems of powder metallurgy*. Moscow: Metallurgiya.
2. Heinike, G. (1987) *Tribochemistry*. Moscow: Mir.
3. Suryanarayana, C. (2001) Mechanical alloying and milling. *Progress in Mater. Sci.*, **46**, 1–148.
4. Grigorieva, T.F., Barinova, A.P., Lyakhov, N.Z. (2001) Mechanical-chemical synthesis of intermetallic compounds. *Uspekhi Khimii*, **70**(1), 2–19.
5. Polkin, I.S., Borzov, A.B. (1991) Mechanical alloying as a new process of production of materials with abnormal properties. *Tsvet. Metall.*, **12**, 54–56.
6. Barua, P., Murty, B., Srinivas, V. (2001) Mechanical alloying of Al-Cu-Fe elemental powders. *Mater. Sci. and Eng.*, **304–306**, 863–866.
7. Nicula, R., Jianu, A., Grigoriu, C. et al. (2000) Laser ablation synthesis of Al-based icosahedral powders. *Ibid.*, **294–296**, 86–89.
8. Borisova, A.L., Tunik, A.Yu., Adeeva, L.I. (2006) Structure and properties of powders of Al-Cu-Fe system alloy for thermal spraying of quasi-crystalline coatings. *The Paton Welding J.*, **12**, 19–26.
9. Borisov, Yu.S., Panko, M.T., Adeeva, L.I. et al. (2001) Technologies for production and properties of powders of the Al-Cu-Fe system for thermal spraying of coatings with quasi-crystalline structure. *Ibid.*, **1**, 45–50.
10. Borisov, Yu.S., Borisova, A.L., Adeeva, L.I. et al. (2005) Thermal coatings with quasi-crystalline phase, properties and applications (Review). *Fizyka i Khimiya Tsv. Tila*, **6**(1), 124–136.
11. Sordelet, D.J., Besser, M.F., Anderson, I.E. (1996) Particle size effects on chemistry and structure of Al-Cu-Fe quasicrystalline coatings. *J. Thermal Spray Technol.*, **5**(2), 161–174.
12. Salimon, A.I., Korshunsky, A.M., Shelekov, E.V. et al. (2001) Crystallochemical aspects of solid state reactions in mechanically alloyed Al-Cu-Fe quasicrystalline powders. *Acta Mater.*, **49**, 1821–1833.
13. Barud, P., Murty, B.S., Srinivas, V. (2001) Mechanical alloying of Al-Cu-Fe elemental powders. *Mater. Sci. and Eng.*, **304–306**, 95–106.



# INFLUENCE OF ELECTROMAGNETIC TREATMENT ON RESIDUAL WELDING STRESSES IN WELDED JOINTS OF CARBON AND LOW-ALLOYED STEELS

A.K. TSARYUK<sup>1</sup>, V.Yu. SKULSKY<sup>1</sup>, S.I. MORAVETSKY<sup>1</sup> and V.A. SOKIRKO<sup>2</sup>

<sup>1</sup>E.O. Paton Electric Welding Institute, NASU, Kiev, Ukraine

<sup>2</sup>SPC «DS Ltd.», Nikolaev, Ukraine

Results of evaluation of electromagnetic effects on residual welding stresses of the I and II kind are presented. It is shown that application of low-density current pulses to low-carbon steel welded joints had a specific effect on stresses of the I kind, however, it did not lead to their substantial decrease. It is established that treatment leads to increase of the size of blocks, decrease of stresses of the II kind, and increase of the crystalline lattice parameter of weld metal.

**Keywords:** steel, welded joints, heat treatment, electromagnetic impact, electrophysical treatment, deformation, residual welding stresses, stresses of the I kind, stresses of the II kind

Electromagnetic impact (EMI) on a metal body allows deforming it under certain conditions without any external load, or influencing its stress-strain state caused by external load or residual stresses induced by different technological operations [1–6]. In most cases EMI are electric current pulses passing through the studied sample, with the following parameters: current density of  $10^2$ – $10^4$  A/mm<sup>2</sup>, pulse duration of  $10^{-3}$ – $10^{-6}$  s. Considering the wide range of thicknesses and dimensions of the actual welded joints and not unlimited capabilities of the currently available current sources, studying the methods of EMI implementation in welding fabrication is urgent for those of them, which can make an effect at minimum current density. If we are talking about application of these processes for welded joints of ferromagnetic materials, it is rational to look for such kinds and modes of EMI, which would allow using the electromagnetic energy accumulated in the material, i.e. energy of the domain magnetic field [7]. The influence of electrophysical treatment (EPHT) on the mechanical properties of welded joints of carbon and low-alloyed steels was assessed earlier [8]. It is shown that owing to specific EMI, EPHT (pulse time of 1–2 s, pause duration of 5–10 s, duration of the fronts of pulse rise and drop of 0.5–1 s, pulse number per EPHT cycle of ~ 100, ranges of variation of current density in the pulse of 5–16 A/mm<sup>2</sup>) promotes producing a more equilibrium structure of HAZ metal of welded joints in these steels, which is manifested in increase of metal impact toughness. The purpose of this work was evaluation of the influence of EPHT with a low current density on the level of residual welding stresses (RWS) of the I kind and stresses of the II kind in welded joints of steels.

To study the influence of EPHT on the level of RWS of the I kind, samples of 300 × 100 × 8 mm size of welded joints of St2ps (semi-killed) and 20KhMFL steels were made, in which a stressed state was in-

duced, which is characteristic for rectilinear butt single-pass joints. A longitudinal stress component was selected as the criterion of RWS level. In order to determine it, a method of cutting and measurement of residual elastic deformations in measurement bases using a mechanical strain meter was selected [9]. A mechanical strain meter with a clock-type indicator designed at the Welding Fabrication Chair at the NTUU «Kiev Polytechnic Institute» was used in the investigations\*. Strain gauge measurement base was 50 mm, indicator division value was 0.001 mm.

One sample of St2ps and 20KhMFL steels each was left in as-deposited condition, three samples of each steel were processed by EPHT (Figure 1). Parameters of treatment current were assigned and maintained by an automatic control system of DS10D unit: pulse shape is trapezoidal, alternating current amplitude is 4–8 kA, amplitude current duration is 2 s, duration of pulse rise and decrease is 1.5 s, duration of pause between pulses is 10 s. Current parameters correspond to electromagnetic field frequency of 0.2 Hz, which is below the critical value  $f_{cr} \approx 2.5$  Hz, for samples of 8 mm thickness, which eliminates skin-effect. Samples were connected to the unit using four pairs of flexible cables with clamps so that the current would flow along the sample. Sample heating temperature at EPHT was controlled using a batch-produced multimeter of M890G model, fitted with chromel-alumel thermocouple.

During EPHT also the nature of sample deformation (one sample of either steel) was controlled. With this purpose the above samples were treated in air by series of 2–10 current pulses. The strain meter was fixed permanently in the base opening in immediate vicinity of the deposited bead.

The other samples (two of either steel) were treated without controlling the nature of deformation. They were placed into a dielectric tank with water to minimize heating as a result of thermal action of welding current.

Figure 2 shows the nature of sample deformation. Sample deformation is presented in the form of two

\* The authors are grateful to I.M. Zhdanov, Professor of the Welding Fabrication Chair, Cand. of Sci. (Eng.), for his assistance.



components: deformation due to thermal elongation of the sample, and deformation related to electrodynamic processes which are caused by electric current pulses. The first component was always positive and increased with the number of pulses applied to the sample, which is characteristic for thermal elongation. The second component of deformation cannot be associated with temperature deformation, as it changed in synchronism with current pulses. As is seen from Figure 3, deformations are not constant even during a short series of current pulses, which is indicated by the change of the sign and values of the measured base. Total number of pulses applied to the samples, and their maximum temperatures upon completion of EPhT cycle are given in Table 1.

The above-mentioned strain meter was used to evaluate longitudinal RWS. Measured  $\sigma$  values were used to plot the epures (Figure 4). For St2ps steel in as-welded condition the active zone fibres are under tension, the maximum of which is observed in the deposited metal and in its value is commensurate with its yield point. In the case of steel 20KhMFL the stresses in the active zone are somewhat lowered, which is related to  $\gamma \rightarrow \alpha$  transformation, which runs at a comparatively low temperature and partial recovery of elastic properties of the metal of the weld and HAZ. Compressive stresses are active in the reactive zone fibres of both the samples. A certain lack of equilibrium in the epures is attributable to overlooking the RWS transverse component. Thus, the epures of longitudinal RWS in samples of either steel in as-welded condition do not contradict the established concepts and are in normal agreement with the earlier derived experimental data [9].

RWS epures of any of the three samples of St2ps and 20KhMFL steel in as-EPhT condition differ only slightly from the respective epures in as-welded condition. No clear dependence is observed between the quantity of pulses applied during EPhT and the RWS level. EPhT influence turned out to be the most noticeable for samples of 20KhMFL steel. It is reduced to redistribution of longitudinal RWS. In the active zone RWS decrease by 3–25 %, in the reactive zone an increase of RWS by approximately 15 % is ob-

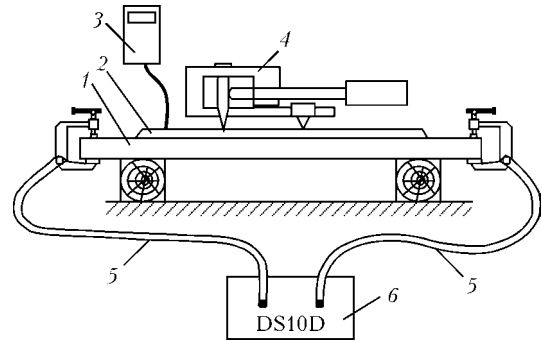


Figure 1. Schematic of conducting EPhT with studying the nature of sample deformation: 1 — treated sample; 2 — weld; 3 — multimeter; 4 — strain meter; 5 — cables; 6 — EPhT unit

served. The same tendencies, but at smaller quantitative values, were noted for samples of St2ps steel. Such an influence can hardly be accounted for by the thermal action of current. Formation of inhomogeneous temperature fields (skin-effect and dynamic pinch-effect) in the sample was eliminated due to the used parameters of current and plate thickness, and any uniform heating should lead to stress lowering in all the points of the sample. Even considering all the errors of measurement of sample metal temperature, one can state that the latter at EPhT did not exceed a value at which water boiling with formation and floating of vapour bubbles starts on the surface of the metal immersed into the water.

The above evaluated stressed state of the welded sample is presented by residual stresses of the I kind, i.e. balanced on the scale of the macroscopic metal body. It is due to the fact that the active zone metal during the thermodeformational deposition cycle went through an incompletely compensated deformation of plastic contraction  $\Delta$ . These stresses can be eliminated by applying along the sample longitudinal axis, a force capable of creating plastic tension in the active zone by a value compensating  $\Delta$ , as it occurs with the mechanical methods of RWS relieving [10]. Considering the features of sample deformation during EPhT, it may be assumed that the revealed redistribution of RWS is caused by action inside the metal of volume forces of electromagnetic origin arising at current pas-

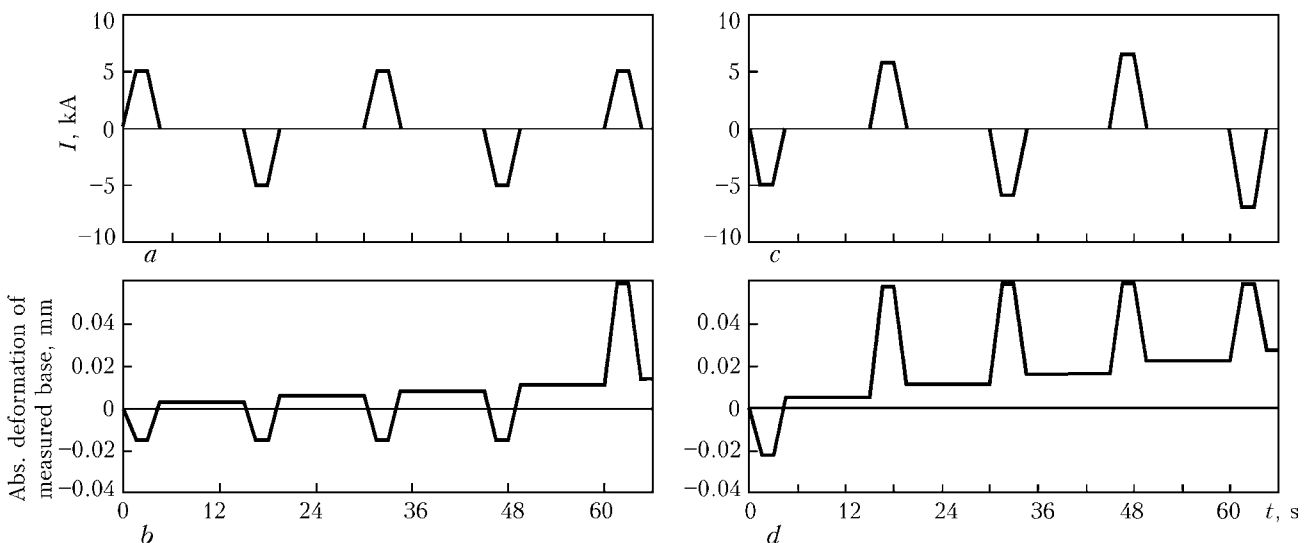
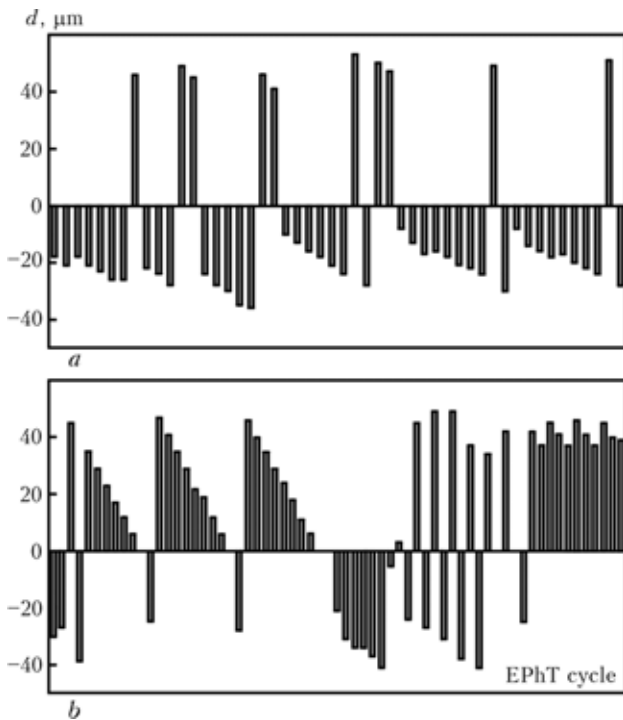


Figure 2. Nature of deformation of an experimental welded sample of St2ps (a, b) and 20KhMFL (c, d) steel



**Figure 3.** Change of electrodynamic component of deformation in an experimental welded sample of St2ps (a) and 20KhMFL (b) steel over a complete EPhT cycle (with subtraction of thermal elongation)

sage through the ferromagnetic. Electrodynamic (force) action of the electromagnetic field can be determined from the expression of a generalized force:  $F_{\eta} = dW/d\eta$ , where  $F_{\eta}$  is the force component;  $W$  is the electromagnetic field energy stored in the considered system volume;  $\eta$  is the generalized coordinate. For a cylindrical sample from a magnetic material a stressed state is induced, which has a compressive radial  $\sigma_r$  and tensile axial  $\sigma_x$  components:

$$\sigma_r = F_r/S = -1/2\mu_0(I/2\pi R)^2 = -1/8\mu_0(jR)^2,$$

$$\sigma_x = F_x/S = 1/4\mu_0\mu(I/2\pi R)^2 = 1/16\mu_0\mu(jR)^2,$$

where  $S$  is the surface to which force  $F_{\eta}$  is applied;  $\mu_0$  is the magnetic permeability of vacuum;  $\mu$  is the relative magnetic permeability of the material;  $I$  is the electric current;  $j$  is the current density;  $R$  is the sample radius.

From ratio  $\sigma_x/\sigma_r = \mu/2$  it follows that for a non-magnetic material ( $\mu = 1$ ) compressive radial mechanical stresses  $\sigma_r$ , and for the ferromagnetic --- tensile longitudinal stresses  $\sigma_x$  prevail, which increase  $\mu$  times (10–10<sup>2</sup> times). Magnetic permeability of the ferromagnetic depends on the intensity of the magnetic field in it. At current increase and respective increase of intensity of the magnetic field induced by this current, magnetic permeability of the material first rises from the initial value  $\mu_{in}$  to maximum value  $\mu_{max}$  due to the internal electromagnetic energy of the domain structure, and then decreases tending to value  $\mu = 1$ . It is exactly at the moment when  $\mu_{max}$  is reached that tensile stresses  $\sigma_x$  increase by an order of magnitude and more.

Stresses  $\sigma_x$  are of a non-polar nature, i.e. are independent on polarity of the flowing current, and allow interpreting the results given in Figure 3. For structural steel parameters and current densities  $j = 6\text{--}16$  A/mm<sup>2</sup> design stress  $\sigma_x$  is equal to 2.1–15.3 MPa. At flowing of the current pulse stress  $\sigma_x$  which is always tensile, interacts with RWS of the samples, which is exactly what leads to redistribution of the resulting stresses. However, the actual value of stresses  $\sigma_x$  and duration of their application are too small for a longitudinal plastic tension of the sample by any significant value during the time of one current pulse. Determination of the conditions necessary and sufficient to achieve the positive effect, is the objective of further studies.

The influence of EPhT on the level of stresses of the II kind in the weld metal of low-carbon steel welded joint was also studied. For this purpose a butt joint on 12 mm steel 20 was welded by multipass manual arc welding with application of UONI-13/55 electrodes. Weld metal contained, wt.%.: 0.085 C; 0.26 Si; 0.58 Mn; 0.13 Ni; 0.07 Cr; 0.019 P; and 0.021 S. Two transverse templates of 36 mm width cut out of the welded joint, were subjected to EPhT in two different modes, selected proceeding from the production experience of SPC «DS Ltd.». Of the remaining parts of the welded joint one was treated by high tempering at the temperature of 650 °C (60 min); and the second --- by annealing at 1060 °C (20 min); the third was left in as-welded condition.

Investigations were conducted using X-ray diffractometer DRON-UM1 on a polished area of 18 ×

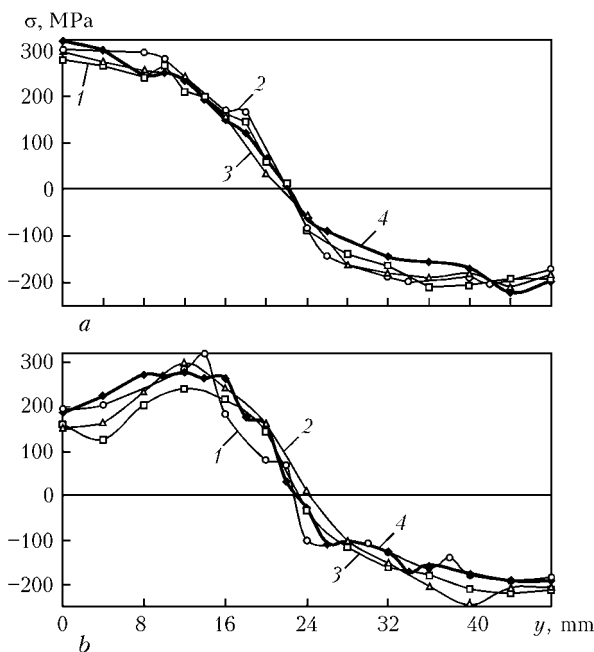


**Figure 4.** Distribution of longitudinal RWS in the cross-section of three samples of St2ps (a) and 20KhMFL (b) steel after EPhT (1–3) against as-welded condition (4)

**Table 1.** Parameters of EPhT of experimental samples

Sample material	Sample #	Total pulse number	Cooling environment	T <sub>max</sub> , °C
St2ps	1	48	Water	65
	2	94		77
	3	50	Air	72
20KhMFL	1	48	Water	65
	2	100		86
	3	65	Air	93



**Table 2.** Results of X-ray diffractometric investigation of deposited metal of steel 20 welded joint

Welded joint condition	Crystalline lattice type ( $a$ , nm)	Size of blocks (areas of coherent scattering), nm	Coefficient characterizing stresses of the II kind
As-welded	96.4 % $\alpha$ -Fe (0.28692); 3.6 % $\gamma$ -Fe (0.36352)	74	0.002
As-tempered (650 °C, 60 min)	$\alpha$ -Fe (0.28691)	78	0.001
As-annealed (1060 °C, 20 min)	$\alpha$ -Fe (0.28681)	97	0.0005
After EPhT by mode 1	$\alpha$ -Fe (0.28697)	127	0.0005
After EPhT by mode 2	$\alpha$ -Fe (0.28704)	135	0.0009

× 18 mm of a microsection containing just the metal of the weld upper passes (Table 2).

Postweld heat treatment (PWHT) brings the weld metal microstructure into a more equilibrium state: the size of blocks reflecting the volume of metal with a relatively perfect lattice increases; level of RWS of the II kind, expressed by the respective coefficient, decreases. With increase of PWHT temperature the noted features are manifested to a greater degree. Thus, the as-welded condition is characterized by the smallest size of the blocks and highest level of RWS, and the as-annealed condition --- by the largest size of the blocks and minimum RWS level.

As is seen from Table 2, EPhT of welded joints also essentially influenced the weld metal microstructure, which is confirmed by changes of diffractometric characteristics. Block size was equal to 127–135 nm, which is by 35 % higher than for annealed metal. EPhT also provided lowering of RWS of the II kind to the level of 0.0005–0.0009.

Metal of a low-carbon weld in as-welded condition contains a small amount of residual austenite. EPhT, similar to PWHT, caused decomposition of the residual  $\gamma$ -phase. Decomposition of quasistable residual austenite in the metal of a low-carbon weld during EPhT is attributable to a change of its magnetic condition, leading to a spontaneous appearance of small single-domain ferromagnetic regions (nuclei) arising and annihilating in a paramagnetic  $\gamma$ -matrix by statistical laws [11], as well as destabilization of the stressed state of comprehensive compression of the austenite regions. In the above-mentioned respect the action of EPhT on the weld metal is similar to PWHT action. On the other hand, the influence of EPhT on  $a$  constant of the crystalline lattice differs from PWHT action. Heat treatment causes a decrease of  $a$  from 0.28692 (after welding) to 0.28681 nm (after annealing), whereas EPhT leads to a noticeable increase of  $a$  to 0.28697–0.28704 nm.

Elementary cell parameter is related to an interatomic spacing corresponding to such a relative position of adjacent atoms, at which the level of potential energy of the system is minimum, whereas the attraction and repulsion forces are equal. The following factors are known from physics of metals, which allow controlling the metal lattice constant: temperature, pressure, stresses of the I kind and alloying. As these conditions were unchanged in all the diffractometric experiments, it is rather difficult to explain the observed influence of EPhT. Among the processes running in steels during PWHT, it is appropriate to mention decomposition of the oversaturated solid solution with new phase precipitation, leading to reduction of

the concentration of interstitial impurities in the solid solution, and, therefore, decrease of  $a$ , which is confirmed experimentally.

Considering the key factors of the influence of low-density electric current and electromagnetic field on the metal microstructure [7, 8], the following cause can be suggested for increase of  $a$  parameter after EPhT. Dislocation slipping (and, possibly, their annihilation), caused by the magnetic field present in the metal at EPhT, led to a more uniform distribution through the volume of  $\alpha$ -phase of interstitial impurity atoms, which were initially concentrated in microsegregational clusters (atmospheres) connected with dislocations. This might have led to increase of the average content of impurities in the solid solution and eventually, caused increase of  $a$  parameter after EPhT. Further research is conducted to provide a more complete explanation of the influence of EPhT on the submicrostructure.

In conclusion it should be noted that EPhT with the selected parameters and technique of performance has a specific influence on the level of RWS of the I kind in welded joints of carbon and low-alloyed steels: in the welded joint active zone RWS decrease by 3–25 %, and in the reactive zone they rise by 0–15 %. EPhT lowers stresses of the II kind to the level, provided by annealing at the temperature of 1060 °C, with a noticeable increase of  $a$  parameter of the crystalline lattice of  $\alpha$ -phase.

1. Golovin, Yu.I., Tyalin, Yu.N., Umrikhin, V.M. (1987) Field of mechanical stresses and strength of cylindrical conductors in pinching electromagnetic fields. In: *Abstr. of 1st All-Union Conf. on Effect of Electromagnetic Fields on Plasticity and Strength of Metals and Alloys* (Yurmala, 29 Sept.–1 Oct. 1987). Moscow: A.A. Blagonravov Institute of Eng. Sci., 37.
2. Strizhalo, V.A., Novogrudsky, L.S., Vorobiov, E.V. (1990) *Strength of alloys of cryogenic engineering under electromagnetic effects*. Kiev: Naukova Dumka.
3. Strizhalo, V.A., Vorobiov, E.V. (2003) Jump-like metal deformation in conditions at pulsed magnetic field and cryogenic temperature impacts. *Problemy Prochnosti*, 1, 137–142.
4. Shcherbakov, I.P., Churaev, D.V., Svetlov, V.N. (2004) Study of submicrorelief change of copper specimen surface in passing of high density electric current pulses through them. *Zhurnal Tekhn. Fiziki*, 74(4), 139–142.
5. Lobanov, L.M., Pashchin, N.A., Skulsky, V.Yu. et al. (2006) Influence of electrodynamic treatment on the stress-strain state of heat-resistant steels. *The Paton Welding J.*, 5, 8–11.
6. Lobanov, L.M., Pashchin, N.A., Loginov, V.P. et al. (2007) Change of the stress-strain state of welded joints of aluminium alloy AMg6 after electrodynamic treatment. *Ibid.*, 6, 7–14.
7. Moravetsky, S.I., Parshenkov, N.A., Sokirko, V.A. (2007) Features of electromagnetic impacts on the metals and their welded joints (Review). *Ibid.*, 6, 14–19.
8. Tsaryuk, A.K., Skulsky, V.Yu., Moravetsky, S.I. et al. (2008) Change of mechanical properties of welded joints of carbon and low-alloyed steels at electromagnetic impact. *Ibid.*, 7, 27–30.
9. Vinokurov, V.A. (1973) *Stress relaxation tempering of welded structures*. Moscow: Mashinostroenie.
10. Kasatkin, B.S., Prokhorenko, V.M., Chertov, I.M. (1987) *Stresses and strains in welding*. Kiev: Vyscha Shkola.
11. Bernshejtn, M.L., Pustovojt, V.N. (1987) *Heat treatment of steel products in magnetic field*. Moscow: Mashinostroenie.

# APPLICATION OF 10KhSNDA, 15KhSNDA ROLLED STOCK IN METAL STRUCTURES OF THE RAILWAY-ROAD BRIDGE ACROSS THE DNEIPER RIVER IN KIEV

V.A. KOVTUNENKO, A.M. GERASIMENKO, V.A. ZADOROZHNY and V.V. RYNDICH  
E.O. Paton Electric Welding Institute, NASU, Kiev, Ukraine

Steel rolled stock used for fabrication of critical building metal structures and bridges has been analyzed. Steels 10KhSNDA and 15KhSNDA according to TU 14-1-5120-92 developed on the basis of 10KhSND and 15KhSND steel (GOST 6713) widely applied in bridge construction, are considered. Problems of application of these steels for construction of the railway-road bridge across the Dnieper River in Kiev are outlined.

**Keywords:** bridge construction, metal structures, steel rolled stock, microalloying, arc welding technologies and modes, welding consumables, welded joint properties

Development of bridge construction is directly related to improvement of steel rolled stock quality. Table 1 gives the data on the use of steels for rolled metal elements in the load-carrying metal span structures according to standard DBN B.2.3-14:2006 «Bridges and pipes. Design rules».

Steels of 10KhSND, 15KhSND grades (GOST 6713) are the most often used in the local bridge building. The alloying base of such steels, are such elements as carbon, silicon, manganese, chromium, nickel and copper. Arc welding modes and technologies and consumables providing the required properties of the welded joints, have been optimized for them. Steel 09G2S (GOST 19281) is rather widely accepted for building metal structures.

Modern requirements to materials for critical metal structures are met by new generation steels — high-strength sparsely alloyed steels 06GBD, 06G2B (C355-490, TU U 27.1-05416923-085:2006), 09G2SYuCh (C325-390, TU U 322-16-127). These steels differ from those usually used in the local metal structures by sparse alloying, high reliability, cold resistance, and good weldability. However in practice of local bridge building predominantly low-alloyed steels with the yield point of up to 350 MPa are used.

Steels 10KhSND of 390 strength class, and 15KhSND of 345 strength class provide high strength properties at a considerable alloying with deficit chromium and nickel.

The main standard regulating the requirements to rolled stock for bridge structures is GOST 6713. It envisages specifying the strength, ductile properties and toughness characteristics. However, it does not guarantee brittle fracture resistance of the metal at negative temperatures by the results of impact toughness testing of samples with a sharp notch (*KCV*). GOST 19281 standard guarantees Charpy (*KCV*) impact toughness of steels 10KhSND, 15KhSND not

lower than 40 J/cm<sup>2</sup> only at temperatures of 0 and -20 °C.

09G2S rolled sheets of C345 strength class have lower values of the yield point and ultimate tensile strength compared to 10KhSND, 15KhSND steels. Impact toughness of the rolled stock on a sample with a *KCV* sharp notch is specified by GOST 19281 standard at not lower than 40 J/cm<sup>2</sup> (testing temperature is 0, -20 °C).

06GBD, 06G2BD rolled stock of strength classes C355-490 to TU U 27.1-05416923-085:2006 has the following *KCV* impact toughness values: at -20 °C — 98 J/cm<sup>2</sup>, at -40 °C — 78 J/cm<sup>2</sup> and at -60 °C — 59 J/cm<sup>2</sup>, respectively. Steels are supplied with guaranteed values of the strength and ductile properties in the direction of the thickness, as well as guaranteed provision of the continuity of rolled plates not lower than continuity class 1, 2 to GOST 27727.

Construction of a road bridge across the entrance to the Harbour of the Podol bridge in Kiev can be an example of application of new generation steels in bridge metal structures. These engineering facilities are interesting in that rolled sheets of two different steel grades of the same strength class C390, namely 10KhSND-2 (GOST 6713) and 06GBD (TU U 27.1-05416923-085:2006) were used in the main metal welded structures (main beams) for the first time in local bridge construction.

The project of the railway-road bridge across the Dnieper River in Kiev (OJSC «Transmost», St.-Petersburg) allows application of 10KhSNDA and 15KhSNDA rolled stock to TU 14-1-5120-92 with modification #6.

In Ukraine 10KhSNDA and 15KhSNDA rolled stock was not applied in the road and railway bridge span structures and it is not mentioned in the standards.

In Russia these steels are not included into SNiP 2.05.03-84\*. Their application in bridges is performed in keeping with the letter of RF Ministry of Construction #13/2 of 04.01.95. This resulted in certain dif-


**Table 1.** List of steels for elements from rolled metal according to DBN B.2.3-14:2006 «Bridges and pipes. Design rules»

Steel grade	Strength class	Rolled stock thickness (mm), incl.		GOST, TU	Additional requirements
		Plate	Shaped		
16D	235	Up to 20		GOST 6713	–
16D	225	21–40		GOST 6713	As in note 3 to Table 1*, 1.14, 1.16
16D	215	41–60		GOST 6713	
15KhSND	345	8–15		GOST 6713	
15KhSND	335	16–50; 16–32		GOST 6713	
10KhSND	390	8–15		GOST 6713	
10KhSND-2	390	8–40	8–15	GOST 6713	It. 2.2.1, 2.2.2, 2.2.3, 2.2.6, 2.2.9, 2.2.11, 2.3 to GOST 19281 Continuity class 1, 2 to GOST 22727
15KhSND-12	345	Up to 32	Up to 10	GOST 19281	
10KhSND-12	390	Up to 40	Up to 15	GOST 19281	Continuity class 1, 2 to GOST 22727
14G2AFD	390	Up to 50	--	GOST 19281	
15G2AFDps	390	Up to 32	--	GOST 19281	
09G2D-12	295D	Up to 32	Up to 20	GOST 19281	
09G2SD-12	295D	21–32		GOST 19281	
09G2SD-12	325D	Above 10 -- up to 20		GOST 19281	
09G2D-12	325D	Up to 10	--	GOST 19281	
09G2SYuCh-2	325	8–50	--	TU U 322-16-127	
09G2SYuCh-2	355	8–50	--	TU U 322-16-127	
09G2SYuCh-3	390	8–50	--	TU U 322-16-127	
E36	355	8–50	--	GOST 5521	
E40	390	8–40	--	GOST 5521	
06GBD	355	8–50	--	TU U 27.1-05416923-085:2006	
06GBD	390	8–50	--	TU U 27.1-05416923-085:2006	
06G2BD	440	8–50	--	TU U 27.1-05416923-085:2006	
06G2BD	490	8–50	--	TU U 27.1-05416923-085:2006	

difficulties for application of this rolled stock in construction of the bridge.

E.O. Paton Electric Welding Institute performed analysis of the data on the properties of rolled stock and welded joints of bridge structures from 10KhSND and 15KhSND steels [1–4].

Rolled stock from 10KhSND and 15KhSND steels is supplied by «Uralskaya Stal Ltd.» to TU 14-1-5120–92 with modification #6. Compared to steels for bridge construction to GOST 6713 these steels are characterized by more cost-effective alloying system, as well as strictly specified requirements on impurity content. Steel composition was modified towards lowering the content of nickel and chromium, sulphur and phosphorus (Table 2). Values of carbon equivalent  $C_{eq}$  of the developed steels compared to steels to GOST 6713 are as follows: for 10KhSND steel --- 0.39–0.52; 15KhSND --- 0.34–0.48; 10KhSND --- 0.35–0.49; 15KhSND --- 0.31–0.49 ( $C_{eq}$  is determined by the following IIW formula:

$$C_{eq} = C + \frac{Mn}{6} + \frac{Cr + Mo + V}{5} + \frac{Ni + Cu}{15}$$

Technical conditions TU 14-1-5120–92 with modification #6 guarantee supply of 10KhSND and 15KhSND rolled stock with not lower than 29 J/cm<sup>2</sup> impact toughness at testing temperature of –40 °C on notched Charpy samples (*KCV*), ensuring the class of rolled

stock continuity 1, 2 to GOST 22727, as well control of the set of properties in Z-direction.

The main point of difference of 10KhSND and 15KhSND steels is presence of strong carbide-forming elements of vanadium and niobium in their composition, which allowed simultaneous improvement of strength properties by the dispersion hardening mechanism and of ductility properties by refining the final ferrite-pearlite structure.

The possibility of improvement of the strength properties allowed reducing the content of carbon, chromium, and nickel, which strengthen the steel by the solid solution mechanism. It was taken into account that minimum content of nickel, chromium, and copper should provide a sufficient resistance to atmospheric corrosion and together with carbon and manganese provide the required degree of stability of over-cooled austenite at heat treatment [3]. This circumstance in combination with special modes of rolling and heat treatment allowed improvement of the rolled sheet properties.

In [3] it is shown that compared to steels to GOST 6713, 15KhSND and 10KhSND rolled stock has higher ductile characteristics and impact toughness at an equal level of strength properties. The cold brittleness threshold of steels in the normalized condition is equal to –70 and –60 °C, respectively. Tensile testing of the rolled stock in Z-direction showed a prac-

**Table 2.** Composition of 10KhSND, 15KhSND, 10KhSNDA and 15KhSNDA steels, wt.%

Steel grade	C	Si	Mn	Cu	Cr	Ni	S	P	V	Nb
10KhSND (GOST 6713)	Up to 0.12	0.80–1.10	0.50–0.80	0.40–0.60	0.60–0.90	0.50–0.80	0.035	0.035	--	--
15KhSND (GOST 6713)	0.12–0.18	0.40–0.70	0.40–0.70	0.20–0.40	0.60–0.90	0.30–0.60	0.035	0.035	--	--
10KhSNDA (TU 14-1-5120-92 with modification #6)	≤ 0.12	0.80–1.10	0.65–0.95	0.40–0.60	0.30–0.60	0.20–0.50	≤ 0.010	≤ 0.015	0.08–0.12	0.03–0.06
15KhSNDA (TU 14-1-5120-92 with modification #6)	0.10–0.15	0.40–0.70	0.60–0.90	0.20–0.40	0.30–0.60	0.20–0.50	≤ 0.010	≤ 0.015	0.08–0.12	0.03–0.06

*Note.* In all the steels N is not more than 0.008 %.

tically same level of strength and ductile properties both in the rolling plane and across the thickness.

Change of composition resulted in the change of metallurgical processes and phase transformations running in the weld pool and near-weld zone. This resulted in the need to look for optimum technologies of welding bridge structures from these steels, both in the shop and in the site conditions [1].

Investigations showed that rolled stock from 10KhSNDA and 15KhSNDA steels has a sufficient margin of welding and technological characteristics [4]. However, in welding of micro-alloyed steels transition of niobium, vanadium, as well as their nitrides and carbonitrides into the deposited metal, can promote and increase of the deposited metal hardness and adversely affect the impact toughness and temperature of weld metal transition into a brittle state.

In [1] site welded joints of these steels were studied and it was established that the metal of the weld and different zones of welded joints of 10KhSNDA and 15KhSNDA steels has the required characteristics of strength and ductility on the level of base metal properties. However, welded joints 12 mm thick of 10KhSNDA and 15KhSNDA steels made by single- and two-pass submerged-arc welding from one side turned out to be sensitive to low-temperature embrittlement, particularly along the fusion line. Embrittlement at testing temperature of  $-60^{\circ}\text{C}$  was more pronounced in the joints made in winter ( $-15 - 20^{\circ}\text{C}$ ). Normalizing with tempering after welding, as well as multilayer filling of the weld, prevent low-temperature embrittlement, except for the fusion zone of the last pass, where a higher sensitivity to low-temperature shock is preserved.

In order to determine the causes for lowering of the cold resistance of welded joints on 10KhSNDA and 15KhSNDA steels, microstructures of the sections cut out of butt joints made with different heat inputs were studied [1].

Microstructural studies of welded joints of 10KhSNDA and 15KhSNDA steels made at a higher heat input showed coarser grain in the near-weld zone. Acicular arrangement of ferrite in the pearlite grain

body is indicative of overheating and Widmanstaetten structure formation. Structure examination in a microscope revealed inclusions of different shapes and dimensions, predominantly in the ferrite grain bulk. Microchemical analysis of the zone recorded presence of carbonitride inclusions of niobium, vanadium and other compounds of metal and non-metal origin in it [1, 5].

According to the performed research [1, 5], welding at higher heat inputs of 10KhSNDA and 15KhSNDA steels microalloyed by niobium and vanadium, leads to a long-term stay of the weld and HAZ metals in the high-temperature range (above  $1300^{\circ}\text{C}$ ). This accounts for a more complete dissolution of carbides and other niobium and vanadium compounds in austenite, austenite grain growth, carbon diffusion from the base metal into the deposited metal and melt saturation by phosphorus from the welding consumables. Subsequent cooling leads to formation of an unfavourable Widmanstaetten structure, precipitation of vanadium and niobium carbonitrides from the austenite and melt, which promote [5–8] local distortion of the crystalline cells of ferrite, lowering of dislocation mobility, particularly at negative temperatures, and, consequently, slowing down of the slip process at deformations. Here, lowering of the metal cold resistance is affected by increased phosphorus content in the fusion zone, and Widmanstaetten structure with ferrite laths and needles in the pearlite grain body, forming in welding of site welds under the conditions of accelerated cooling of a highly overheated steel [1].

Experimental data were the basis to develop the modes of welding at lower heat inputs and parameters of edge preparation of site joints in bridge structures of 10KhSNDA and 15KhSNDA steels providing cold resistance and equivalent strength of the joints.

By the statement of the Ministry of Construction of Russia 10KhSNDA, 15KhSNDA rolled stock (TU 14-1-5120-92 with modification #6) with not more than 0.010 % S, not more than 0.015 % P and not less than 50 % of fibrous structure in the fracture, can be used in road-bridge structures.

**Table 3.** Performance of rolled stock of 10KhSNDA and 15KhSNDA steels

Steel grade to TU 14-1-5120-92	Rolled stock thickness, mm	Mechanical properties			$KCU, J/cm^2$ , at temperature, °C			Bend angle, deg	Fraction of fibrous structure in the fracture, %
		$\sigma_t$ , MPa	$\sigma_y$ , MPa	$\delta_5$ , %	-60	-20	20 (after mechanical ageing)		
10KhSNDA	12	568–574	429	27.0–30.0	135–159	147–162	148–160	120	100
10KhSNDA	16	565–567	370–386	27.0–27.3	60–85	62–74	90–125	120	100
15KhSNDA	16	528–532	370–377	26.6–29.3	160–207	168–200	174–217	120	95–98
10KhSNDA	20	558–569	359–397	28.8–35.8	200–209	198–205	209–222	120	97–100
10KhSNDA	32	593–605	400–405	27.0–37.0	161–230	170–218	213–237	120	95–100

Performance of in-coming control of the mechanical properties, impact toughness on samples with a sharp notch ( $KCV$ ) at the temperature of  $-40$  °C and metal structure in the fracture of each rolled stock batch in keeping with the specification requirements is mandatory.

In case of structure fabrication and assembly in the shop, it is necessary to check the applied welding modes and consumables by determination of mechanical properties of the joints and weld metal by the procedures and in the scope specified by the currently valid standards on the technology of shop and site welding.

Experience of application of rolled stock from 10KhSNDA and 15KhSNDA steels at construction of the railway-road bridge in Kiev shows that making welded joints runs into certain difficulties, which restrain the procedure of including these steels into the standards.

Problems arising at construction of the railway-road bridge across the Dnieper River in Kiev using a considerable scope of span metal structures which are made of steels of 10KhSNDA and 15KhSNDA grades by CJSCs «Kurganstal-most» and «Ulan-Udestal-most», were of a comprehensive nature and required a coordinated solution. With this purpose PWI studied the rolled stock properties (Table 3), performance of welded joints of 10KhSNDA and 15KhSNDA steels (Table 4). Macrostructure of welded joints of 15KhSNDA, 10KhSNDA rolled stock metal 16, 20, 40 mm thick was also studied. The results meet the requirements specified for welded joints in SNIIP III-18-75.

Proceeding from the conducted investigations and experience of application of rolled stock from 15KhSNDA, 10KhSNDA steel to TU 14-1-5120-92 with modification #6 in the Russian bridge construction (bridges across Ob, Kama, Don, Volga, Oka and other rivers) adaptability of these steels to fabrication

**Table 4.** Performance of welded joints on 15KhSNDA and 10KhSNDA steels (welding consumables: 5 mm Sv-10NMA wire, AN-47 flux; root passes were made with UONI-13/55 electrodes)

Steel grade (thickness, mm)	$\sigma_t$ , MPa	$KCU_{-60}, J/cm^2$		Weld		
		Weld axis	Fusion line	$\sigma_t$ , MPa	$\sigma_y$ , MPa	$\delta_5$ , %
15KhSNDA (12)	561–570	45–53	52–100	736–778	598–644	20–22
15KhSNDA (16)	641–647	62–89	36–75	637–662	513–584	21–23
15KhSNDA (20)	767–773	61–71	47–86	587–658	460–478	23–27
15KhSNDA (40)	565–597	49–72	37–133	736–799	705–720	18–23
10KhSNDA (12)	541–554	51–59	81–110	753–771	647–690	21–22
10KhSNDA (16)	680–692	49–55	35–42	688–700	595–603	20–23
10KhSNDA (20)	602–606	70–84	38–65	612–685	402–484	24–30
10KhSNDA (40)	649–652	66–85	30–99	675–688	420–425	21–22

**Table 4 (cont.)**

Steel grade (thickness, mm)	Vickers hardness		
	Base metal	Near-weld zone	Weld
15KhSNDA (12)	135–140	163–174	178–185
15KhSNDA (16)	158–166	170–172	190–210
15KhSNDA (20)	152	159–165	171–174
15KhSNDA (40)	138–145	160–173	186–195
10KhSNDA (12)	148–155	174–177	200–209
10KhSNDA (16)	154–162	171–177	201–217
10KhSNDA (20)	159–165	174–177	197–209
10KhSNDA (40)	159–171	177–186	209–217

Note. Samples of all the joints failed across the base metal at testing, bend angle was 120°.

was assessed and temporary specifications were developed, which regulate application of 15KhSNDA, 10KhSNDA rolled stock in the metal structures of the railway-road bridge across the Dnieper River in Kiev (with approach zones) in the Kiev-Moskovsky-Darnitsa railway section. Scientific-engineering support of the assembly-welding operations is performed by PWI specialists.

1. Cheprasov, D.P., Ivanajsky, E.A., Platonov, A.S. et al. (1998) Properties of site joints of bridge structures from 10KhSNDA and 15KhSNDA steels. *Svarochm. Proizvodstvo*, **6**, 16–19.
2. Cheprasov, D.P., Petrov, V.P., Ivanajsky, E.A. (2003) Hydrogen brittleness of erection welded joints of bridge structures from 10KhSNDA and 15KhSNDA steels. *Ibid.*, **3**, 12–16.
3. Pemov, I.F., Morozov, Yu.D., Stepashin, A.M. et al. (2004) New generation bridge steels on the base of naturally-alloyed ores of Khalilov deposit. *Metallurg*, **9**.
4. Platonov, A.S., Pemov, I.F., Podberezny, N.I. (1996) New types of rolled steel stock for bridge construction. *Transport. Stroitelstvo*, **3**, 12–14.
5. Dobrotina, Z.A., Litvinenko, S.P., Rozanova, G.A. et al. (1979) Cold resistance of 08G2SFB steel welded joints. *Svarochm. Proizvodstvo*, **1**, 25–27.
6. Gudkov, A.A. (1989) *Crack resistance of steel*. Moscow: Metallurgiya.
7. (1988) *Embrittlement of structural steels and alloys*. Moscow: Metallurgiya.
8. Grabin, V.F. (1982) *Metals science of fusion welding*. Kiev: Naukova Dumka.

## PERFORMANCE OF FLASH BUTT WELDED JOINTS ON RAILWAY FROGS

S.I. KUCHUK-YATSENKO<sup>1</sup>, Yu.V. SHVETS<sup>1</sup>, A.V. KAVUNICHENKO<sup>1</sup>, V.I. SHVETS<sup>1</sup>  
S.D. TARANENKO<sup>2</sup> and V.A. PROSHCHENKO<sup>2</sup>

<sup>1</sup>E.O. Paton Electric Welding Institute, NASU, Kiev, Ukraine

<sup>2</sup>Open Joint Stock Company «Dnepropetrovsk Railway Switch Factory», Dnepropetrovsk, Ukraine

Results of investigation into performance of joints on railway frogs, made by flash butt welding through an intermediate insert of steel 12Kh18N10T, are presented. It is shown that strain hardening of austenitic components of a welded joint occurs during the operation process. This leads to levelling of hardness over the roll surface, thus limiting the local wear. Investigations of structural changes in the joint resulting from operation under cyclic loading and at a low temperature have been carried out.

**Keywords:** flash butt welding, railway frog, pulse flash-ing, Hadfield steel, steel M76, austenitic insert, performance of joints

Improving service characteristics and reliability of switch points is one of the topical problems in construction of railroads. Joining of a tailing part of the core to a rail with bolts through cover plates leads to a sharp drop of the vertical rigidity and causes a local

wear of the roll surface of the frog core ends and adjoining rail. The most promising method for increasing service strength of a frog consists in using new designs of the frogs with the rail ends welded to them. Lately, the welded frogs find an increasingly wide application on modern high-speed railways.

The E.O. Paton Electric Welding Institute developed the technology and equipment for flash butt welding of railway frogs under industrial conditions [1]. The technology is based on pulse flash welding [2], which allows making joints between high-manganese steel 110G13L and railway steel M76 through an intermediate insert of chrome-nickel austenitic steel 12Kh18N10T.

Open Joint Stock Company «Kakhovka Factory of Electric Welding Equipment» manufactured welding machine K924M using designs worked out by the E.O. Paton Electric Welding Institute. The machine has been employed to advantage at the Open Joint Stock Company «Dnepropetrovsk Railway Switch Factory» since 2002, including for manufacture of new types of welded frogs.

Specialists of the E.O. Paton Electric Welding Institute and «Dnepropetrovsk Railway Switch Factory» have monitored the state of welded frogs during their entire service life: measured deviation of the roll surface from linearity within the HAZ and insert region, and investigated structural changes, which could take place under the effect of cyclic loads and low service temperatures.

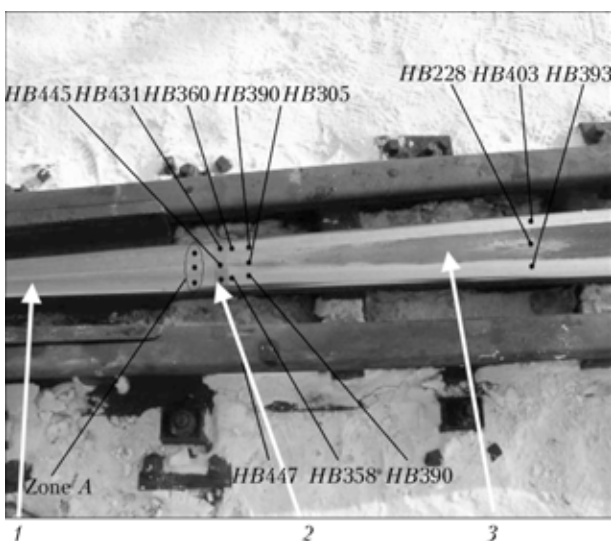


**Figure 1.** Appearance of welded frog and results of measurements of hardness on roll surface: 1 — frog core (steel 110G13L); 2 — insert (12Kh18N10T); 3 — rail end (M76); zone A — hardness above HB 450

Results of investigation of local deviation of roll surface from linearity within the welded joint zone at the Pridneprovskaya Railway

No.	Location of laying down	Tonnage passed, gross freight, mln t	Width of insert, mm	Deviation from linearity (recess), mm	Hardness <i>HB</i> at insert centre
1	Verkhovtsevo station	65.20	18–22	0.75	441
		196.6	18–22	0.80	445
2	Varvarovka station	48.37	40–42	0.80	420
3	Samojlovka station	48.57	18–20	0.50	410
4	Sinelnikovo station	96.50	18–22	0.50	435

As shown by practical application, no such characteristic defects as metal spalling in the tailing end of a frog, breakoff of a cast part of the check rail, transverse cracking in a rack part of the tail, which substantially reduce service life, were formed in the welded frogs.

Figure 1 shows appearance of a welded frog laid down on a track at the Verkhovtsevo station of the Pridneprovskaya Railway, as well as the values of hardness of the roll surface after passing of a gross freight of 196.6 mln t.

The insert of steel 12Kh18N10T in a joint has the lowest hardness at the initial stage of operation. The Table gives results of measurements of deviations of the roll surface from linearity, as well as values of hardness of the central part of the inserts in four frogs laid down on a track in regions of the Pridneprovskaya Railway with a high turnover of freight. As can be seen, the maximal deviation of profile of the roll surface from linearity, which occurs in the central part of the insert, is 0.5–0.8 mm.

The insignificant local deviation of the roll surface from linearity forms in the insert region at the initial stage of operation, when hardness of the insert is lower than that of the rail steel. This is confirmed by the measurements made on the same frog after passing of different tonnages of freight (Table, pos. 1). Formation of a local deviation from linearity is attributable to a different degree of the initial deformation required to achieve practically identical hardness of rail steel M76, chrome-nickel austenitic steel 12Kh18N10T and high-manganese steel 110G13L in work hardening.

Investigations and analysis of distribution of Brinell hardness in a joint were carried out on a frog, on which a 42.2 mln t gross freight was passed (Figure 2). The form of the curves of hardness distribution in a neck and flange of the frog is indicative of

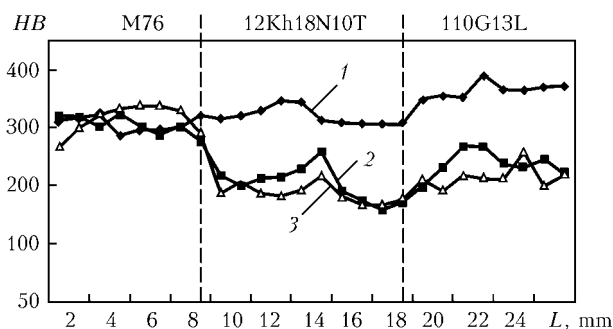


Figure 2. Distribution of Brinell hardness in welded frog: 1 — head; 2 — neck; 3 — flange

the fact that these rail regions experienced no work hardening, i.e. the hardness distribution corresponds to that which was observed after manufacture of the welded frog [1, 3]. The curve of hardness distribution on the roll surface also corresponds to the earlier one, plotted in measurements with a bigger pitch in a longer region.

As proved by comparative analysis, hardness of a joint on the roll surface grows both in the insert region and in the high-manganese steel as a result of work hardening. It becomes close to hardness of a rail within the insert region, and a bit higher in the high-manganese steel region. The latter is associated with a higher sensitivity of steel 110G13L to strain hardening, compared with steel 12Kh18N10T [3].

Levelling of hardness within the joint region during operation is a positive factor, in terms of a local deviation of the roll surface from linearity.

It is a known fact that work hardening is a result of structural transformations. So, investigations were conducted to study microstructure of the metal layer adjoining the roll surface, and distribution of microhardness in this layer (Figure 3). It was found that depth of the hardened layer in all the steels was practically identical and equal to about 2 mm. The curve of distribution of microhardness in the hardened layer monotonously grew with distance to the surface. Microhardness of steel 12Kh18N10T increased from 1800 to 3500–3800 MPa, that of steel 110G13L increased from 1800 to 3900–4100 MPa, and that of steel M76 — from 3600 to 5000 MPa (Figure 3).

Structure became refined in the hardened layer of steel 12Kh18N10T (Figure 4, a, b), and grain coarsening took place in the hardened layer of steel 110G13L (Figure 4, c, d). In both cases the steels remained austenitic. Austenite grains contained nu-

HV 0.5, MPa

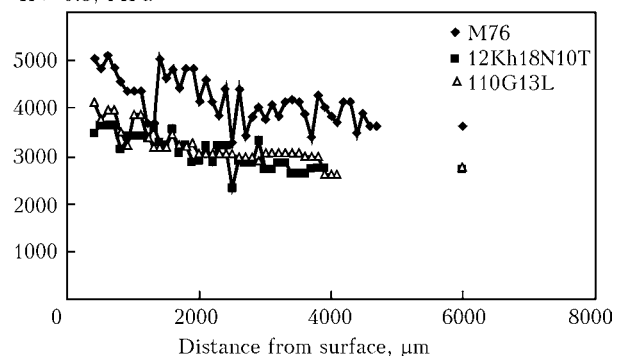
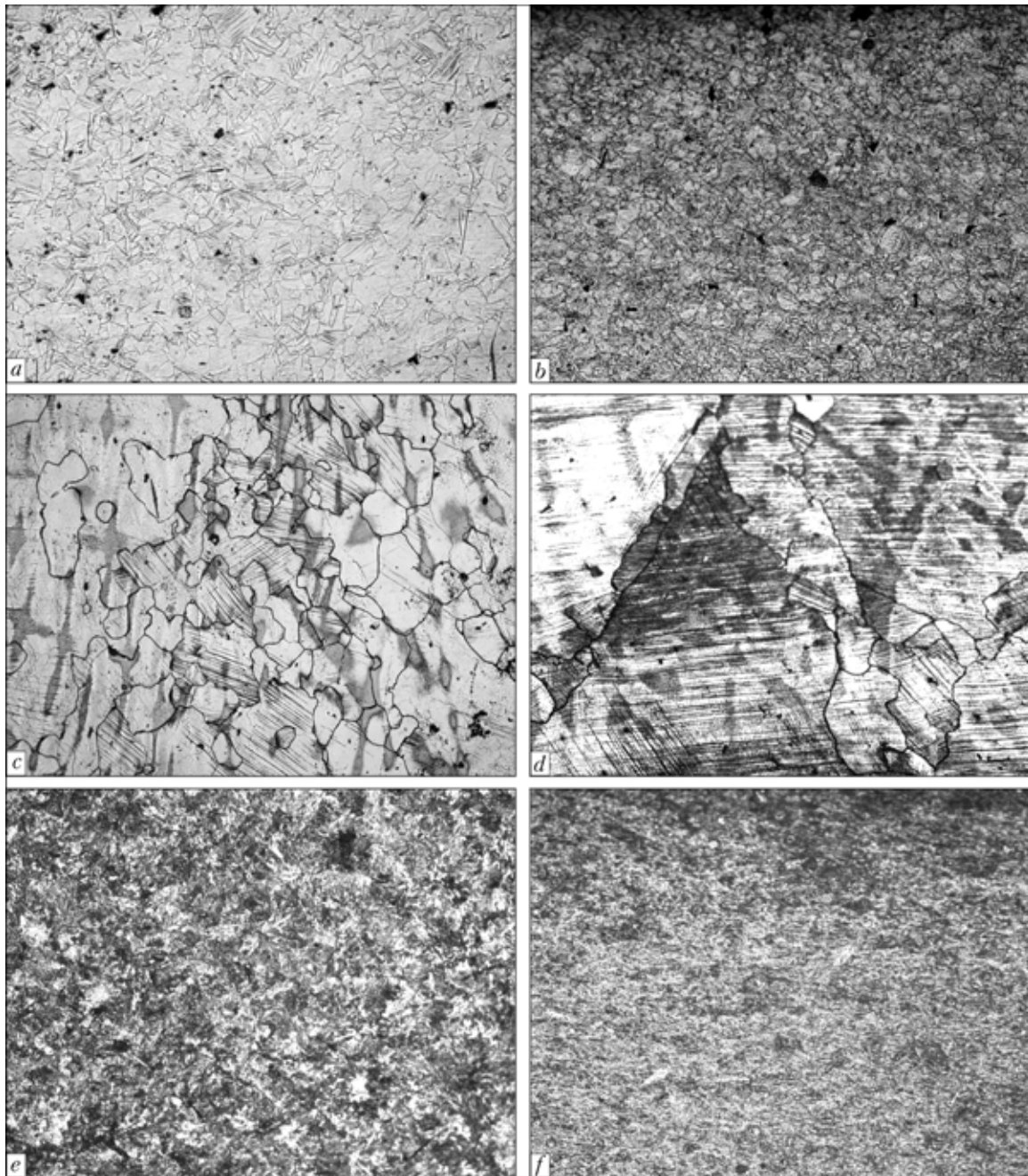
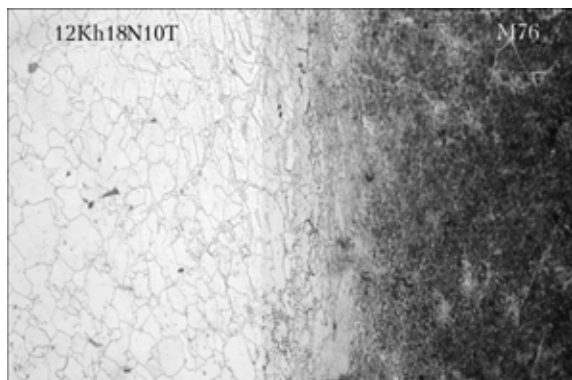


Figure 3. Distribution of microhardness in metal layer adjoining roll surface



**Figure 4.** Microstructure of steels 12Kh18N10T (*a, b*), 110G13L (*c, d*) and M76 (*e, f*) in the bulk (*a, c, e*) and near roll surface (*b, d, f*) ( $\times 100$ )



**Figure 5.** Microstructure of transition zone at interface of the 12Kh18N10T + M76 joint ( $\times 25$ )

merous strain slip lines. This was especially pronounced for steel 110G13L. The issues related to nature of strain hardening are studied in detail in [4]. Intensive refining of sorbite grains took place in the hardened layer of rail steel M76 (Figure 4, *e, f*).

The transition zone at interface between steels 12Kh18N10T and 110G13L consisted of austenitic components of intermediate chemical composition [5], the structural changes in which were similar to those in the base metal.

Structure of the transition zone at interface between steels 12Kh18N10T and M76 was more complex [3]. The interface layer of the rail steel comprised an interblock structural component formed under the temperature-deformation conditions of welding as a



result of mass transfer of the melt over the fused structural boundaries [3]. The interblock structural component was the alloyed unstable austenite. Needles of quenching structures were present in the bulk of individual interblock structural components. Further decomposition of austenite may take place under the effect of external loads and negative service temperatures, which will lead to a strength loss.

Analysis of microstructure showed (Figure 5) that decomposition of austenite in the hardened layer at interface between the rail and insert steels did not develop. The same result was also obtained in metallography of the frog, which was in operation in winter of 2006 at temperatures of down to  $-30^{\circ}\text{C}$ . This evidences that austenite in interblock structural components is sufficiently stable for such service conditions.

## CONCLUSIONS

1. Hardening and levelling of hardness on the roll surface occur within the zone of the core–insert–rail end welded joint during operation of the frogs with the rail ends welded to them.

2. Insignificant local deviation from linearity of the roll surface within the insert zone occurs at the

initial stage of operation. It is attributable to a different degree of the initial deformation required to level hardness of rail steel M76, chrome-nickel austenitic steel 12Kh18N10T and high-manganese steel 110G13L in work hardening. Further operation does not lead to any increase in local deviation of the roll surface from linearity.

3. No formation of defects, and no transformation of unstable austenitic structural components to form quenching structures take place in a welded joint under service conditions.

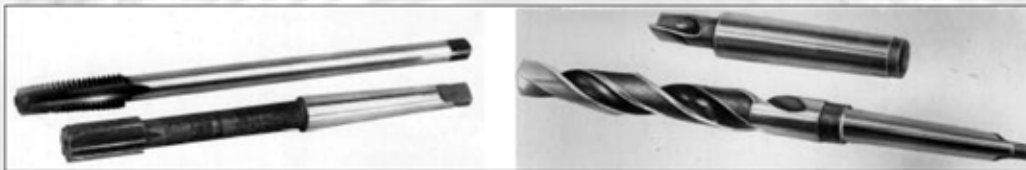
1. Kuchuk-Yatsenko, S.I., Shvets, Yu.V., Dumchev, E.A. et al. (2005) Flash butt welding of railway frogs with rail ends using an intermediate insert. *The Paton Welding J.*, **1**, 2–4.
2. Kuchuk-Yatsenko, S.I., Didkovsky, V.V., Bogorsky, M.V. et al. *Method of flash butt welding*. Pat. 46820 Ukraine. Publ. 17.06.02.
3. Kuchuk-Yatsenko, S.I., Shvets, Yu.V., Kavunichenko, A.V. et al. (2007) Influence of the width of stainless steel insert on performance of joints of railway frogs with rail ends. *The Paton Welding J.*, **3**, 2–5.
4. Bogachev, I.N., Rozhkova, S.B. (1963) Strengthening of austenitic steels in cold plastic deformation. *Izvestiya Vuzov. Chyorn. Metallurgiya*, **7**, 162–168.
5. Kuchuk-Yatsenko, S.I., Shvets, V.I., Gordan, G.N. et al. (2006) Features of formation of structure of joints of rail steel M76 to steel 110G13L made by flash-butt welding. *The Paton Welding J.*, **1**, 2–8.

## TECHNOLOGY AND EQUIPMENT FOR FLASH-BUTT WELDING OF CUTTING TOOLS

E.O. Paton Electric Welding Institute developed technology and equipment for flash-butt welding of tool steel to structural steel, in particular, high-speed steel of R6M5 grade to structural steels 45, 20Kh, 40Kh, etc., for making bimetal metal-cutting point tools (drills, taps, broaches, finger mills).

The developed technology guarantees producing sound flash-butt welded joints of cutting tools equivalent to the base metal.

The welding process is fully automated, has program control and a system for real time monitoring of welding parameters.



Samples of welded bimetal tools

The developed technology was the basis for designing specialized and upgrading all-purpose flash-butt welding machines K802, K793, K724A, K838, which allow welding tool billets of 7 to 8000 mm<sup>2</sup> cross-section. This equipment can be applied independently or as part of automated lines of tool manufacturing.

**Purpose and application.** Technologies and equipment for flash-butt welding of bimetal tools are designed for application in the tool and machine-tool construction industries.

**Status and level of development.** Developed technologies and equipment for their implementation correspond to the world standards and are protected by foreign patents and authors' certificates.

**Forms of co-operation.** To be determined during negotiations. Technology and equipment can be introduced, and all-purpose equipment can be upgraded on contract basis.

Contacts: Prof. Kuchuk-Yatsenko S.I.  
E-mail: chvertko@paton.kiev.ua

# METAL-ABRASIVE GRINDING WASTES, METHODS OF THEIR PROCESSING AND EXPERIENCE OF APPLICATION IN SURFACING MATERIALS

I.P. LENTYUGOV, I.A. RYABTSEV, O.G. KUZMENKO and Yu.M. KUSKOV  
E.O. Paton Electric Welding Institute, NASU, Kiev, Ukraine

Methods for preparation of metal-containing grinding wastes for processing and technologies for processing metal-abrasive wastes are considered. Foreign and domestic experience in application and processing of such wastes is described.

**Keywords:** metal-abrasive grinding wastes, processing of wastes, electroslag remelting, surfacing materials, flux-cored wires

In state-of-the-art surfacing materials of various designations such expensive alloying elements as tungsten, vanadium, chromium, molybdenum, etc. are used [1], whereby their price and respectively price of the surfacing materials continuously increases. One of the ways for reducing cost of the latter is application in their production of wastes from different fields of production, in particular, metal-abrasive grinding wastes (slurries). Data, presented in [2], prove that at industrial enterprises of Ukraine, especially at metallurgical ones, within one year accumulates significant amount of such wastes (Table 1).

Metal-containing grinding wastes consist of the mixture of fine-dispersed metal microchips with abrasive powder (products of destruction of grinding wheels and residues of the lubrication-cooling liquid (LCL)) [2, 3].

Attempts were undertaken to use directly metal abrasive wastes in welding and surfacing materials [4–6]. In [4] experience of application of pulverous wastes of abrasive scarfing of rolled metal from low and medium-carbon steels in production of electrodes for welding of cast iron, which were manufactured according to traditional technologies — the wastes were added into coating of the electrodes, is described. Composition of the metal, deposited by

means of these electrodes, corresponded to a low-carbon non-alloyed steel ( $C \leq 0.07\%$ ), which significantly limited its application in industry.

Experiments were carried out on application of wastes of processing of the alloyed steel ingots and alloys in the charge of flux-cored wires [5]. Several experimental flux-cored wires were produced from the wastes. Using one of them, in particular the one that ensures production of the deposited metal, composition of which is close to that of the tool steel, the rolls were surfaced, which demonstrated satisfactory results in operation.

Possibility of using the wastes, produced in scarfing on roughing-grinding machines of ingots from the EP109, EP199 and EP33 alloys, for plasma surfacing of the fixture parts of rolling mills and rolls of roller conveyers that transport heated billets, i.e. parts, subjected to friction wear without lubrication at increased temperatures, was investigated [6]. Before surfacing the wastes were sieved by fractions and calcinated in electric furnaces at 200–250 °C. For deposition powder of 125–315 μm fractions was used. The experiments showed that presence in the powder of 3–4 wt.% of oxides worsened formation of the deposited metal.

All these works were of experimental character and were not used on wide commercial scale because the wastes were selected randomly. The experiments showed that one should not use metal-abrasive wastes

**Table 1.** Metal-abrasive wastes of a number of metallurgical enterprises of Ukraine [2]\*

Enterprise	Group of processed steel	Method of waste collection	Mass of metal-abrasive wastes per year, t
«Dnepropetsstal», Zaporozhie	Tool, high-speed, corrosion-resistant, bearing	Hopper-accumulator	> 3000
«Zaporozhstal», Zaporozhie	Carbon, structural, alloyed, corrosion-resistant	Same	200
Enakievo metallurgical plant	Tool, high-speed, corrosion-resistant, bearing	»	> 1000
Alchevsk metallurgical works	Structural medium-alloyed	Container	~ 100
«Krivorozhstal», Krivoj Rog	Structural carbon	Hopper-accumulator	

\* In [2] the data are presented collected early in 1990s. As far as volumes of metal production in metallurgical industry of Ukraine are approximately the same, masses of the collected metal wastes approaches those indicated in Table 1.

in production of surfacing materials without preliminary preparation and selection of chemical composition.

In order to use metal-abrasive wastes for production of surfacing materials, the wastes themselves and technology of their processing should meet the following requirements:

- relative constancy of chemical composition of the metal component;
- presence of expensive alloying elements (tungsten, molybdenum, chromium, vanadium, etc.) in metal component of the wastes;
- adaptability to manufacture and profitability of preparation of the metal-containing wastes for processing;
- adaptability to manufacture and profitability of processing of the wastes into foundry alloys and similar charge materials, which are easily milled and fit for production of surfacing materials (flux-cored wires, tapes, powders, etc.).

For production of surfacing materials the wastes are needed, which are produced at high-speed grinding of the high-alloy steel ingots and alloys in the process of abrasive processing of the metal-cutting tools, because exactly in them such expensive alloying metals as tungsten, vanadium, chromium, molybdenum, etc. are contained.

According to GOST 1639-93 «Scrap and wastes of non-ferrous metals and alloys», pulverous wastes from sharpening of the hard-alloy tools and high-speed tool steels should be collected into separate containers, which makes easier their utilization and allows producing from them foundry alloys and powders of practically constant chemical composition.

**Preparation of metal-containing grinding wastes for processing.** Experience showed that metal-containing grinding wastes may contain up to 50 % of abrasive component and LCL [7]. Because of this reason majority of existing methods of disposal of such wastes envisage their preliminary preparation for processing — removal of LCL and magnetic separation for the purpose of reducing content of the non-metallic component. For removal of the LCL residues calcination of metal-abrasive wastes at temperature 200–400 °C is envisaged [8–10]. It is also suggested to use for this purpose a high-speed centrifugal stirrer [11] or degreasing of the wastes by tetrachloroethyl and drying at 80–120 °C [12].

In process of calcination the wastes may turn into small stakes, which it is necessary to mill, after which magnetic separation of wastes on a separator of periodic action [8, 10–12] is performed for production of the concentrate, containing 95–98 % of metal and 2–5 % of mineral components (Figure 1) [13]. Such content in the wastes of the abrasive component after magnetic separation is explained by the fact that abrasive grains and metal chips in process of calcination join (set) with each other rather strongly; in addition, spiral of metal chips may mechanically retain abrasive grains.

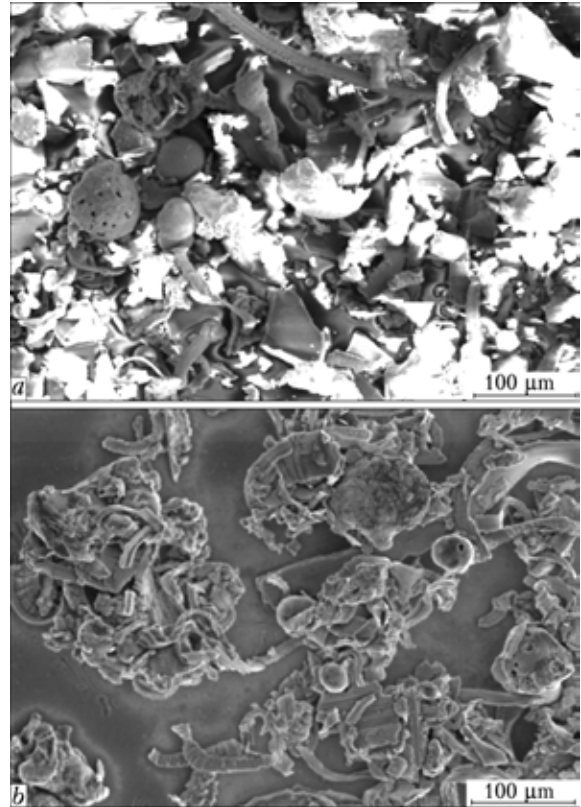


**Figure 1.** Appearance of metal-abrasive wastes before (a) and after (b) magnetic separation

For more efficient cleaning of the metal-abrasive wastes magnetic separation is supplemented by chemical-metallurgical methods of regeneration. However, because of introduction of such technological operations cost of the final product significantly increases. So, for example, in the US patent [12] it is suggested to oxidize after magnetic separation the wastes at temperature 850–1000 °C within 2 h, after which the oxidized product is reduced in hydrogen at 1050–1200 °C.

Rather complex technology of disposal of the metal-abrasive wastes is also suggested in Austrian patent [9]. After calcination for removal of LCL 10–20 %  $\text{CaCO}_3$  were added to the wastes, then this mixture was heated up to 1100 °C, soaked at this temperature for 2 h, and then cooled in water. Produced product was treated in 10 % solution of  $\text{MoCo}_3$  at temperature 90 °C. According to author of this patent, in process of leaching up to 100 wt.% W, 90 wt.% Mo, and 95 wt.% V are recovered from the wastes. Subsequent treatment of the residue using 15 % solution of hydrochloric acid allows recovering about 93 wt.% Ni and 90 wt.% Co.

From all considered methods of preparation of the metal-containing slurry for processing the most simple for implementation is calcination at 200–400 °C for removal of LCL, and in case of significant content in them of abrasive residues — magnetic separation.

**Processing of metal-abrasive wastes. Remelting in arc furnaces.** At the electrometallurgical plant «Elektrostal» (Elektrostal, RF) technology for disposal of wastes of grinding of precision alloys without



magnetic separation by means of their remelting into a certified billet in five-ton electric arc furnaces has been developed and introduced [14]. These wastes form in process of abrasive scarfing of continuously cast billets from the 5ON, 29NK, and 47ND alloys and represent a mechanical mixture of oxidized metal chips of 0.5–5.0 mm length and products of the abrasive tool wear.

The charge consists of the chips, produced as a result of turning processing of the ingots, and lumpy and grinding wastes. Amount of the wastes constituted 30–50 % of total mass of the remelted materials.

The developed technology ensures assimilation (on average) up to 90 wt.% Co and 93 wt.% Ni, contained in metal component of the metal-abrasive wastes, and 75–80 wt.% Fe. Produced charge ingots were used in melting of branded metal of respective precision alloys in arc or induction furnaces. Share of these ingots constituted up to 25 % of the metal charge mass.

At metallurgical works «Zaporozhstal» (Zaporozhie, Ukraine) in technology of production of strips and sheets from corrosion-resistant stainless steel scarfing of the latter is envisaged, due to which a fine-dispersed slurry is formed, containing such valuable components as nickel (6–7 wt.%), chromium (up to 13 wt.%), and iron (up to 54 wt.%) [15].

Melting of certified ingots was carried out in a seven-ton furnace with addition into the initial charge up to 1.7 t grinding slurry. Addition of the grinding wastes increased content in the finished metal of chromium by 0.83–0.96 wt.% and nickel by 1.48–0.68 wt.%, whereby for removal of LCL it is recommended to preliminarily anneal slurry in heating devices.

*Electroslag remelting (ESR).* Great prospects for processing of mentioned wastes open electroslag technologies [16], whereby ESR may be performed with application of consumable and non-consumable electrodes, which are used rarely. So, in the patent [17] the method for recovery of metal components from grinding dust by means of sintering from it of consumable electrodes with their subsequent ESR is described. More rational is ESR of metal-abrasive wastes with application of non-consumable electrodes, whereby labor-consuming operation of manufacturing consumable electrodes from the wastes is excluded and continuity of the melting process is ensured.

At Oskol plant of metallurgical machine building (RF) technology for processing of abrasive grinding wastes of high-speed tungsten-containing steels has been developed, which includes drying, magnetic separation, and ESR of the produced intermediate product with application of a non-consumable graphite electrode. Remelting is carried out into the closed bottom mould or a short mould with drawing of an ingot [18]. In ESR efficient sulfur removal occurs, due to which content of sulfur reduces from 0.023 to 0.010–0.008 wt.%. Melting loss of such elements as molybdenum, chromium and tungsten is practically absent. Yield of efficient ingots equals about 85 %.

In manufacturing of magnates from the UNDK alloy (on basis of Fe–Al–Ni–Cu–Co according to GOST 17809–79) [19] also forms significant amount of grinding wastes. Laboratory and industrial experiments on remelting of metal-abrasive wastes of this alloy in electric arc and electroslag crucible furnaces were carried out. In the course of the experiments it was established that electroslag method of remelting significantly increases coefficient of the metal recovery from the wastes. Possibility of combining the waste remelting and refining processes in the electroslag furnace was confirmed [19].

In electroslag crucible remelting fine wastes are filled into the layer of molten flux, where they melt. The produced product meets by content of the impurities strict requirements of high-quality UNDK or Alnico alloy. Irrecoverable losses of metal in this process are comparatively small and significantly lower than in case of melting in the arc furnace [16, 19].

For the purpose of reducing production cost of alloyed steels and alloys in manufacturing from them of metal products of the required quality the technology for production of ingots of the assigned composition from a fragmented charge (chips, metal-abrasive wastes, etc.) using ESR method was developed. Depending upon requirements, established for the ingot, chlorine-oxygen oxidation refining of the metal, deoxygenation and desulfurization, recovery of the metal component from pulverous metal abrasives, deoxidation, and alloying of the molten metal pool by direct introduction of deoxidizers and alloying elements through the slag are carried out in ESR [20]. The process proceeds continuously with periodic discharge of the ingots on the commercial installation [21]. The developed technology allows producing quality ingots of alloyed steels from the fragmented charge.

In the E.O. Paton EWI [22] investigations of ESR of slurries, produced in anode-mechanical cutting of billets from the EI437BU alloy, and electrocontact scarfing of billets from the JS6KP alloy were carried out. Experimental melts were performed on the A-550 installation in a water-cooled mould of 160 mm diameter. The slurry was charged into the mould batchwise.

Taking into account the fact that the slurries have rather high content of  $Al_2O_3$ , the  $CaF_2$  fluorite — main component of majority of kinds of slag used in electroslag technologies — was chosen as the slag for ESR. Transition of  $Al_2O_3$  from the slurry into the slag in process of melting ensured production of the slag, chemical composition of which corresponded to the ANF-6 flux that allowed increasing amount of remelted slurry without partial renewal or complete replacement of the used slag.

Produced intermediate product may be used in melting of alloyed steels. For remelting of slurry the metal water-cooled electrodes with tungsten or molybdenum tips may be used, application of which in ESR brought good results [22].

So, considered technologies of electric arc remelting and ESR of the metal-abrasive wastes allowed



**Table 2.** Results of chemical analysis of composition (wt.%)\* of wastes before and after special preparation as well as produced from them foundry alloys

Experiment No	Material, method of its preparation and foundry alloy	C	Si	Al	Cr	W	V	Mo	Co
1	Wastes	1.8	16.0	15.0	1.2	5.0	0.9	0.9	0.4
	Foundry alloy	3.7	12.5	0.2	3.5	5.2	0.8	1.4	0.5
2	Wastes	1.8	16.0	15.0	1.2	5.0	0.9	0.9	0.4
	Wastes after magnetic separation	1.7	5.0	4.0	3.6	9.5	1.3	1.4	0.6
	Foundry alloy	4.1	1.1	0.6	3.9	11.4	0.7	2.3	0.3
3	Wastes	1.8	16.0	15.0	1.2	5.0	0.9	0.9	0.4
	Wastes after oxidation	2.2	5.8	3.9	2.4	4.4	0.8	0.8	0.3
	Foundry alloy	4.5	1.3	0.3	1.3	10.7	0.4	2.3	0.2

\*The rest is iron.

producing either certified ingots, which may be used in subsequent melting of high-alloy steels, or directly ingots of respective grades of high-alloy steels. However, these technologies were not used for production of foundry alloys and other charge materials fit for production of flux-cored surfacing wires. As it was mentioned above, such materials should be relatively easily ground into powders.

For the purpose of producing from metal-abrasive wastes of high-alloy foundry alloys that would meet formulated above requirements, in the E.O. Paton EWI technology for processing wastes of grinding of tools from high-speed steel was suggested [23]. Taking into account the fact that at present nomenclature of used grades of high-speed steels is relatively small and is frequently limited by the R6M5 steel, production of the charge of approximately the same composition does not cause great difficulties.

Originally the technology for processing of wastes, including operations of calcination, magnetic separation for cleaning from components of abrasive wheels, ESR with application of a non-consumable graphite electrode, milling and sieving of the charge into required fraction, was developed. During performance of the experiments it was established that for ensuring stability of the ESR process and maximum yield of quality foundry alloy, specific power should be not less than  $100 \text{ W/cm}^2$ , whereby rate of the slurry feeding should be 2–3 kg/min.

Composition of the produced foundry alloy includes sufficient amount of such expensive alloying

elements as tungsten, molybdenum, vanadium, it also contains more than 3 wt.% C and because of this reason is easily ground (Table 2, Figure 2).

Chemical analysis of the foundry alloy, produced from the wastes, which were not subjected to preliminary preparation (experiment No 1, Table 2) showed that it, as a rule, contained more than 12 wt.% Si, which is not always admissible. Such high content of silicon in the foundry alloy is explained by the fact that silicon carbide from the abrasive wheels gets into the wastes. Preliminary magnetic separation of the wastes allows significant reducing content of silicon in the foundry alloy (experiment No 2, Table 2), but this is rather expensive operation that requires for application of special equipment.

It is known that silicon carbide may reduce oxides of majority of other metals, due to which silicon dioxide is formed that is easily removed into slag in ESR. Experiments on replacement of magnetic separation for preliminary high-temperature oxidation of metal-abrasive wastes at temperature  $900^\circ\text{C}$  were carried out, which resulted in a certain increase of the slurry mass. During performance of experiments on ESR of oxidized wastes in a water-cooled copper mould dependence between degree of the material oxidation  $K$  (ratio of the oxidized slurry mass to the initial slurry mass) and content of silicon in the melted foundry alloy was established. So, at  $K = 1.0$ – $1.05$  content of silicon in the foundry alloy remains rather high — 9–12 wt.%, at  $K = 1.1$ – $1.2$  it reduces down to 4.8–6.9 %, and at  $K = 1.3$ – $1.5$  — down to

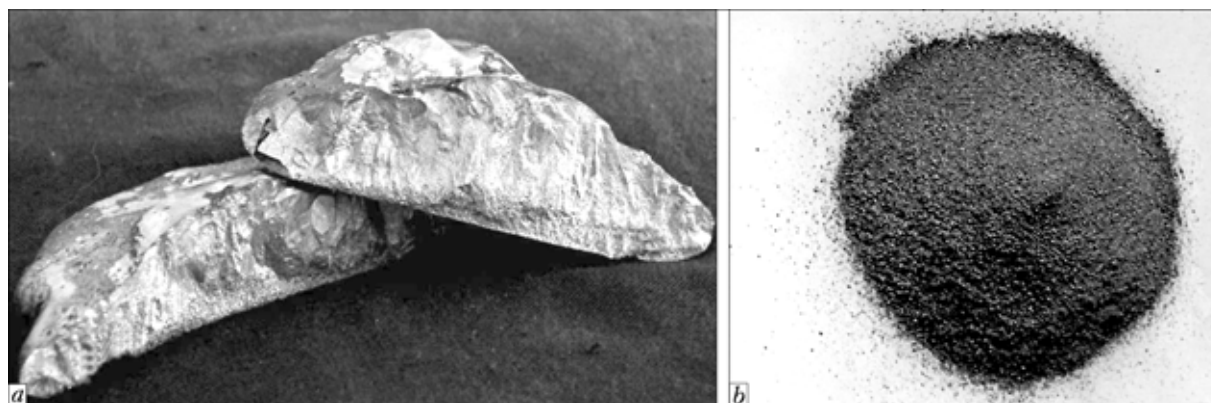


**Figure 2.** Appearance of foundry alloy produced from metal-abrasive wastes of high-speed steel grinding before (a) and after (b) refining



1.3 wt.% (experiment No 3, Table 2). So, by changing degree of the charge oxidation one may control content of silicon in the foundry alloy, whereby content of other alloying elements in foundry alloys, melted from preliminarily oxidized charge, is within the same range as in the foundry alloy, produced from the wastes that passed magnetic separation.

Using this foundry alloy experimental lots of the TsP-AN132 and PN-AN147 flux-cored wires were produced, which ensured production of deposited metal of the tool steel type [24]. Flux-cored wires of this type are widely used for surfacing of rolls, stamps, and stamp fitting-out of different types [1]. Besides the foundry alloy, into the charge of flux-cored wires ferroalloys were additionally added for the purpose of producing a deposited metal, composition of which would correspond to the grades of mentioned wires. Investigations of the metal, deposited using experimental flux-cored wires, showed that its hardness and other mechanical properties corresponded to the metal, deposited using standard PP-AN132 and PP-AN147 flux-cored wires. These experiments confirmed efficiency of developed in the E.O. Paton EWI technology for processing metal-abrasive wastes of high-speed steel that included high-temperature oxidation and ESR with application of a non-consumable water-cooled electrode, and good prospects of application of the produced foundry alloy for production of high-alloy surfacing materials.

## CONCLUSIONS

1. Metal-abrasive wastes of grinding of high-alloy steels, collected at metallurgical and machine-building enterprises, may be used as raw material for production of foundry alloys for surfacing materials. In order to use such wastes for production of surfacing materials, they and technology of their processing should meet a number of requirements.

2. In the E.O. Paton EWI technology for processing metal-abrasive wastes of high-speed steel that includes high-temperature oxidation and ESR with application of a non-consumable water-cooled electrode has been developed. Good prospects of application of the produced foundry alloys for production of high-alloy surfacing materials have been experimentally confirmed.

- Ryabtsev, I.A. (2004) *Surfacing of machine parts and mechanisms*. Kiev: Ekotekhnologiya.
- Kiparisov, S.S., Padalko, O.V., Levinsky, Yu.V. et al. (1993) Resource-saving and natural potential of powder materials and technologies: realization in field of processing of waste resources. *Poroshk. Metallurgiya*, **6**, 1–4.
- Gabrielov, I.P., Kerzhentseva, L.F. (1985) Properties of powder produced from metal-abrasive waste of high-speed steel. *Ibid.*, **9**, 133–136.
- Babij, V.M., Kondratenko, Z.F., Rybalka, V.I. (1989) Use of dust-like waste of abrasive dressing of rolled metal in production of electrodes for welding of cast iron. *Svarochn. Proizvodstvo*, **10**, 32–33.
- Pozdeev, G.A., Sheenko, I.N., Titarenko, V.I. et al. (1990) Hardfacing of section mill rollers by flux-cored wire with charge of metal waste of alloy steel and doped alloy ingots. In: *Abstr. of Pap. of All-Union Seminar on Recovery and Strengthening of Metallurgical Unit Parts by Hardfacing, Spraying and Heat Treatment* (Moscow, Sept. 1990). Moscow: TsNITEI ChM.
- Pozdeev, G.A., Olejnik, V.A. (1990) About possibility of application of mechanical treatment waste of ingots for plasma arc surfacing. *Svarochn. Proizvodstvo*, **10**, 32–33.
- Tager, L.R., Zhabin, I.Ya., Gorshkov, B.T. et al. (1972) Effective processes of abrasive machining. *Bull. In-ta Chernetinformatsiya*, **15**, 11–16.
- Tambovtsev, Yu.I., Burachonok, I.N. *Electromagnetic separator*. USSR author's cert. 944659. Int. Cl. B 03 C 1/08. Publ. 23.10.80.
- Hans, W., Steinmark, K., Wolfgang, M. et al. *Method of swarf processing, in particular, of grinding dust*. Pat. 377240 Austria. Publ. 25.02.85.
- Gabrielov, I.P., Rapoport, L.A., Slabodkin, V.Yu. (1989) Processing of fine-fractional waste of alloy steel. *Stal*, **10**, 39.
- Radzikowski, W., Piecuch, T. (1988) Badanie i opracowanie technologii odzysku stopow AlNiCo ze szlamow poszlifier-skich. In: *Proc. of Symp. on Optym. Wykorzyst. Sur. Miner. Proces, Przerobki i przerworstwa* (Zakopane, 25–27 pazdz., 1988). Krakow, 25–27.
- Holman, J.L., Neumeier, L.A. *Extraction of metals from slurry produced in grinding*. Pat. 4409020 USA. Int. Cl. C 22 C 1/04, B 02 F 9/04. Publ. 11.10.83.
- Dovgy, I.I., Volobuev, V.F., Ankudinov, N.V. (1980) *Stocking and processing of recycled metals*. Moscow: Metallurgiya.
- Tager, L.R., Karavaev, V.M. (1979) Recycling of grinding waste of precision alloys. *Bull. In-ta Chernetinformatsiya*, **21**, 37.
- Pavlishchev, V.B., Salo, G.D. (1985) Application of swarf in melting of corrosion-resistant steel. *Stal*, **10**, 42–43.
- Volkotrub, N.P., Latash, Yu.V. (1981) Study of possibilities of metal component extraction from slurry by means of electroslag melting. *Spets. Elektrometallurgiya*, **46**, 32–35.
- Sointag, G., Valash, H. *Method of recovery of metal components from grinding dust*. Pat. 2505378 Germany. Int. Cl. C 21 C 5/52. Publ. 14.08.78.
- Volkov, A.E., Bedrin, N.I. (1994) Specifics of electroslag remelting of abrasive dust. *Stal*, **3**, 70–71.
- Sokolov, V.M., Fedorenko, I.V. (2001) Improved technology of refining remelting of slag and grinding waste of alloy YuNDK. *Protsessy Litiya*, **3**, 81–84.
- Bogdanov, S.V. (1990) Prospects of application of ESR technology for recycling of metal waste. *Stal*, **6**, 36–37.
- Yakovenko, V.A., Lyuty, I.Yu. (1989) Unit UO-105 for electroslag melting and refining of metals and alloys from non-compact charge. In: *Series Spetsselektrometallurgiya*. Kiev: PWI.
- Lyuty, I.Yu., Volkotrub, N.P., Latash, Yu.V. (1976) To problem of application of cooled non-consumable electrodes in electroslag treatment of metals. *Spets. Elektrometallurgiya*, **30**, 28–33.
- Lentyugov, I.P. (2003) Development of technology of foundry alloy production for flux-cored wires using the waste of grinding production. In: *Abstr. of Pap. of 2nd All-Ukr. Sci-Tech. Conf. of Junior Scientists and Specialists* (Kyiv, 25–27 June, 2003). Kiev: PWI.
- Ryabtsev, I.A., Kuskov, Yu.M., Kuzmenko, O.G. et al. (2002) Production of flux-cored wires for surfacing and arc metallization using the grinding waste of high-speed steel in charge. In: *Abstr. of Int. Conf. (Benardos Lectures) on Welding and Related Technologies* (Kiev, 22–26 April, 2002). Kiev: PWI, 44–45.



## THESES FOR A SCIENTIFIC DEGREE



**E.O. Paton Electric Welding Institute, NASU.**

**S.G. Vojnarovich** (PWI) defended on 25th of June 2008 candidate's thesis on topic «Development of technology of microplasma spraying of bioceramic coating».

The thesis is devoted to development of technology of microplasma spraying of the coating from hydroxyapatite (HA) on parts of endoprostheses with ensuring of the required phase composition and structure.

Experimentally range of parameters of the plasmatron operation with a remote anode of 1–2 kW power was established for conditions of spraying of the coatings and its volt-ampere characteristics were determined. It was established that VAC of the MP-004 plasmatron had a linear form and were ascending, arc voltage under conditions of microplasma spraying with application of pure argon as a plasma gas equaled 22–32 V. Investigation of influence of the plasma gas consumption on conditions of outflow of the microplasma jet showed that within range of currents 30–45 A stable laminar outflow of the jet was observed which preserved at flow rate of the plasma gas 40–120 l/h, whereby length of the microplasma jet equaled 100–150 mm.

Influence of technological parameters (current, consumption of the plasma gas) on efficiency of the plasmatron, enthalpy, and temperature of argon plasma was determined using method of flow calorimetric measurement. It was established that efficiency of the plasmatron increased by means of increase of the plasma gas flow rate and achieved 55 %. It was shown that in working range of the spraying parameters enthalpy constituted 11,000–32,000 J/l

which corresponded to the mass average initial temperature of argon jet 10,000–13500 K.

Investigation of the metal spraying figure and spraying spot for conditions of the HA microplasma spraying showed that the metal spraying figure had a profile that was described with high accuracy by Gauss distribution (correlation factor equaled 0.933–0.996), and spraying spot had shape of ellipse with ratio of the axes 1.1–1.3 and size 8–15 mm depending upon parameters of the spraying process. Carried out calculations of losses of the material being sprayed showed that total losses of the material in microplasma spraying on implants having cross-section 8–10 mm constituted 20–40 %, which is 2–4 times lower than in traditional plasma spraying.

Investigation of influence of main parameters of the microplasma spraying process (current, consumption of the plasma gas, distance of spraying, consumption of powder) on morphology and structural-phase transformations in the HA coatings showed that by means of change of these parameters, which caused change of conditions of heating and movement of particles of the material being sprayed, it was possible to control phase composition of the HA coatings within 88–98 % content of the HA crystalline phase, degree of amorphism from 0 to 7 %, content of tricalcium phosphate from 0 to 6 % and formation due to this of the HA coatings with the assigned phase composition. It was established for the first time that under conditions of microplasma spraying formation of texture (with coefficient 0.48–0.74) is possible in the HA coatings. Linear regression models were calculated which showed degree of influence of each parameter on formation of a complex of the HA coating characteristics.

It was established that phase composition of the HA coatings and characteristics of the texture changed over thickness of the layer in direction from the coating surface to interface with the base.

Strength of the coating adhesion to the base was determined depending upon presence of the sublayer and material of the latter. In spraying of the HA coatings with application of titanium as the coating sublayer, strength of adhesion equaled  $24.17 \pm 0.85$  MPa.

The results obtained were used in development of technological recommendations for application of the HA coatings on implants for interbody spondylosynthesis and femoral endoprostheses. Positive results of clinical tests were obtained.



E.O. Paton Electric Welding Institute, NASU.

**A.V. Ignatenko** (PWI) defended on 2nd of July 2008 candidate's thesis on topic «Mechanism of origination of induced by hydrogen cracks in welded joints of high-strength low-alloy steels».

For solution of raised in the work issues theoretical investigations and numeric modeling of the processes, which occur in a grain of a metal with the body-center lattice during origination and development of a submicrocrack, were carried out.

Mathematical model of hydrogen transfer by moving edge dislocations was suggested. Influence of the metal temperature, rate of movement of the edge dislocations and concentration of the diffusion hydrogen on amount of carried by the dislocations hydrogen to the place of a submicrocrack formation was investigated. It was established that at increase of rate of movement of an edge dislocation or at reduction of

the diffusion hydrogen concentration, amount of the carried out hydrogen reduced, and maximum of the curve  $N(T)$  shifted into the area of higher temperatures.

Ziener–Strau model of submicrocrack formation according to the dislocation mechanism was improved. Temperature-rate dependence of the degree of the metal brittle strength reduction  $\delta(T)$  was investigated using numeric methods and the calculations were compared with the experiment. It was discovered that the  $\delta(T)$  dependence had minimum in the area of room temperature, reduction of the metal strength under action of hydrogen might reach 50 % of strength of the metal without hydrogen. The calculations showed that at the same temperature at increase of the relative plastic strain rate, the  $\delta(T)$  value increases and minimum of the  $\delta(T)$  curves shift into area of higher temperatures. Numeric modeling showed that temperature-rate peculiarities of influence of hydrogen on strength of items from HSLA steels were explained by dependence between temperature of the metal, rate of plastic strain and amount of hydrogen which is carried by the dislocations to the place of a microflaw origination. It was shown that reduction of the diffusion hydrogen concentration caused increase of the  $\delta(T)$  values.

Calculation-experimental methodology for determining parameters of energy traps of hydrogen in the weld metal, such as energy of the hydrogen-trap interaction and density of the traps, was developed. Influence of parameters of energy traps on kinetics of mass transfer of hydrogen in the metal and its redistribution in a welded joint was analyzed. Recommendations for prevention of microlevel origination in a welded joint of induced by hydrogen cold cracks were given.

## MEASURING SYSTEM FOR DETERMINATION OF RESIDUAL STRESSES IN ELEMENTS OF STRUCTURES USING THE ESPI METHOD



At the E.O. Paton Electric Welding Institute a compact measuring system and technology for determination of residual stresses, occurring in welded, brazed, cast and other metallic structures, have been developed. The developed system and technology can be also used for determination of stresses, caused in structures by applying the loads.

Residual stresses are determined on the basis of data about the value of in-plane displacements, measured by the method of electron speckle-interferometry in the vicinity of a blind hole. The in-plane displacements are the result of an elastic unloading of residual stresses after drilling of a blind hole.

The accuracy of determination of residual stresses is 10 % of value of yield strength of the material examined.

The measuring system consists of speckle-interferometer 1, CCD-camera 2, light guide 3, laser 4, computer with a board of pattern interference fringes figuring 5.

**Proposals for co-operation.** Measurement of residual stresses in elements of metallic structures, parts and sub-assemblies of machines. Manufacture of the measuring system and its delivery to the Customer, training of personnel.

Contacts: Prof. Lobanov L.M.  
Tel.: (38044) 289 95 78



## NEWS

### MAVR-150 MOBILE UNIT FOR AIR-PLASMA CUTTING

State holding company «Artyom-Contact» produces a mobile unit for air-plasma cutting (MAVR), designed for manual or automated cutting of low-carbon and stainless steels, aluminium and other metals within wide range of thickness.

Power source of MAVR is made on basis of original scheme of a high-frequency transistor inverter.

MAVR has the following advantages:

- transistor power source ensures reliability of operation and stability of the process;
- ignition of the arc is performed using the oscillator;
- scheme of protection against overloads is envisaged;
- low weight and compactness in repair and maintenance due to block design of the unit;
- possibility of operation from an independent power source of 30 kV·A power.

The unit has following technical characteristics: input voltage  $380 \pm 15\%$  V; range of output currents 50–150 A (I stage — 50, II — 100, and III — 150 A);



consumed power — not more than 25 kV·A; thickness of cutting up to 50 mm; power factor — 0.91; ambient temperature —  $-10$ – $+40$  °C; duty cycle at 10-minute cycle and current (100 A) 150 A is (100) 60 %; overall dimensions —  $400 \times 280 \times 600$  mm; mass — 45 kg.

### MGM-50K WELDING ELECTRODES

At the enterprise «Mezhgosmetiz» (Minsk, Oryol oblast) started production of the MGM-50K coated electrodes with a rutile kind of the coating for welding of carbon and low-alloy steels of increased strength ( $\sigma_t = 490$ – $660$  and  $\sigma_{0.2} > 375$  MPa) on alternating or direct current of reverse polarity in all spatial positions, except vertical one. High mechanical properties of the weld metal are achieved due to optimum composition of coating of the electrodes and introduction into it of rare-earth elements. These advantages allow using the electrodes for wide range of steels, including steels of increased strength.

The MGM-50K welding electrodes have in contrast to other alternating current electrodes higher welding-technological properties:

- easiness of the primary and repeated ignition of arc by the electrode due to application of ionization coating on the electrode end and introduction of ionized additives into composition of the coating;
- stable burning of short, medium and long (up to 20 mm) arc on alternating and direct current;
- self-separation of the slag;
- quality formation of the weld;
- possibility of welding within wide ranges of current;



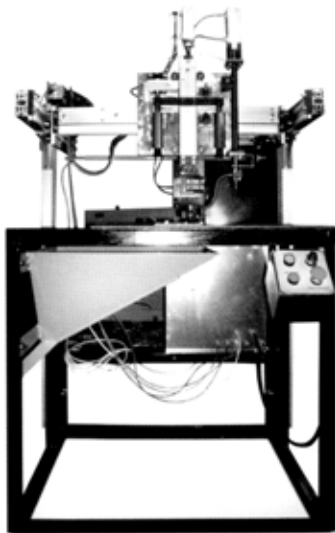
- possibility of welding at short-term moistening of the electrode surface without reduction of the deposited metal quality and welding-technological properties;
- possibility of using during performance of repair welding works of metal structures, containing rust, foreign matter and moisture.

The electrodes are certified by «UkrSEPRO», BelSt, GOST-R, Marine and River register of shipping industry of Russia and produced under SMK conditions, certified according to ISO GOST-R 9001:2001.



## ADFS-2001 INSTALLATION FOR AUTOMATIC WELDING OF REINFORCEMENT BARS TO EMBEDDED PARTS

The installation, produced by TC «Tekhnosvar» (Pskov, RF), is designed for automatic submerged-arc welding of reinforcement bars of 8–20 mm diameter to embedded parts. Material of the reinforcement bars is low-carbon and low-alloy steels.



Simultaneously one bar is welded. To a plate several bars may be welded.

The installation has the following composition: mechanisms for clamping a plate and a reinforcement bar; a mechanism for vertical movement of the bar according to the preset cycle; a table with guides and carriages; an oscillator for ignition of the arc; a pneumatic device; a unit for controlling the welding process; a set of wires and hoses; a source of welding current — a 1200 A rectifier.

The welding installation meets requirements and rules of labor protection and safety rules. Average productivity of the installation is 250 welding operations per hour. Design of the installation ensures manual placement of the parts to be welded and their removal after welding. Filling and removal of the flux is performed by the operator. The installation ensures horizontal movement of the bar clamping mechanism with its subsequent fixation during welding in order to make it possible to weld anchors according to the preset coordinates. The control unit ensures necessary cycle of operation in automatic mode: feeding of the reinforcement bar to the plate, switching of the welding current source and its disengagement after ignition of the arc, movement of the bar upwards and its lowering under welding current into molten metal, and cut off of the welding current source. Switching off of the welding process is performed automatically.

### TECHNOLOGY OF ARGON-ARC WELDING AND SURFACING WITHOUT PREHEATING OF STEELS WITH AN INCREASED CONTENT OF CARBON

The increased content of carbon in a hardening steel causes such difficulties in their welding and surfacing, as the susceptibility of welded joints to cracking, overheating and embrittlement. The advanced methods of their overcoming, including combination of welding at low heat inputs with preheating and application of austenitic welding consumables, are expensive, labor and power consuming. Besides, the effectiveness of these methods is reduced with increase in carbon content in steels. As a result, a whole group of steels with carbon content above 0.5 % is referred to those being not recommended for welding.

The offered technology allows welding and surfacing without preheating of hardening steels with carbon content up to 0.8 % using welding consumables close to the parent metal by the chemical composition. The given technology of welding and surfacing provides control of formation of structure of welded joint metal by control of conditions of its heating and cooling. In this case, a fine-grain structure with high characteristics of toughness and ductility is formed in metal of joints, thus increasing their resistance to the crack formation and embrittlement.

Technology is realized in standard welding equipment with control systems developed at the E.O. Paton Electric Welding Institute.

**Application.** Machine building, power engineering, agricultural machine building and other branches of industry, in which steels with increased carbon content are used, and also repair workshops.

**Proposals for co-operation.** Development and implementation of technologies; designing, manufacture and delivery of equipment; training of personnel.

Contacts: Prof. Savitsky M.M.  
E-mail: savitsky@paton.kiev.ua



## INTERNATIONAL CONFERENCE «TITANIUM-2008 IN CIS»

Traditional Annual International Conference «Titanium-2008 in CIS» arranged by the Inter-State Association «Titanium» was held on 18–21 May in St.-Petersburg (Russia). The Conference was attended by over 250 people from Russia, Ukraine, Belarus, Tajikistan, USA, Germany, Italy, Japan, Luxemburg, Poland and other countries.

Scientists and specialists in the field of titanium from leading research institutions and industrial enterprises of Russia, Ukraine, Belarus and other countries made presentations at the Conference: Federal State Unitary Enterprise «All-Russian Institute of Aircraft Materials», Federal State Unitary Enterprise «Central R&D Institute of Structural Materials «Prometej», A.A. Bajkov Institute of Metallurgy and Materials Science of RAS, Open Joint Stock Company «All-Russian Institute of Light Alloys», K.E. Tsiolkovsky Russian State Technological University «MATI», Ural State Technical University «UPI», Open Joint Stock Company «VSMPO-AVISMA Corporation», Federal State Unitary Enterprise «Giredmet», Open Joint Stock Company «Uralredmet», Closed Joint Stock Company «Zubtsovsky Machine-Building Factory», Open Joint Stock Company «Kaluzhsky Turbine Factory», State Research and Design Institute of Titanium, E.O. Paton Electric Welding Institute of NASU, G.V. Kurdyumov Institute for Metal Physics of NASU, Institute of Geological Sciences of NASU, Zaporozhie State Engineering Academy, State Enterprise «Zaporozhie Titanium-Magnesium Works», O.K. Antonov Aviation R&D Complex, Open Joint Stock Company «Ukrainian Graphite», State Research University «Physical-Technical Institute of NASB», etc. Totally, over 100 presentations were made.

Traditionally, many papers at the Conference were presented by specialists of the VSMPO-AVISMA Corporation. At present, it is one of the world leading manufacturers of critical-application titanium semi-finished products, meeting the 100 % demand for titanium parts for shipbuilding and aircraft engineering enterprises of Russia, Ukraine and Uzbekistan, 40 % demand — for the Boeing Company, and 60 % demand — for the EADC Company (including AIRBUS). VSMPO-AVISMA Corporation is an enterprise offering a full technological cycle in manufacture of titanium products: from production of titanium sponge to manufacture of tubes, rods, plates and forgings, and it continuously improves its production. The main area of its development is mastering of new, more technology-intensive stages of manufacture of titanium products: finishing machining of press-formed parts for disks of gas turbine engines, landing gears of air liners, heat exchangers, etc.

Also, many papers were presented by scientists of K.E. Tsiolkovsky Russian State Technological University MATI, which is active in investigations in the

field of materials science for titanium and titanium alloys, including for medical applications. Representatives of the Zaporozhie Titanium-Magnesium Works covered in detail the main trends in upgrading of the technology for production of titanium sponge in Ukraine, and further development of the Works. It should be noted that in 2008 an electron beam unit will be started up at this Enterprise to produce titanium ingots and slabs up to 5 t in weight, and they study the possibility of arrangement of a rolling shop for processing of ingots into plates.

Specialists of the E.O. Paton Electric Welding Institute made presentations on production of ingots up to 1200 mm in diameter and up to 20 t in weight by electron beam melting, investigation of the mechanisms of removal of titanium nitride inclusions from the titanium melt, electroslag remelting of titanium with electromagnetic stirring of the melt, as well as heat treatment of welded joints in new domestic titanium alloy T110. The papers presented by associates of the Institute generated high interest of the Conference participants.

Out of a wide variety of welding technologies, the greatest attention at the conference was given to explosion welding of bimetal plates to manufacture heat exchangers, and production of cast-welded structures to reduce costs of the products.

Much consideration at the Conference was given to the issues of application of titanium in aircraft engineering, power engineering, shipbuilding and production of medical-application items (endoprostheses, implants, instruments, etc.). Dramatic growth of volumes of utilisation of composite materials in manufacture of a new generation of aircraft has led to increase in a proportion of parts made from titanium alloys, which are the best structural materials for manufacture of load-carrying structures of the aircraft frame.

Among the new and quickly growing fields of application of titanium, we have to note construction of liquefied gas production factories and regasifying terminals (up to 250 t of titanium rolled stock per plant), as well as nuclear engineering (e.g. heat exchangers for nuclear power stations).

Because of a substantial growth of output of titanium, especially in China, the current titanium market is characterised by an increased level of competition, which causes reduction of prices for titanium products and increase of requirements to their quality. Further development of these trends opens up good prospects for increasing the volumes of utilisation of titanium in various civil industries.

In conclusion, we would like to note a high level of holding of the Conference, and express gratitude to its organisers represented by the Closed Joint Stock Company «Inter-state Association «Titanium» and its Chairman A.V. Aleksandrov.

*Prof. S.V. Akhonin (PWI)*

## FOURTH INTERNATIONAL CONFERENCE «MATHEMATICAL MODELLING AND INFORMATION TECHNOLOGIES IN WELDING AND RELATED PROCESSES»

From May 27 to 30, 2008 the Fourth International Conference «Mathematical Modeling and Information Technologies in Welding and Related Processes» was held in Katsiveli township at the «Katsiveli» House of Creativity of Scientists of NASU.

Conference organizers were the National Academy of Sciences of Ukraine, E.O. Paton Electric Welding Institute of NASU, International Association «Welding».

More than 60 specialists from Ukraine, Russia, Belarus, Germany and Poland took part in the Conference. The Conference was organized in the form of plenary and poster sessions, Conference working languages were Russian and English, with synchronous translation of the presentations.

20 papers were presented in the plenary session. We would like to note some of the presentations, which give an idea about the range of the covered subjects:

*Mathematical simulation of electromagnetic processes in the «welding arc–evaporating anode» system allowing for the anode voltage drop* (I.V. Krivtsun, V.F. Demchenko, A.B. Lesnoj, V.V. Nakvasnyuk, O. Mokrov, I. Zabirov, U. Raizgen, V. Pavlyk; E.O. Paton Electric Welding Institute of

NASU, Kiev, Ukraine; Institute of Welding, Aachen, Germany);

*Procedure of computer dynamic testing of welded structures* (S.V. Medvedev, M.V. Petrushina, O.P. Chiz; United Institute of Information Sciences, Minsk, Belarus);

*Mathematical simulation of thermal, electromagnetic and hydrodynamic processes at stationary arc TIG and A-TIG welding* (K.A. Yushchenko, I.V. Krivtsun, V.F. Demchenko, D.V. Kovalenko, A.B. Lesnoj, I.V. Kovalenko; E.O. Paton Electric Welding Institute of NASU, Kiev, Ukraine);

*Stress-strain state at diffusion welding of materials with differing physico-mechanical properties* (V.I. Makhnenko, V.V. Kvasnitsky, G.V. Ermolaev; E.O. Paton Electric Welding Institute of NASU, Kiev; NTU «Kiev Polytechnic Institute», Kiev; Admiral Makarov National University of Shipbuilding, Nikolaev, Ukraine);

*Mathematical simulation of the processes of producing large-diameter ingots* (T.V. Koroleva; E.O. Paton Electric Welding Institute of NASU, Kiev, Ukraine);

*Investigation of the influence of energy traps on the kinetics of hydrogen removal from the weld metal*



Conference participants during their visit to Livadia Palace, Yalta



of HSLA steels by numerical methods (V.S. Sinyuk; E.O. Paton Electric Welding Institute of NASU, Kiev, Ukraine);

*Deterministic chaos in the electric circuit with the welding arc* (V.N. Sydorets; E.O. Paton Electric Welding Institute of NASU, Kiev, Ukraine);

*Mathematical simulation of the turbulent flow of arc plasma formed by the plasmatron with the anode wire* (M.Yu. Kharlamov, I.V. Krivtsun, V.N. Korzhik, S.V. Petrov, A.I. Demianov; V. Dal East-Ukrainian University, Lugansk; E.O. Paton Electric Welding Institute of NASU, Kiev, Ukraine).

After the Conference was over a round table discussion on «Computational physics of the processes of welding and allied technologies — goals and problems» was held under the leadership of Prof. V.F. Demchenko and I.V. Krivtsun, Corresp. Member of NASU, during which the «venerable» and young scientists in a maximum open form discussed different issues of conducting a computational experiment, from

the engineering design, physical and mathematical models to algorithmization and software development.

Paper abstracts with the Conference program were published by the Conference start. Conference proceedings will be published before the end of 2008. These proceedings, as well as the proceedings of the First (2002), Second (2004) and Third (2006) International Conferences on «Mathematical Modelling and Information Technologies in Welding and Related Processes» can be ordered from the Editorial Office of «The Paton Welding Journal».

The next, 5th International Conference on «Mathematical Modelling and Information Technologies in Welding and Related Processes» will be held in Katsiveli township, Crimea, Ukraine in the last decade of May 2010.

*A.T. Zelnichenko, Cand. of PhM Sci.  
I.Yu. Romanova, Cand. of Sci. (Eng.), PWI*

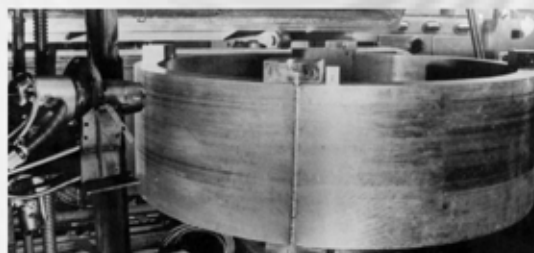
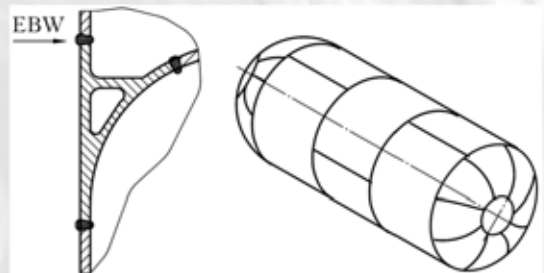
## TECHNOLOGY FOR EBW OF LIGHT ALLOY TANKS AND OTHER SHELL STRUCTURES WITH WALL THICKNESS OF UP TO 150 MM

Integrated technology was developed for application of electron beam welding to manufacture cylindrical or conical shells and tanks from 300 to 8000 mm in diameter, used as airframes of space rocket vehicles, casings of fuel systems, pressure vessels or cryogenic tanks of aluminium or magnesium alloys.

In addition to welding operations, the technology also comprises designing of the weld edges for different types of the joints, preparation of surfaces and edges for welding, meeting of accuracy requirements, selection of spatial position of the joints, as well as selection of rational methods for quality control and strength tests of welded joints, including at cryogenic temperatures.

The technology provides a 15–20 % increase in tensile strength of the joints in heat-hardened and intensively cold-worked aluminium alloys, 4–5 times decrease in residual welding stresses, and 5–7 times reduction in the HAZ width, compared with arc welding methods.

**Proposals for co-operation.** Development of technical documents, transfer of know-how for the technology, technical consultations and engineering services in commercial application of the technology.



Contacts: Prof. Ishchenko A.Ya.  
Tel.: (38044 287 44 06)

# SUBSCRIPTION FOR «THE PATON WELDING JOURNAL»

If You are interested in making subscription directly via Editorial Board, fill, please, the coupon and send application by fax or e-mail.

The cost of annual subscription via Editorial Board is \$324.

Telephones and faxes of Editorial Board of «The Paton Welding Journal»:

Tel.: (38044) 287 6302, 271 2403, 529 2623

Fax: (38044) 528 3484, 528 0486, 529 2623.

«The Paton Welding Journal» can be also subscribed worldwide from catalogues of subscription agency EBSCO.

<b>SUBSCRIPTION COUPON</b>			
Address for journal delivery			
<b>Term of subscription since</b>	200	till	200
<b>Name, initials</b>	_____		
<b>Affiliation</b>	_____		
<b>Position</b>	_____		
<b>Tel., Fax, E-mail</b>	_____		



## ADVERTISEMENT IN «THE PATON WELDING JOURNAL» (DISTRIBUTED ALL OVER THE WORLD)

### «АВТОМАТИЧЕСКАЯ СВАРКА»

#### RUSSIAN VERSION OF «THE PATON WELDING JOURNAL» (DISTRIBUTED IN UKRAINE, RUSSIA AND OTHER CIS COUNTRIES)

**External cover, fully-colored:**

- First page of cover (190×190 mm) – \$570
- Second page of cover (200×290 mm) – \$400
- Third page of cover (200×290 mm) – \$400
- Fourth page of cover (200×290 mm) – \$400

**Internal cover, fully-colored:**

- First page of cover (200×290 mm) – \$400
- Second page of cover (200×290 mm) – \$400
- Third page of cover (200×290 mm) – \$400
- Fourth page of cover (200×290 mm) – \$400

**Internal insert:**

- Fully-colored (200×290 mm) – \$340
- Fully-colored (double page A3) (400×290 mm) – \$570
- Fully-colored (200×145 mm) – \$170

- Article in the form of advertising is 50 % of the cost of advertising area
- When the sum of advertising contracts exceeds \$1000, a flexible system of discounts is envisaged

**Technical requirement for the advertising materials:**

- Size of journal after cutting is 200×290 mm
- In advertising layouts, the texts, logotypes and other elements should be located 5 mm from the module edge to prevent the loss of a part of information

**All files in format IBM PC:**

- Corell Draw, version up to 10.0
- Adobe Photoshop, version up to 7.0
- Quark, version up to 5.0
- Representations in format TIFF, color model CMYK, resolution 300 dpi
- Files should be added with a printed copy (makeups in WORD for are not accepted)